DE TTK

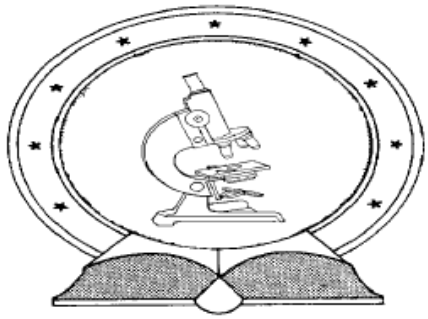

1949

Robust thallium(III) complexes with inorganic and organic multidentate ligands

PhD thesis

Tamás Fodor

Supervisor: Dr. Imre Tóth

University of Debrecen

Debrecen, 2016

Ezen értekezést a Debreceni Egyetem Természettudományi Doktori Tanács Kémiai Doktori Iskola koordinációs kémiai programja keretében készítettem a Debreceni Egyetem természettudományi doktori (PhD) fokozatának elnyerése céljából.

Debrecen, 2016. szeptember 13.

a jelölt aláírása

Tanúsítom, hogy Fodor Tamás doktorjelölt 2011.- 2016. között a fent megnevezett Doktori Iskola koordinációs kémiai programjának keretében irányításommal végezte munkáját. Az értekezésben foglalt eredményekhez a jelölt önálló alkotó tevékenységével meghatározóan hozzájárult. Az értekezés elfogadását javasolom.

Debrecen, 2016. szeptember 13.

a témavezető aláírása

A doktori értekezés betétlapja

Robust thallium(III) complexes with inorganic and organic multidentate ligands

Értekezés a doktori (Ph.D.) fokozat megszerzése érdekében
a koordinációs kémia tudományágban

Írta: Fodor Tamás okleveles vegyész

Készült a Debreceni Egyetem Kémiai doktori iskolája (K/2 koordinációs kémia programja) keretében

Témavezető: Dr. Tóth Imre

A doktori szigorlati bizottság:
elnök:: Dr. ……
tagok: Dr. ……
Dr. ……

A doktori szigorlat időpontja: 20… . …… … .

Az értekezés bírálói:
Dr. ….....
Dr….....
Dr. ….....

A bírálóbizottság:
elnök: Dr. ….....
tagok: Dr. ……..
Dr. ……..
Dr. ……..
Dr. ……..

Az értekezés védésének időpontja: 20… . …… … .

1. Introduction 4

2. Bibliographic review 9

2.1. Thallium chemistry 9

2.2. Polyoxometallates 12

2.3. Macrocyclic polyamino-polycarboxylate ligands 19

3. Experimental section 22

3.1. Materials and Preparation of Solutions 22
3.2.1. pH-potentiometry 27
3.2.2. Iodide-selective potentiometry 28

3.3. Spectrophotometry 28

3.4. NMR measurements 29

3.5. Crystal structure analysis 30

3.6. DFT calculations 31

4. Results and Discussion 33

4.1. Detailed characterization of $[Tl(dota)]^-$ 33
4.1.1. X-ray crystal structure 33
4.1.2. Solution structure and mixed-complex formation 39
4.1.3. Studies on the stability and kinetic inertness of $[Tl(dota)]^-$ by UV-vis Spectroscopy 44
4.1.5. Solution dynamics study with ^{13}C-NMR 55

4.2. Characterization of $[Tl(cdo2a)]^+$ and its iodido mixed-ligand complex 64
4.2.1. Background of ligand choice 64
4.2.2. Dissociation kinetics of $[Tl(cdo2a)]^+$ 65
4.2.3. Acid-base properties of $[Tl(cdo2a)]^+$ 66
4.2.4. Investigation of the iodido-mixed ligand complex [Tl(*c*do2a)I] 67
4.2.5. Comparison with a rigidified open-chain complex $[Tl(cdtabba)]^+$ 69

4.3. Study of the ternary complex formation between [Al(nota)] and F^+ 73

4.4. Characterization of $[Tl_2\{B\text{-}\beta\text{-}SiW_8O_{30}(OH)\}_2]^{12-}$, a newly synthesised thallium-containing polyoxometallate 77
4.4.1. X-ray crystal structure 77
4.4.2. Solution structure study 79
4.4.2.1. Simulation of Tl NMR spectra *81*
4.4.3. Solution behavior and overall robustness 86
4.4.4. Antibacterial activity 90

5. Summary 99

6. Összefoglaló 106

8. Scientific publications of Tamás Fodor 125

9. Acknowledgement 130

1. Introduction

Thallium is the heaviest element in Group 13 of the periodic table, with atomic number 81 and relative atomic mass of 204.38. It was discovered by Sir William Crookes in 1861 during a search for tellurium in sulphuric acid plant residue. The metallic element was named after the bright green colour of its emission line, derived from the greek word „θαλλός" which means „budding twig". Called the "forgotten element" of the periodic table by some, thallium research cannot be described as either widespread or mainstream. There are few books that deal mostly, or exclusively with inorganic thallium chemistry and the bulk of scientific papers on the subject are from a small number of researchers.[1,2,3,4] Indeed to most people, both outside and within the scientific community, the most widely known properties of thallium are its toxicity and its use as poison for rodents and sometimes humans. Ongoing inorganic thallium chemistry is mostly confined to its redox reactions, high-temperature superconductors, metal-metal bonds and coordination chemistry.[5,6,7,8,9]

The element can be found in the Earth's crust in 0.1–3 ppm, mostly in sulphide ores. It is widely distributed in nature and has no commercially important source mineral (the few thallium-based minerals such as lorándite ($TlAsS_2$), crookesite ($(Cu,Tl,Ag)_2Se$), and avicennite (Tl_2O_3) are very rare). This wide distribution can be mostly attributed to Tl^+ being able to replace potassium in various minerals.[10,11]

It is manufactured commercially as a by-product from flue dusts created during the roasting of pyrite ores, in sulphuric acid plants, and from the smelting of lead, zinc, and copper. Elemental thallium is recovered by electrolytic reduction of Tl(I) sulfate solutions.

Thallium is used in the optical industry to increase the density and refractive index of glass, or create IR optical elements from TlBr–TlI crystals. In the field of electronics, thallium oxysulfide is used in the so-called 'Thalofide cell', which is highly sensitive to low-intensity, long-wavelength light and thallium-activated NaI or NaCl crystals are used in some types of scintillation detectors. Thallium-containing alloys are also used as good quality bearings, having a very high resistance to corrosion and low friction coefficients. The only current medical application of thallium is its use in the form of intravenous injections of ^{201}Tl (half-life = 72.9 hours) for myocardial imaging.

Thallium is toxic to a variety of life forms, including humans. The biochemical behaviour of Tl^+ is similar to that of K^+, enabling it to replace potassium to some degree and interfere with K^+–dependent biological reactions. The lethal dose of thallium is in the range of 10–50mg/kg. Compared to (both natural & synthetic) „true" poisons, this means that one needs to absorb quite a lot of thallium for a fatal dose (600 mg for humans). The symptoms appear in 1–5 days and are paresthesia of the extremities, hypersecretion, hair loss, uncontrolled muscle movements, convulsions, delirium, coma and ultimately, death by respiratory failure.

The metal accumulates in the body and can be absorbed by ingestion or through the skin and membranes, seemingly regardless of chemical form. The most effective known antidote is colloidal Prussian Blue, $(KFe^{3+}[Fe^{2+}(CN)_6]\cdot nH_2O)$, acting as an ion exchanger for Tl^+ in the intestines and accelerating its elimination.

Although it is not an outstanding poison, thallium has garnered considerable infamy. This is in part due to the early (1920 to 1970) use of

thallium compounds as pesticides, in medicine and as cosmetics. Thallium has been used internally in the treatment of gonorrhoea, syphilis, dysentery, and tuberculosis and externally as a depilatory. Thallium-based pesticides were most often poisoned bait, which distributed the metal into the nearby environment and wildlife and even children were severely poisoned via ingesting said bait. This mixture of direct and indirect poisoning routes has lead to serious, sometimes fatal cases and the withdrawal of such products.

Thallium has two naturally occurring stable isotopes: ^{203}Tl and ^{205}Tl. Both isotopes have a nuclear spin of ½, their natural abundances are 29.5% and 70.5% respectively. Numerous radioactive Tl-isotopes exist in the mass range 184–210, there are 41 isotopes including 16 with half-lives longer than 10 minutes.[12] As mentioned before, ^{201}Tl is used in diagnostics in what is called a *thallium stress test.* It is a form of scintigraphy, where the amount of ^{201}Tl detected in cardiac tissues correlates with tissue blood supply. Normal cardiac cells have normal Na^+/K^+ ion exchange pumps and thallium is transported into the cells via the K^+ pumps. Widening of normal coronary arteries (vasodilation) is triggered either by exercise or medication. Coronary steal occurs from areas of ischemia where arteries are already maximally dilated, infarct areas and ischemic tissue will remain "cold". Differences in thallium distribution pre- and post-stress may indicate areas that may require surgery, redistribution indicates the existence of coronary steal and the presence of ischemic coronary artery disease.[13] The electron configuration of ground-state thallium is $[Xe]4f^{14}5d^{10}6s^26p^1$, its common oxidation states are I and III. In contrast to other elements of the group, Tl(I) is the more stable state and the investigation of the Tl(III) – Tl(I)

redox system is a large part of thallium chemistry. While its $6s^2$ electrons do display the inert pair effect, this alone does not provide a sufficiently high ionization energy barrier to stabilize Tl(I). The bond energies in Tl(III) halides however, are much weaker than those found in analogous gallium and indium compounds, making its formation significantly less favourable. Thallium can also exist in the formal oxidation state II, though no stable compounds of Tl(II) are known in aqueous solution. Tl(II) intermediates have been detected in reactions with one-electron reactants with half-lives of 0.5 ms by flash photolysis.

The standard reduction potential of Tl(III)/Tl(I) is E^0= +1.25 V.[14] Tl(III) strongly hydrolyses in aqueous solutions even in acidic conditions, producing $TlOH^{2+}$, $Tl(OH)_2^+$ (their hydrolysis constants being $K_1 = 69\times10^{-3}$ and $K_2 = 25\times10^{-3}$ respectively) and brown solid Tl_2O_3. The influence of complexation and hydrolysis on formal redox potentials are especially important in thallium redox systems, as they have been shown to vary greatly ($TlCl/TlCl_3$ = +0.77 V in 1M HCl; $TlOH/Tl(OH)_3$ = −0.05 V in alkaline solution). The difference to E^0 can be attributed to the highly dissimilar complexation properties of the two oxidation states.
Thermodynamic stability of Tl(III) can be vastly increased by the addition of complexing anions as it forms much more stable complexes than Tl(I), especially with softer ligands such as halides or pseudohalides (see later).

As mentioned before, thallium research is not very widespread and the element itself has mostly found niche uses. Data on the chemical properties of thallium compounds is also quite scarce, especially compared to most other group 13 elements and even more from outside the group. This is also true when Tl(III)-aminocarboxylates are

considered, as there is little to no data on their solution chemistry, with the exception of a few open-chain ligands such as NTA-complexes and $[Tl(edta)]^-$ (see later). The data that does exist, suggests that thallium has remarkable properties that could perhaps be utilized more widely or present a completely novel approach to well-known problems. This requires intense research into the chemistry of complexes of Tl(III) with multidentate ligands.

In this work, we sought to examine various lesser-known and/or novel Tl(III)-compounds in detail, with focus on the structural properties both in solid and solution. The core aims of this work are summarized below:

Exploring the structural properties of $[Tl(dota)]^-$ both in solid phase and solution.

Elucidating the solution dynamics of $[Tl(dota)]^-$.

Investigating the acid–base properties and affinities towards mixed–complex formation for $[Tl(cdo2a)]^+$ and $[Tl(dota)]^-$ with a number of small anions.

Obtaining information on the dissociation kinetics of $[Tl(cdo2a)]^+$ and $[Tl(dota)]^-$.

Preparing and investigating the properties of $[Al(nota)F]^-$ as analogs of mixed ligand complexes mentioned above.

Examining the solution structure of thallium–containing POMs and providing a stability estimate for $[Tl_2\{B\text{-}\beta\text{-}SiW_8O_{30}(OH)\}_2]^{12-}$

2. Bibliographic review

2.1. Thallium chemistry

Thallium(III) is classified as a „soft" metal ion, in contrast to other elements of the group, which are classified as „hard" ions. The „softness" of Tl(III) is shown in its strong interactions with „soft" donor ligands such as sulphur or larger halides. Tl(I) is classified however, as a borderline ion sharing similarities both with the alkali metal ions, which have comparable ionic radii, and also with Ag^+. Complexes of Tl(I) are quite weak due to the inert s^2 electron pair, which are σ–antibonding in all stereochemistries.

As such, Tl(III) forms strong chloride and bromide complexes of type TlX_n^{3-n}, where *n* is less than or equal to 4. These species are more stable in aqueous solution than analogous complexes of other group 13 elements and are among the most stable metal–halide complexes known. Complexes where *n* = 5 or 6 also exist is solution, they are however much weaker and only appear if halide concentration is high enough.[15,16]

There is a systematic change in the coordination geometry of the Tl(III) complexes TlX_n^{3-n} (X = Cl, Br). The $Tl(H_2O)_6^{3+}$ cation has a regular octahedral geometry, which is unchanged by the coordination of the first two halides ($TlX(H_2O)_5^{2+}$ and $TlX_2(H_2O)_4^{+}$), the X–Tl–X^+ unit is linear in aqueous solution. The solids $TlCl_3 \cdot 4H_2O$ and $TlBr_3 \cdot 4H_2O$ are isomorphous, both have trigonal bipyramidal coordination around Tl(III). X-ray diffraction studies indicate that the three halide ligands are coordinated in a trigonal arrangement with two water molecules completing the coordination sphere. In aqueous solution, the geometry is

essentially the same in $TlBr_3(H_2O)_2$, but the chloride complex likely has distorted tetrahedral geometry.[17] In the TlX_4^- complexes where X = Cl, Br, or I, the coordination sphere is tetrahedral with no water molecules in the inner sphere, either in solution or in the solid phase. TlX_5^{2-} and TlX_6^{2-} are again octahedral.[5,18]

Knowledge of the Tl(III)–iodide complexes is limited because Tl(III) oxidizes iodide in solution. This can be countered by a large excess of iodide, avoiding redox reactions and a highly stable TlI_4^- complex has been observed; β_4 = ca. 5×10^{35}.[19]

Tl(III) forms stable cyanide complexes (the overall formation constants, $\beta_n = 10^{13.2}$, $10^{26.5}$, $10^{35.2}$ and $10^{42.6}$ in 4 M ionic strength for n = 1, 2, 3 and 4 respectively). These species are in fact the most stable monodentate–Tl(III) complexes.[20] The extra stability of the $Tl(CN)_2^+$ species is noteworthy, as the diorganothallium(III) compounds containing the linear C–Tl–C group (as does the dicyanide) are also very stable. The redox stability of the $Tl(CN)_4^-$ complex might be explained in a similar manner to that of TlI_4^-.

Complexes of Tl(III) with oxoanions are also much more stable than those of Tl(I). The coordination of perchlorate to Tl(III) cannot be ruled out; however, ClO_4^- is considered to be the best noncoordinating counterion for equilibrium studies. Related stability constant values (K_1) are: $Tl(NO_3)^{2+}$, $10^{0.9}$; $TlSO_4^+$, $10^{1.95}$; $TlHSO_4^{2+}$, $10^{1.2}$; $Tl(OAc)^{2+}$, $10^{6.2}$. The overall stability constant $\beta_4 = 10^{18.3}$ for $Tl(OAc)_4^-$. Some mixed hydroxo complexes have also been detected, including $Tl(OH)_2NO_3$ and $Tl(OH)(OAc)^+$.[4,21]

In case of Tl(III)–organic ligand systems, it is important to consider that $Tl(H_2O)_6^{3+}$ is easily hydrolyzed, forming Tl_2O_3 even at pH = 2–3 and

Tl(III) itself is a strong oxidant. Tl(III)–oxide is also known to oxidize organic molecules even in cases where $Tl(H_2O)_6^{3+}$ does not.[22] Both these effects prevent the formation or study of many such complexes. Conversely, the multidentate ligands can stabilize the cation against both hydrolysis and reduction. These effects are exemplified in the $[Tl(edta)]^-$ complex, which is one of the most stable metal–edta species known ($K = 10^{37.8}$)[23,24,25]; only $[Co^{III}(edta)]^-$ has higher stability.[23] $[Tl(edta)]^-$ is stable up to pH = 12 and has pK = 8.00**;** $Tl(edta)(OH)^{2-}$ is formed in alkaline solutions. The solid phase structure of the Tl(III)–edta complex is yet unknown, but may very well be seven coordinate, including a water molecule in its inner coordination sphere, as it forms ternary $Tl(edta)X^{2-}$ complexes with monodentate ligands readily, without reduction of Tl(III) (log $K_{mix[Tl(edta)X]}^{2-}$ = 2.30, 3.50, 2.70, and 8.72, where X = Cl^-, Br^-, SCN^-, and CN^-, respectively). In solid $Na_2Tl(edta)CN{\cdot}3H_2O$, the thallium(III) ion is hemispherically encased by the hexadentate edta, strongly coordinating one further CN^- in its inner sphere.[26]

The metal-metal interactions have recently become a focus in heavy element coordination chemistry.[27] Tl(I) is often used as a large crystallization counter cation for anionic metal complexes, however its role might be more complicated as seen in $Tl_2Pt(CN)_4$. This solid compound involves two Pt–Tl bonds with a weakly covalent character, differing from other $M_2Pt(CN)_4$ salts that show Pt–Pt "linked" columnar structures. The strong luminescence due to these Pt-Tl bonds is lost in solution.[28,29] Conversely the ligand supported metal–metal bond in $[Tl^I(crown\text{-}P_2)Pt^{II}(CN)_2]NO_3$ (P = diphenylphosphinomethyl) stays intact in solution.[30] A family of cyano compounds containing direct platinum–thallium metal–metal bonds, unsupported by ligands and their formation,

structure, equilibrium, and kinetics have been reported.[31,32,33,34,35] Four dinuclear species represented by a general formula $[(NC)_5Pt–Tl(CN)_{n-1}]^{(n-1)-}$ (n = 1–4) and a trinuclear complex $[(NC)_5Pt–Tl–Pt(CN)_5]^{3-}$ are shown to form in aqueous solution. These are true equilibrium complexes, their solutions also include the parent complexes $Pt(CN)_4^{2-}$ and $Tl(CN)_n^{3-n}$ (n = 0–4), and can be shifted to either side of the equilibrium by changing cyanide concentration and/or pH in the solution. Multinuclear NMR- (^{13}C, ^{195}Pt, ^{205}Tl), IR-, Raman spectroscopy, Electron Spectroscopy for Chemical Analysis (ESCA), X-ray, and Extended X-ray Absorption Fine Structure (EXAFS) studies confirm direct, short (2.60–2.64 Å) Pt–Tl bonds. The spin-spin coupling pattern is consistent with 4 + 1 + 1 equivalent $^{13}CN^-$ ligands (I = 1/2), respectively and one ^{195}Pt nucleus (natural abundance 33.8%, I = 1/2). The compounds are diamagnetic, and the electronic states and the nature of the Pt–Tl bonds have been elucidated by Density Function Theory (DFT) calculation.[36]

2.2. Polyoxometallates

Polyoxometalates [37, 38] are polyoxoanions that are composed mainly, or completely of transition elements, distinguishing them from their main group analogues (such as silicates), which are both structurally and chemically distinct. The typically water-soluble polyoxometalates (POMs) are most often highly symmetrical anions with molecular structures incorporating multiple metal centers, the current record being 368. Also known as addenda, these metal centers are mainly transition metals of groups 5 and 6 in high oxidation states, such as W(VI) and

V(V). Addenda are octahedrally coordinated to six oxygens, forming MO_6 building blocks that are joined by corner- or edge- (rarely face-) sharing oxygen atoms in a self–assembly manner. The terminology „polyoxo" is due to the large number of coordinated oxygens, usually present as bridging and terminal oxo ligands. Natural POMs may be found in minerals such as sherwoodite ($Ca_{4.5}[AlV^{IV}_2V^{V}_{12}O_{40}]\cdot H_2O$) and mendozavilite ($(Na(Ca,Mg)_2Fe^{III}(PO_4)_2[PMo_{11}O_{39}](OH,Cl)_{10}\cdot H_2O$), as well as in the Mo & W storage proteins of Azotobacter vinelandii, which contain ~100 of the respective atoms as individual clusters with 3–8 metal centers.[39,40]

The polyoxoanions of Group 5 & 6 are traditionally classified as either isopolyanions, which are composed solely of addenda and oxygens, or heteropolyanions which incorporate a number of metallic or non-metallic heteroatoms. The heteroatom and its coordinated oxygens constitute a heterogroup, which is commonly connected to the surrounding MO_6 groups by edges or corners. As the coordination environment of the heteroatom most often defines the structural type of the heteroPOM and virtually any element of the periodic table can serve as a heteroatom, the number of known heteropolyanions is great and continually increasing. Addenda atoms are dominantly octahedrally coordinated and retain either one or two (mutually *cis*) terminal oxygen atoms that comprise the outermost layer of the POM structure in nearly all cases.

The first POMs were described by Berzelius[41] in 1826 (yellow ammonium–12– molybdophosphate and –arsenate, and their reduced „blue" derivatives), but detailed reports on the chemistry of many polymolybdates and polytungstates only began to emerge in the late 19th

century. Keggin introduced the use of X-ray diffraction into POM chemistry in 1933, investigating the structure of $H_3[(PO_4)W_{12}O_{36}]\cdot 6H_2O$.[41]

The formation of polyoxoanions from mononuclear oxoanions is driven by acidic condensation of MO_6 octahedra, resulting in the kinetic and eventually the thermodynamic products under the formation conditions. (Polytungstates and some polyvanadates usually equilibrate much more slowly than molybdates). This also means that all polyoxoanions undergo dissociation in alkaline media. The required pH may, at times, not be achievable in aqueous solutions though.

The expected initial step in the polymerization of a tetrahedral oxoanion is condensation of the monoprotonated version. This is the case for V(V) and Cr(VI) but not for Mo(VI) and W(VI). That V, Mo, and W can generate an extensive chemistry of large POMs is a result of their ability to coordinate a largely variable amount of oxygen atoms (4 – 7) (one may mention that Cr cannot).

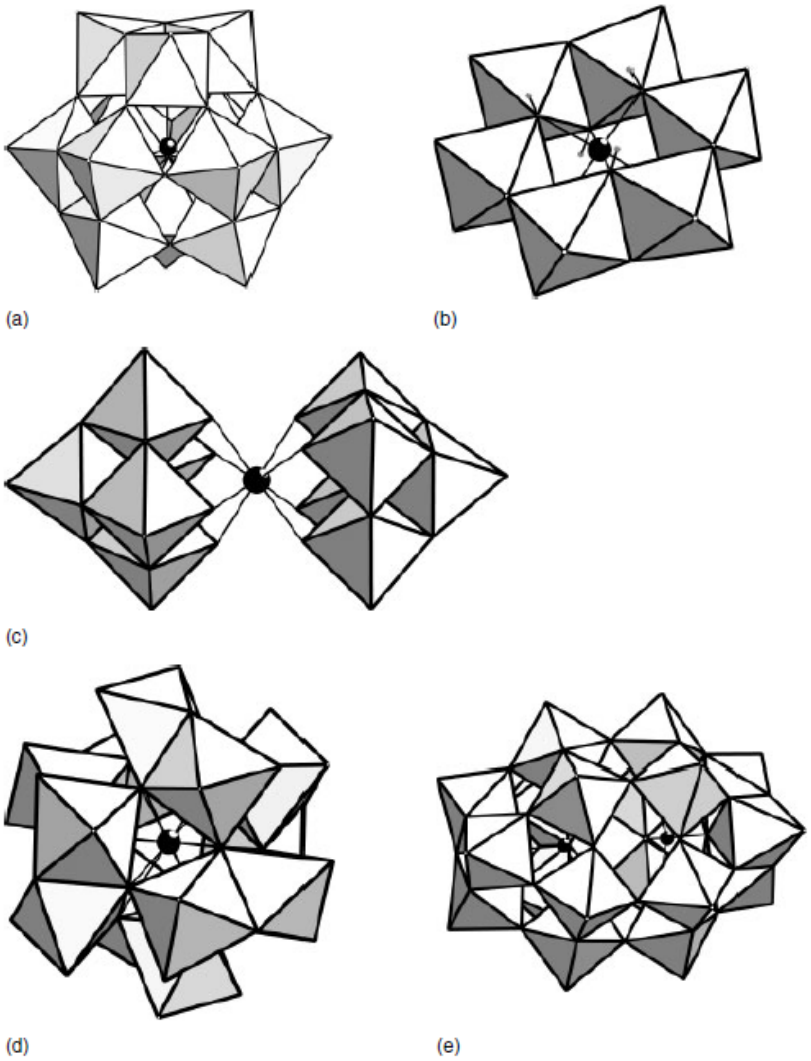

Figure 2.2.1 Examples of POM structures. (a) α-$[(PO_4)W_{12}O_{36}]^{3-}$ *(Keggin)*. (b) $[(Te^{VI}O_6)W_6O_{18}]^{6-}$, $[\{Cr^{III}(OH)_6\}Mo_6O_{18}]^{3-}$ *(Anderson–Evans)*. (c) $[(U^{IV}O_8)W_{10}O_{28}]^{8-}$ *(Weakley–Yamase)*. (d) $[(Ce^{IV}O_{12})Mo_{12}O_{30}]^{8-}$ *(Dexter–Silverton)*. (e) α-$[(AsO_4)_2Mo_{18}O_{54}]^{6-}$ *(Wells–Dawson)*

Several parameters such as pH, temperature, ionic strength, concentration and ratio of reagents greatly influence the resulting POM structures and can be „tuned" to provide a large variety of polyanions. As mentioned, polyanions are formed by self–assembly and in the formation of heteroPOMs, the heterogroup functions as an important template.

Closed-shell POMs have low surface–oxygen basicity, making them chemically inert towards electrophiles, and are also known as plenary structures. They usually only react with metal ions in terms of ion pair formation.

The Keggin structure (XW_{12}) has become the symbol of POM chemistry and most published research in this field deals with these type of polyanions. Keggin anions may form many structural isomers, of which the best known are those of C_{3v} symmetry, designated β, in which one of the four equivalent edge-shared M_3O_{13} triads found in the original „α" Keggin anion of T_d symmetry, is rotated by 60°. Each triad corresponds to three edge–shared MO_6 octahedra, which are corner–linked by μ_4–oxo bridges to the central heteroatom. Two, three, and all four edge-shared groups, when rotated, produce γ, δ, and ε structures, respectively.[42] Each additional rotation destabilizes the Keggin ion, as the number of edge–shared MO_6 connections is increased.

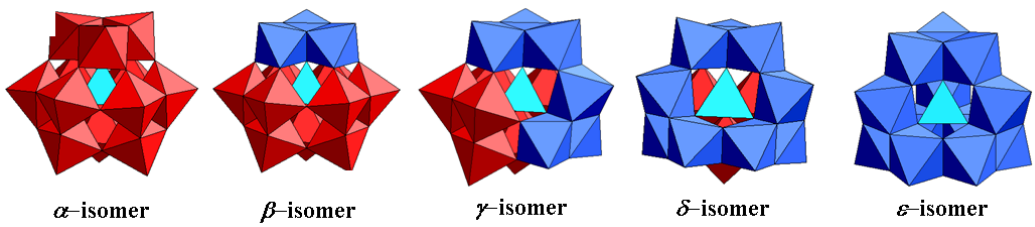

Figure 2.2.2 Structural isomers of $XM_{12}O_{40}^{n-}$ Keggin anions

The number of possible isomers greatly increases in „mixed-addenda" POMs, such as $[(PO_4)V_2W_{10}O_{36}]^{5-}$, which has five „positional" isomers of α configuration, and 13 β–isomers. The existence of these isomer types has been well established by NMR spectroscopy.

The so-called *lacunary*, or vacant derivatives of certain polyanions, notably the Keggin and Wells–Dawson structures, are also known. These structures can be prepared by controlled basic hydrolysis and are markedly more reactive than their parent POMs. For heteropolytungstates, loss of W–centers along with their terminal oxo-ligands leads to structures with varying vacant site numbers (mono– to hexavacant) (e.g. $[GeW_{11}O_{39}]^{7-}$, $[\gamma\text{-}SiW_{10}O_{36}]^{8-}$, $[P_2W_{15}O_{56}]^{12-}$, $[H_2P_2W_{12}O_{48}]^{12-}$).

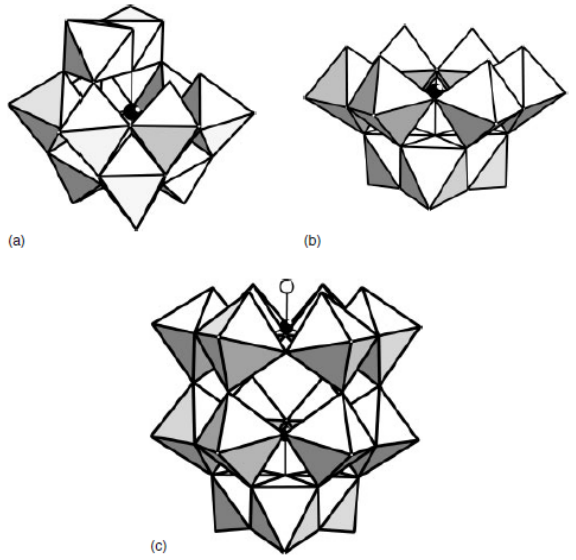

Figure 2.2.3 Some lacunary anion structures. (a) $[(PO_4)W_{11}O_{35}]^{7-}$. (b) $[(PO_4)W_9O_{30}]^{9-}$. (c) $[(PO_4)_2W_{15}O_{48}]^{14-}$

The removal of each cationic $(WO)^{4+}$ unit also negates some of the mentioned inertness, as the overall negative charge of the resulting lacunary POM is raised, also increasing nucleophilicity and thus, reactivity. Such vacant POMs are, in essence, inorganic multidentate ligands and may be modified by incorporating additional heteroatoms or –groups into the vacant sites.

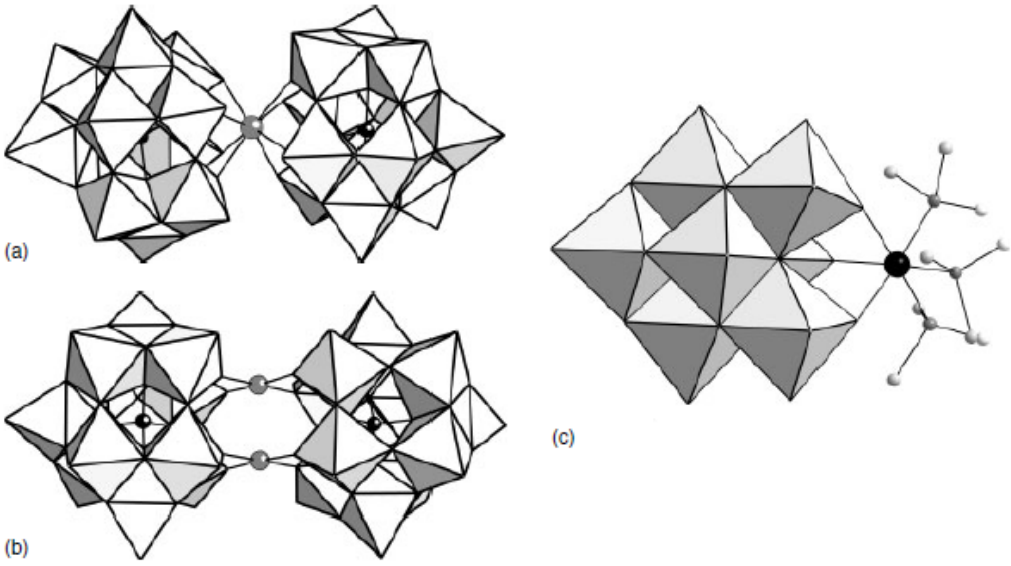

Figure 2.2.4 Two lacunary POM sandwich type structures (a) $[U^{IV}(SiW_{11}O_{39})_2]^{12-}$; (b) $[Pd^{II}{}_2(PW_{11}O_{39})_2]^{10-}$ and one substituted lacunary POM (c) $[Mo_7O_{24}\{Os(dmso)_3\}]^{3-}$.[43]

These secondary heteroatoms, depending on their inherent coordination geometry, may reconstruct the original POM structure (such as a Keggin anion), or they may be sandwiched between two lacunary POMs.

The POMs, being a large and highly diverse group of compounds, are applied in a wide variety of fields.[44,45,46,47] One of the earliest uses is

in analytical chemistry: trace–level colorimetric determination of elements that are prone to Keggin–anion formation, namely silicates and phosphates. Phosphotungstic acid ($H_3PW_{12}O_{40}$) is a general stain for electron microscopy. More recent organic derivatives allow highly selective, targeted imaging applications.[48] POMs have proven to be successful phasing agents in the structural crystallography of several large biomolecules, the most noteworthy recent case being $[P_2W_{18}O_{62}]^{6-}$ used for the high-res structure of ribosomes (2009 Chemistry Nobel Prize). POMs also find use as industrial–grade catalysts:[49,50,51,52,53] molybdophosphates in the oxidation of methacrolein to methacrylic acid; tungstophosphoric acids in the production of hydroxoalkanes via alkene hydration; molybdovanadophosphates in alkene oxidation and aromatic coupling, etc. POMs are also breaking ground into medicine, as many of them are biologically active[54]: smaller vanadates and molybdates selectively inhibit enzyme function[55] and many polytungstates have been found to possess antitumoral, antibacterial and antiviral activity.[56,57,58]

2.3. Macrocyclic polyamino-polycarboxylate ligands

Macrocyclic amino-carboxylate ligands are widely used in clinical chemistry including medical diagnosis and therapeutic applications involving metal complexes. The ligands consisting of polyaza-macrocyclic rings and pendant arms show high selectivity if the size of the ring and the radius of the metal ion match perfectly. Moreover, the nature of the pendant arm attached to the N-atoms of the macrocycle can be used to tune the physico-chemical properties (stability and selectivity) of the metal complexes. In case of bifunctional ligands, there is also a

conjugated biological vector (peptide, antibody etc.), i.e. a covalently bonded entity in the molecule, responsible for the selective targeting of the complexes in living organisms.[59] The most widely studied complexes are the MRI-contrast agents, where the macrocyclic ligands are often the 1,4,7,10-tetraazacyclododecane-1,4,7,10-tetraacetate (dota) and its derivatives, known as the most versatile ligands for medical imaging applications. [60] With a suitably sized cavity and four potentially coordinating pendant arms, this macrocyclic ligand forms complexes with many cations (i.e., Ln^{3+} ions, Sc^{3+},[61] Y^{3+},[62] Ga^{3+},[63] Bi^{3+},[64] Ca^{2+},[65] Sr^{2+},[66] Zn^{2+},[67] and transition metal ions such as Fe^{3+},[68] Co^{2+},[63] Ni^{2+}, and Cu^{2+}).[69] The complexes are usually thermodynamically very stable [70] and kinetically quite inert.[71,72] These behaviors together make dota a very safe metal-binder because it can carry the metal component in biological fluids without risk of decomplexation, which would result in uncontrolled distribution of the components (i.e., metal ion and ligand) in the biological system and may cause toxic effects or a decrease in the signal (e.g., relaxivity, luminescence, radioactivity).

The advantages of providing high stability and inertness (often called kinetic stability in medical papers) are partly counterbalanced by the slow formation of metal−dota complexes.[73] While this is hardly a technical problem for stable metal ions, the long formulation time could be a crucial point for short-lived radioisotopes.[74] Very intensive research during the last 2 to 3 decades has produced a trove of chemical knowledge about dota complexes, i.e., the stability constants, formation and dissociation kinetics, and structure in both the solid state and solution have been explored for many metal ions.[75] A significant portion of the information that has allowed general conclusions to be established

regarding dota complexes has been collected in lanthanide(III)−dota systems, particularly the Gd^{3+} complex. This is related to the fact that $[Gd(dota)]^-$ is a very good and safe general (nonselective) magnetic resonance imaging (MRI) contrast agent (CA) widely used in clinical practice under the trade name Dotarem. Dota complexes are also of great importance in other diagnostic fields, such as radiology (Single Photon Emission Computed Tomography, SPECT and Positron Emission Tomography, PET). The use of macrocyclic complexes, such as dota-derivatives for targeted radioisotope delivery is a relatively fresh and heavily investigated field. One example is Dota-octreotate, an amide of dota and (Tyr^3)-octreotate which binds to somatostatin receptors and is therefore selective towards a number of neuroendocrine tumors. Radionuclides commonly transported with DOTATATE (trade name) are ^{68}Ga for tumor diagnosis with PET [76] and ^{177}Lu for ß-radiation treatment.[77]

It was also reported recently, that macrocyclic metal complexes may be used to bind and deliver certain radioisotopes in anionic form: Al(III)-complexes of peptide-linked amide derivatives of 1,4,7-triazacyclononane-1,4,7-triacetate (nota) were shown to bind the PET isotope ^{18}F with promising in vivo results.[78,79]. This type of radionuclide transport also foregoes bonding the isotope to the backbone of the carrier molecule and most complications associated with the process. It is therefore quite tolerant of low half-life isotopes and allows virtually any modification to the ligand to take place before labeling, such as linkage of a targeting vector.

3. Experimental section

3.1. Materials and Preparation of Solutions

Tl(III) stock solution

The stock solution of $Tl(ClO_4)_3$ was prepared by anodic oxidation of $TlClO_4$. The electrolytic cell (see scheme 3.1.1.1.) was filled with 6M perchloric acid, bubbles were removed mechanically from the cylinders and by opening the stopcock on the bridge to let any air out.

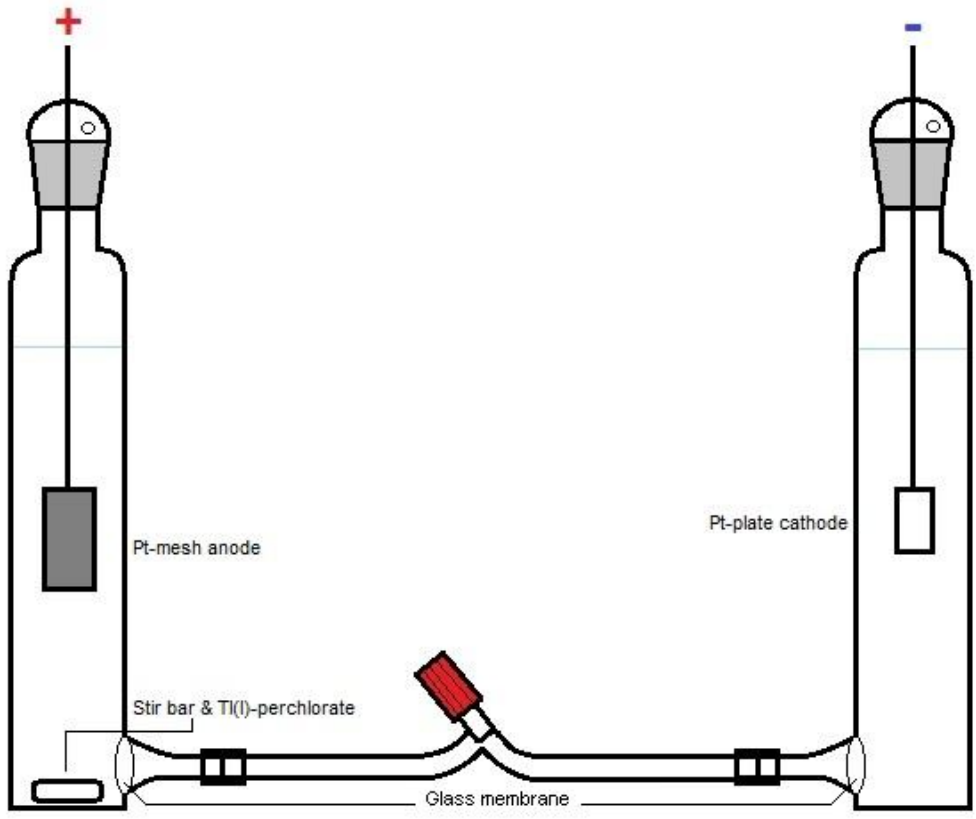

Scheme 3.1.1 Scheme of the Tl(III)-perchlorate electrolysis cell

A portion of solid $TlClO_4$ and a stirrer were added to the anode compartment. Electrolysis took place between a fine platinum mesh anode and a platinum plate cathode with an initial current strength of 120 mA. This gradually dropped to ~80 mA during the process, which took a total of ~51 hours. The remaining portions of $TlClO_4$ were added as the anode compartment was slowly cleared of solids. In our case 21 grams of $TlClO_4$ were used, split up into 7 g portions.

Analysis of the Tl(III) stock solution

The analysis of the $Tl(ClO_4)_3$ stock solution was performed as follows: A carefully measured volume of the stock solution (300 μL) was pipetted into a previously weighed titration flask and weighed. An excess of sodium-chloride was added to avoid the hydrolysis of Tl(III), the sample was diluted with 5 ml distilled water and the acid content was determined by titration with 0.200M NaOH, using methyl red as indicator. 2 ml of concentrated hydrochloric acid was added to re-acidify the solution and the concentration of Tl^+ was determined by titration with 0.0100M $KBrO_3$ at ~95°C. In the absence of Tl^+ methyl-red is oxidized turning the solution colorless, which signals the endpoint of the titration. The solution was brought to a low boil and SO_2 was bubbled through for ~30 minutes to reduce all thallium to Tl^+. (The excess of SO_2 was removed by further boiling for ~10 minutes.) The process for Tl^+-determination was repeated with 0.100M $KBrO_3$.[80] This method yields the density, c_{Tl+}, $c_{Tl(III)}$ and c_{H+} data for the stock solution. The data for the stock solution used for the studies described herein were: ρ=1.72g/cm^3, c_{Tl+}=9.25mM, $c_{Tl(III)}$=1.192M, c_{H+}=3.96M.

[Tl(dota)]⁻ solutions

$[Tl(dota)]^-$ solutions were prepared by (a) adding small portions of the $Tl(ClO_4)_3$ stock solution to a mildly basic (pH ~ 8) solution of dota and dropwise addition of ~20% NaOH to neutralize the acid (high acidity causes [TlH(dota)] to precipitate), (b) adding the required amount (1 equivalent) of dota in one portion to a solution of $Tl(OOCCH_3)_3$ (prepared by mixing a portion of the $Tl(ClO_4)_3$ stock solution (1 equivalent) and a tenfold excess of acetic acid/sodium-acetate buffer) and (c) following method (a) but using guanidine carbonate instead of NaOH. The pH of the resulting solutions was set to ~4 to ensure that only $[Tl(dota)]^-$ was present (any excess of Tl(III) precipitates as Tl_2O_3.). Photochemical decomposition was avoided by keeping the solutions in the dark.[81]

Synthesis of cdo2a

0.89 g (2.52 mmol) of 1,4-dibenzyl-1,4,7,10-tetraazacyclododecane, 0.77g (5.55 mmol, 1.1 eq. per target nitrogen) of bromoacetic acid and a stir bar were added to a 100 ml Erlenmeyer flask. 20 ml of distilled water was added and the reaction mixture was stirred at room temperature until everything dissolved, producing a clear, faintly yellow solution. Two drops of phenolphthalein indicator were added and the reaction was heated to ~80°C. 20 % NaOH was added in small portions until the intermittent opalescence disappeared and the indicator turned violet. The reaction was stirred at ~80°C for 3 hours, with periodic additions of 20% NaOH when the color of phenolphthalein began to fade (every 20-30 minutes). The reaction was deemed complete when the violet colour remained intense for more than 30 minutes and was then left to cool to

room temperature. With stirring, ~6 M HCl was added slowly until the violet color completely disappeared. The resulting slightly yellow solution was evaporated to dryness under reduced pressure, producing an off-white solid. The crude 1,4-dibenzyl-1,4,7,10-tetraazacyclododecane-7,10-diacetic acid (dibenzyl-*c*do2a) was purified via HPLC using a Luna 10u-Prep C18(2) 100A (*250*×21,20 mm*;* 10 μm) column and an acetonitrile / 5 mM TFA eluent system.

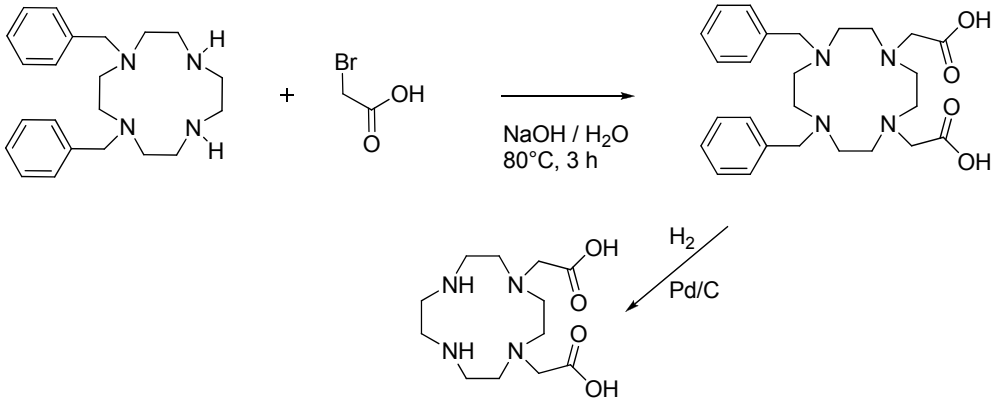

Scheme 3.1.1 Synthesis scheme of *c*do2a

The fractions collected were acidified with ~6 M HCl and evaporated to dryness under reduced pressure. The benzyl groups were removed by hydrogenation of the intermediate in 70 ml of methanol with Pd/C catalyst under 5 bar H_2 pressure for 6 hours. The mixture was then filtered and evaporated to dryness, resulting in a yellow oil. The crude product was purified by dissolving it in 2 ml of methanol, passing it through a small silica column (6 ml total immobile phase volume) and washed with 30 ml methanol and 100 ml of distilled water. The aqueous fraction was freeze-dried to yield the desired product as a light-yellow

solid (0.69 g, 95%). ^{1}H NMR [360 MHz, D_2O] δ 2.80–3.25 (16H, m, ring CH_2); 3,36 (4H, s, acetace CH_2). ^{13}C NMR [100 MHz, D_2O] δ 42.2 (2C, s, ring CH_2); 43.6 (2C, s, ring CH_2); 50.6 (2C, s, ring CH_2); 51.4 (2C, s, ring CH_2); 56.3 (2C, s, acetate CH_2); 174.4 (2C, s, acetate CO).

[Tl(cdo2a)]$^{+}$ solutions

[Tl(*c*do2a)]$^{+}$ solutions were prepared similarly to method (a) described above with the following differences: the ligand solution was used without pH adjustment and the $Tl(ClO_4)_3$ was added in one portion. This caused a similar white precipitate to appear, which was redissolved as the pH was raised to ~4 with slowly added NaOH (~20%).

[Tl(cdtabba)]$^{+}$ solutions

The ligand cdtabba was prepared in our lab, by Zoltán Garda. [Tl(cdtabba)]$^{+}$ solutions were prepared in the same way as [Tl(*c*do2a)]$^{+}$ solutions. The only notable difference is that after complete dissolution of the initial precipitate, these solutions have a tendency to foam.

[Al(nota)] + F^{-} NMR samples

The NMR samples were prepared by mixing Al(III), nota and F^{-} in equimolar ratio (4 mM of $AlCl_3$, NaF and nota each, in acetate buffer at pH = 4) and heated at 100 °C for various time periods. Their ^{19}F-NMR spectra were recorded after an additional 24 h. The pH was adjusted by stepwise addition of 0.2 M NaOH and HCl solutions. An attempt to prepare $[Al(NOTA)(F)]^{-}$ was also undertaken in 50% ethanol ($AlCl_3$,

NOTA and F^- solutions were mixed in water and the appropriate amount of ethanol added lastly.

$(NH_4)_5K_7[Tl_2\{B\text{-}\beta\text{-}SiW_8O_{30}(OH)\}_2]\cdot 19H_2O$

The polyanion was synthesized by W. Ayass (Bremen, Germany) as follows: the dilacunary POM precursor $K_8[\gamma\text{-}SiW_{10}O_{36}]$ was first prepared according to the published procedure.[11] A 20 mL solution of this POM precursor (400 mg, 0.135 mmol) in double deionized water was added to solid thallium nitrate $Tl(NO_3)_3\cdot 3H_2O$ (0.060 g, 0.135 mmol) under vigorous stirring for 30 minutes at room temperature. Once the solution was added, a temporary formation of brown Tl_2O_3 was observed. The dark brown color changed to light brown after a few seconds under vigorous stirring. After 30 minutes, the excess of Tl_2O_3 was finely filtered, resulting in a clear, colorless solution. Around 2 mL of 1 M NH_4Cl was added to the solution resulting in a final pH of around 4.2. Approximately 2 weeks later, white colorless crystals of $(NH_4)_5K_7[Tl_2\{B\text{-}\beta\text{-}SiW_8O_{30}(OH)\}_2]\cdot 19H_2O$ (yield: 60 mg, 17%) suitable for X-ray analysis were formed upon slow evaporation at room temperature in a 50 mL beaker.

3.2. Potentiometric measurements

3.2.1. pH-potentiometry

The pH values were measured by a Metrohm 6.0234.100 combined glass electrode connected to a Delta Ohm HD 8705 pH-meter. The bridge electrolyte (3M KCl) in the electrode was replaced with 1M NaCl to

avoid $KClO_4$ precipitation in the membrane. The pH-meter was calibrated with KH-phthalate (pH = 4.005) and KH_2PO_4-Na_2HPO_4 (pH = 6.865) buffers and the H^+ concentrations were calculated from the measured pH values by applying the method proposed by Irving et al.[82]

3.2.2. Iodide-selective potentiometry

Free iodide concentrations were measured using a Metrohm 6.0502.160 iodide–selective electrode with an Ag/AgCl electrode as reference. As previously stated, electrolytes containing K^+ were replaced with 1M NaCl. Measurements were performed at 25 (±0.1) °C, in 1M $NaClO_4$ under a constant argon stream. Calibration of the electrode was performed by titrating a blank 1 M $NaClO_4$ solution with NaI.

3.3. Spectrophotometry

UV-VIS spectra were recorded in quartz cuvettes ranging from 1.0 mm to 1.0 cm path length with a Varian Cary 1E UV-Visible Spectrophotometer at 25 °C in the wavelength range 350-200 nm, with data points every 0.5 nm and a scan rate of 100 nm/min, unless otherwise stated. Short-term dissociation kinetics was followed by repeated recordings of spectra, with delay times of 1 hour. The UV-light was cut off from the sample during the delays to avoid photochemical decomposition. Long-term kinetics were followed by separate recordings, with delay times of 1 day or 1 week.

3.4. NMR measurements

^{1}H and ^{13}C spectra were recorded with a Bruker DRX 400 spectrometer at 400.1 MHz and 100.6 MHz, respectively. In spite of lacking matching NMR probes capable of ^{205}Tl-measurement, thallium spectra were obtained with a Bruker AM 360 spectrometer by inserting a 500 MHz BB probe and tuning the x-channel to the frequency of ^{205}Tl (207.8 MHz). This setup does not interact with ^{1}H or ^{2}H and does not enable locking or ^{1}H-decoupling to be used. Probe temperatures were kept at 25 (±0.1) °C if not stated otherwise. Calibration was performed using the signal of D_2O (4.79 ppm) for ^{1}H-spectra, tetramethylsilane (0 ppm) for ^{13}C-spectra and with 50 mM Tl(I)- and Tl(III)-perchlorate solutions (Tl^{+}: -4.72 ppm, Tl^{3+}: 2039 ppm) for ^{205}Tl-spectra. Line-shape analysis was carried out with a home-made program written in MatLab, using the algorithm developed by Reeves and Shaw.[83] This program fits a signal-shape function simulating the change of coupling-free NMR signals caused by chemical exchange, using modified Bloch-equations (the coupling-free approximation implies that the same exchange rate is applied to both sets of signals). The relative position of the two doublet signals used for the analysis were fixed, while the integrals (populations) and the line widths within the doublets were assumed to be identical. Five parameters were estimated: two to define the baseline, one for the intensity, the frequency specific to the position of the signal and the exchange rate constant. The calculated rate constants were then fitted to the Eyring-Polanyi equation [$\ln(k/T) = -\Delta H^{\neq}/RT + \ln(k_B/h) + \Delta S^{\neq}/R$, where k is the rate constant, T is

the absolute temperature, k_B is the Boltzmann constant, R is the ideal gas constant, h is the Planck constant and $\Delta H^{\neq}$ and $\Delta S^{\neq}$ are activation enthalpy and activation entropy.

376.5 MHz ^{19}F NMR spectra were collected using a Bruker DRX 400 NMR spectrometer. Calibration was performed with 10 mM slightly basic NaF for ^{19}F spectra (0 ppm).

3.5. Crystal structure analysis

The sodium salt of $[Tl(dota)]^-$ could not be crystallized in spite of repeated trials. Thus, we used the guanidine cation, which is known to aid the preparation of single crystals due to its strong ability to form hydrogen bonds.[84] Single crystals of $\{C(NH_2)_3\}[Tl(dota)]\cdot H_2O$ could be grown at the interface between 96% ethanol and a solution prepared by method (c) described above.

Diffraction intensity data collection was carried out at 293(2) K on a Bruker-Nonius MACH3 diffractometer equipped with a point detector using graphite-monochromated Mo-$K\alpha$ radiation (λ = 0.71073 Å). The structure was solved with the SIR-92 program[85] and refined by the full-matrix least-squares method on F^2. All non-hydrogen atoms were refined with anisotropic thermal parameters using the SHELXL-97 package.[86] Hydrogen atoms were located geometrically and refined in the rigid mode, except for hydrogen atoms of water molecules, which could be found in the difference electron density map. The remaining electron density peaks were found close to the Tl atom. Crystal data and structure refinement details: Formula: $C_{17}H_{32}N_7O_9Tl$; MW: 682.87; crystal system: triclinic; space group: P-1; a = 7.498(10) Å; b = 12.406(5) Å; c =

12.800(4) Å; α = 91.01(1)º; β = 90.86(4)º; γ = 107.31(6)º; V = 1136.3(16) Å^3; Z = 2; D_{calc} = 1.996 g cm^{-3}; $F(000)$ = 672; μ = 7.17 mm^{-1}; Reflections collected: 4909; Unique reflections with I > 2σ(I): 4117; Parameters refined: 331; GOF on F^2 = 1.09; $R[F^2 > 2\sigma(F^2)]$ = 0.057; R_{int} = 0.046; $wR(F^2)$ = 0.156; $\Delta\rho_{max}$ and $\Delta\rho_{min}$ = 3.58 and –4.05 e Å^{-3}.

3.6. DFT calculations

All calculations were performed in aqueous solution employing DFT within the hybrid GGA approximation with the B3LYP exchange-correlation functional[87] and the Gaussian 09 package (Revision B.01).[88] Full geometry optimizations of the [Tl(dota)]$^-$ system were performed in aqueous solution without symmetry constraints. In these calculations we used the relativistic effective core potential (RECP) of Ross. et al for Tl (CRENBL), which includes 68 electrons in the core, with the valence space (5d, 6s and 6p) represented by an uncontracted (3s3p4d) basis set.[89] The ligand atoms were described using the standard 6-311+G(d,p) basis set. The stationary points found on the potential energy surfaces as a result of geometry optimizations were tested to represent energy minima rather than saddle points via frequency analysis.

The relative free energies of the different conformations of [Tl(dota)]$^-$ complexes were calculated in aqueous solution at the B3LYP/CRENBL/6-311+G(d,p) level, and they include non-potential-energy contributions (zero point energies and thermal terms) obtained through frequency analysis. The arm rotation and ring inversion processes of [Tl(dota)]$^-$ were investigated by means of the synchronous transit-guided quasi-Newton method at the B3LYP/CRENBL/6-31+G(d,p)

level.[90] The nature of the saddle points (one imaginary frequency) was characterized by frequency analysis. The free energy barriers calculated include non-potential energy contributions obtained by frequency analysis.

The NMR shielding tensors of the $[Tl(dota)]^-$ system were calculated in aqueous solution using the B3LYP functional and the GIAO method.[91] In these calculations the more extended 6-311G+(d,p) basis set was used for the ligand atoms. For ^{13}C-NMR chemical shift calculation purposes the NMR shielding tensors of TMS were calculated at the same level.

Throughout this work solvent effects were included by using the polarizable continuum model (PCM), in which the solute cavity is built as an envelope of spheres centered on atoms or atomic groups with appropriate radii. In particular, we used the integral equation formalism (IEFPCM) variant as implemented in Gaussian 09.[92] The default values for the integration grid (75 radial shells and 302 angular points) and the SCF energy convergence criteria (10^{-8}) were used in all calculations.

4. Results and Discussion

4.1. Detailed characterization of $[Tl(dota)]^-$

4.1.1. X-ray crystal structure

Crystals of $\{C(NH_2)_3\}[Tl(dota)]\cdot H_2O$ contain the $[Tl(dota)]^-$ complex, a guanidinium cation and a water molecule. A view of the structure of the complex and bond distances of the metal coordination environment is provided in Figure **4.1.1.**1. The Tl^{3+} ion is directly coordinated to the eight donor atoms of the ligand, with the metal coordination environment being best described as twisted square antiprismatic (TSAP). The stereochemistry of eight- and nine-coordinate metal complexes of dota is well documented; the coordination of the ligand to the metal ion introduced two sources of chirality, one associated to the conformation of the cyclen moiety [(δδδδ) or (λλλλ)], and another related to the layout of the four acetate pendant arms [represented as Δ or Λ]. The combination of these two sources of helicity gives rise to four possible stereoisomers existing as two diastereoisomeric pairs of enantiomers. These enantiomeric pairs provide either a square antiprismatic [SAP, Δ(λλλλ)/Λ(δδδδ)] or a TSAP [Λ(λλλλ)/Δ(δδδδ)] coordination around the metal ion.[16e, 93] Inspection of the structure of $\{C(NH_2)_3\}[Tl(dota)]\cdot H_2O$ shows that crystals contain the Λ(λλλλ)/Δ(δδδδ) enantiomeric pair, the two enantiomers being centro-symmetrically related in accordance with the centro-symmetric character of the space group P-1. Both the guanidinium cations and the water

molecules are involved in hydrogen-bonding interactions with the oxygen atoms of the acetate groups of the ligand.

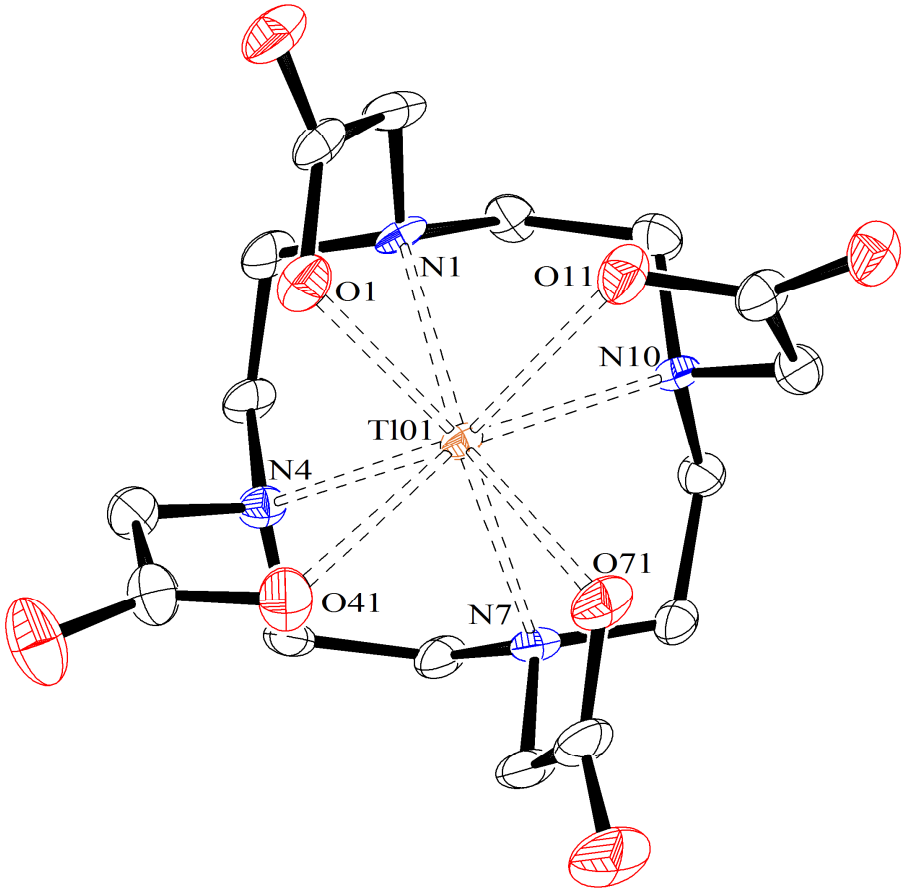

Figure 4.1.1.1 View of the structure of the $[Tl(dota)]^-$ complex present in crystals of $\{C(NH_2)_3\}[Tl(dota)]\cdot H_2O$. The ORTEP plot is at the 30% probability level. Bond distances (Å): Tl01-N1, 2.454(8); Tl01-N4, 2.497(9); Tl1-N7, 2.443(8); Tl01-N10, 2.458(9); Tl01-O1, 2.322(8); Tl01-O11, 2.438(8); Tl01-O41, 2.383(8); Tl01-O71, 2.316(7)

Table 4.1.1.1 Structural parameters observed for selected $[M(dota)(H_2O)]^-$ and $[M(dota)]^-$ complexes in the solid state.

M	La	Gd	Bi	Sc	Tm	Tl
Ionic radius / Å[a]	1.216	1.107	1.17	0.87	0.994	0.98
M-O / Å[b]	2.467	2.368	2.538	2.150	2.279	2.365
M-N / Å	2.770	2.663	2.526	2.441	2.529	2.464
M-O / M-N	0.89	0.89	1.00	0.88	0.90	0.96
M-Q_O / Å[c]	0.728	0.715	1.112	1.007	1.064	1.252
M-Q_N / Å[d]	1.810	1.632	1.434	1.327	1.466	1.324
Q_O-Q_N	2.54	2.35	2.55	2.33	2.53	2.58
Twist Angle / º[e]	23.2	38.5	25.9	41.1	24.4	25.4
Isomer	TSAP	SAP	TSAP'	SAP'	TSAP'	TSAP'

[a] Ionic radii for coordination number 8 (Bi, Sc, Tm and Tl) or coordination number 9 (La and Gd) taken from reference 94. [b] Average bond distances between the metal ion and the O atoms of the acetate arms. [c] Distance between the metal ion and the least squares plane defined by the coordinated O atoms of acetate groups. [d] Distance between the metal ion and the least squares plane defined by the N atoms of the macrocycle. [e] Calculated as the average value of the four torsion angles N-C_N-C_O-O, where N and O are the donor atoms defining a five-membered chelate ring and C_N and C_O represent the centroids of the Q_N and Q_O planes, respectively.

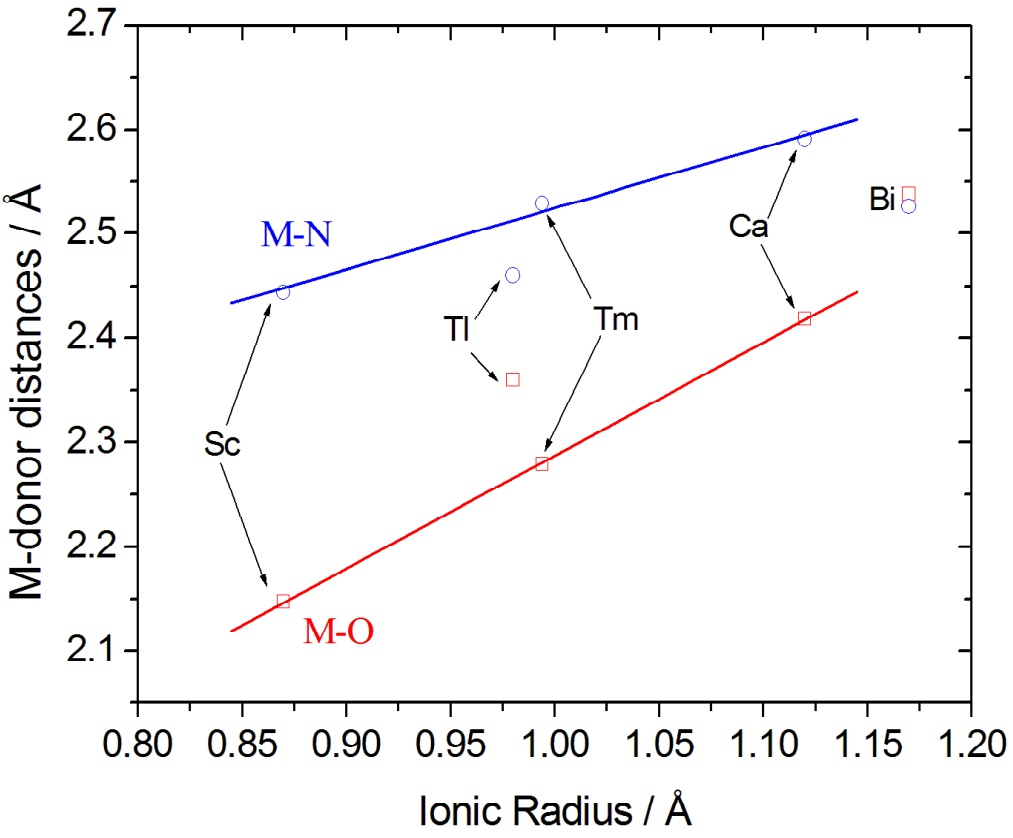

Figure 4.1.1.2 Variation of the M-N and M-O bond distances with the ionic radius in $[M(dota)]^-$ (M = Tm, Sc, Bi or Tl) and $[Ca(dota)]^{2-}$ complexes. The solid lines are the linear fits of the data reported for the Ca^{2+}, Sc^{3+} and Tm^{3+} complexes (see text)

Dota-like complexes with the light Ln^{3+} ions are usually nine-coordinated, where the ligand acts as eight-dentate and one water molecule is in the inner coordination sphere. Eight-coordination with the absence of a coordinated water molecule is typical for the heavier Ln^{3+} ions such as Tm^{3+}. In both sub-groups SAP (Ln= Pr, Nd, Sm, Dy) and

TSAP (Ln= Ce, Tm) geometries are found. Eight coordinate complexes that lack the apical water molecule are often labeled as SA' and TSAP' to differentiate them from the nine-coordinate SAP and TSAP complexes.[63a] $[Sc(dota)]^-$ adopts a SAP' geometry,[63a] in contrast with the TSAP' coordination observed for $[Ca(dota)]^{2-}$, $[Bi(dota)]^-$ and $[Tm(dota)]^-$.[63a,65,66] In $[Tl(dota)]^-$ the coordination geometry around Tl^{3+} is TSAP'. The distinctive structural feature that discriminates SAP and SAP' versus TSAP and TSAP' structures is represented by the twist angle between the two square planes of the antiprism, the basal plane comprised of the four nitrogen atoms of the macrocycle, and the upper plane containing the four coordinated oxygen atoms of the pendant arms. The average twist angle observed for $[Tm(dota)]^-$ (25.4º) is close to that expected for a regular twisted square antitiprism (22.5º) and also similar to those found for other complexes having TSAP or TSAP' structures (Table **4.1.1.**1).

Table **4.1.1.**1 provides a comparison of structural parameters reported in the literature for $[M(dota)]^-$ complexes (M = Sc^{3+},[63a] Tm^{3+},[63a] and Bi^{3+},[65]) with those of the Tl^{3+} analogue. Additionally, we have also included the corresponding data for selected $[M(dota)(H_2O)]^-$ complexes, with M = La[95] or Gd[69] as representative members of the earlier and middle members of the lanthanide series, respectively. The average M-O bond lengths are in the range of 2.54-2.15 Å, while the M-N distances range between 2.44 and 2.77 Å. The distances between the virtual planes defined by the four N atoms of the macrocycle (Q_N) and the four donor oxygen atoms of the pendant arms (Q_O) are ca. 2.53-2.58 Å for the complexes with TSAP and TSAP' coordination and 2.33-2.35 Å for those with SAP and SAP' geometries. Thus, the Q_O-Q_N distances for a given coordination polyhedron remain nearly unaffected by the nature of the

metal ion or the presence of a coordinated water molecule,[96] while the position of the metal ion with respect to the Q_O and Q_N planes varies significantly. As expected, the M-Q_O and M-Q_N distances are substantially different for complexes having different coordination numbers (see for instance the values for La, Gd and Tm in Table **4.1.1.**1).[98] However, different M-Q_O and M-Q_N distances appear to be also related to important changes in the ratio of the M-O and M-N distances. The M-O/M-N ratio is very similar for the complexes with the hard metal ions La^{3+}, Gd^{3+}, Tm^{3+} and Sc^{3+} (0.88-0.90), and increases to 0.96 and 1.00 for the Tl^{3+} and Bi^{3+} complexes, respectively. For the latter complex the M-O and M-N distances are nearly identical, while for the complexes with La^{3+}, Gd^{3+}, Tm^{3+} and Sc^{3+} the M-N bond distances are clearly longer than the M-O ones, and the $[Tl(dota)]^-$ complex presents an intermediate situation. A plot of the M-donor distances versus the ionic radii of the metal ions for the $[M(dota)]^-$ (M = Tm, Sc, Bi or Tl) and $[Ca(dota)]^{2-}$ complexes (Figure **4.1.1.**2) shows that both the M-N and M-O distances vary linearly with the ionic radius for the set of complexes with the "hard" metal ions Tm^{3+}, Sc^{3+} and Ca^{2+}, while the Bi-O and Tl-O distances are longer, and the Bi-N and Tl-N distances are shorter, to the values expected from the linear trends. Thus, the "soft" nature of Tl^{3+} and Bi^{3+} according to the Pearson classification[97] provokes a strengthening of the coordination bonds with the softer N donor atoms, which results in a deeper penetration of the metal ion into the macrocyclic cavity. This effect becomes obvious when comparing the structural data reported in Table **4.1.1.**1 for the complexes with Tm^{3+} and Tl^{3+}, which possess nearly identical ionic radii.

4.1.2. Solution structure and mixed-complex formation

The ^{205}Tl nucleus has a nuclear spin of I=½ and very good sensitivity, therefore ^{205}Tl-NMR is quite useful to follow the formation of metal complexes in aqueous solution.[98] The ^{205}Tl-NMR chemical shift range is huge and very sensitive to the oxidation state of the Tl ion in the particular compound.[99] The (proton coupled) ^{205}Tl-NMR spectrum of [Tl(dota)]$^-$ shows a single signal at δ = 2218 ppm with a chemical shift very similar to that measured earlier for [Tl(edta)]$^-$ (δ = 2301 ppm).[27] The positions of these signals are within the range expected for a Tl(III) compound, while the lack of Tl(I) signal at around δ = 0 ppm indicates that there was no reduction of Tl(III) to Tl(I) during the preparation of [Tl(dota)]$^-$.[100] Furthermore, the absence of a signal due to Tl^{3+}_{aq} at δ = 2039 ppm confirms the full complexation of the metal ion by the ligand. The broad ^{205}Tl-NMR signal observed at 298 K ($w_{½}$= 2200 Hz) did not show multiplicity caused by ^{1}H spin-spin coupling to the protons of the dota ligand, which is likely related to the fluxional behavior of the complex (see below). However, the multiplicity due to ^{1}H-^{205}Tl coupling could be observed in the spectrum recorded at 289 MHz and 268 K, which is observed as a pseudo-nonuplet with an apparent ^{1}H-^{205}Tl coupling constant of ~500 Hz. This suggests that the ^{1}H-^{205}Tl coupling pattern in [Tl(dota)]$^-$ is dominated by the coupling to eight of the 24 proton nuclei of the ligand..

^{205}Tl-NMR shifts are very sensitive to small changes in the chemical environment around Tl-center, and therefore can be used to follow the protonation/deprotonation of the [Tl(dota)]$^-$ complex measuring the ^{205}Tl chemical shift at different pH values. Adding a strong

acid to a solution of $[Tl(dota)]^-$ indeed causes significant changes of the observed ^{205}Tl-NMR shift (Figure **4.1.2.**1). Plotting the chemical shift values vs. pH shows a typical S-shaped curve with an inflection point at pH=1.4, which can be attributed to the protonation of $[Tl(dota)]^-$ according to:

$$[Tl(dota)]^- + H^+ \rightleftharpoons [HTl(dota)]$$

(**4.1.2.**1)

$$K^H_{Tl(dota)} = [HTl(dota)] / [H^+][Tl(dota)^-]$$

(**4.1.2.**2)

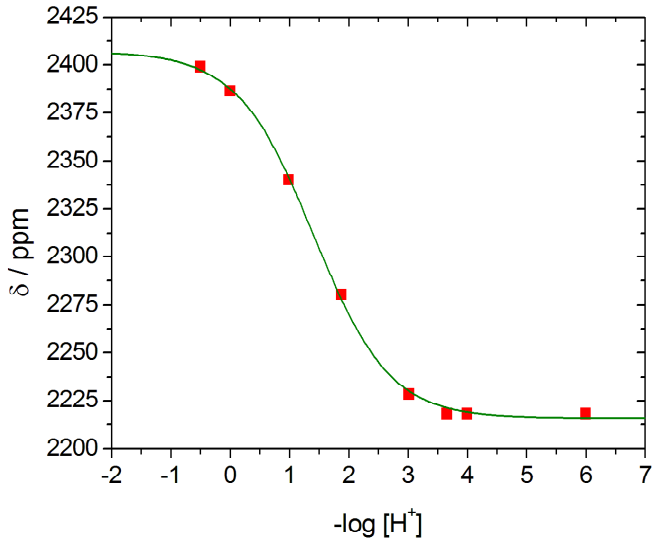

Figure 4.1.2.1 ^{205}Tl-NMR shift of $[Tl(dota)]^-$ vs. $-lg[H^+]$

The analysis of the $\delta - c_{H+}$ curve provides $pK^H_{Tl(dota)} = 1.4\pm0.1$ ($\delta_{[HTl(dota)]}$= 2405±3 ppm and $\delta_{[Tl(dota)]}$= 2216±1 ppm). The protonation process most likely involves the protonation of one of the carboxylate

arms. However the accuracy of this constant was limited by several conditions: 1) it was not possible to keep the ionic medium constant, i.e. the most acidic sample contained 3 M perchloric acid; 2) the samples were not homogenous. Formation of the charge-neutral [Tl(Hdota)] species at 1.0 M and 0.1 M acid concentrations might be responsible for the precipitation of a white solid from the solution of $[Tl(dota)]^-$ in acidic conditions (see experimental Section above). Even so, the pK value could be calculated from the δ_{205Tl} vs. pc_H curve without knowing the total concentration of the $[Tl(dota)]^-$ species; 3) At higher acid concentrations (3 M) the solution became homogeneous, which might be attributed to the formation of a charged diprotonated $[Tl(H_2dota)]^+$ species, with the two protonation steps being strongly overlapped. In any case the evaluated protonation constant can be considered as a reasonable estimate.

The ^{205}Tl-NMR chemical shift of $[Tl(dota)]^-$ was constant in the pH range of 4-11, indicating the lack of formation of the $[Tl(dota)(OH)]^{2-}$ mixed ligand complex. Considering the strong tendency of Tl(III) to undergo hydrolysis, this can be taken as a strong indication of a very tight coordination of the octadentate $dota^{4-}$ ligand to the central Tl^{3+} ion. For instance, in the case of $[Tl(edta)]^-$ the formation of a ternary hydroxo complex characterized by a pK = 6.0 has been reported.[24,26,101]

The decreased reactivity of $[Tl(dota)]^-$ compared to $[Tl(edta)]^-$ is also evidenced by the very limited tendency of the former to form mixed ligand complexes with bromide and cyanide ions. In comparison, $[Tl(edta)]^-$ forms relatively stable mixed ligand complexes with the "soft" halide ions (i. e. $K_{Tl(edta)Br} = [Tl(edta)Br^{2-}] / [Tledta^-]\,[Br^-] = 10^{3.5}$),[102] while similar mixed ligand complexes could not be detected for the $[Tl(dota)]^-$ - Br^- system even using a large excess of halide over

$[Tl(dota)]^-$ ($c_{Tl(dota)}$ = 5 mM, I = 1 M $NaClO_4$, pH ~ 3, c_{Br}= 0- 154 mM). Only the signal of $[Tl(dota)]^-$ at a constant shift (δ = 2218 ppm) was observed, while neither signals due to any mixed ligand complex, nor the signal of $[TlBr_4]^-$ at 1310 ppm that would indicate complex dissociation could be detected.[103]

The formation of a mixed $[Tl(dota)(CN)]^{2-}$ complex could be however detected using ^{205}Tl-NMR experiments on the $[Tl(dota)]^-$ - CN^- system at high pH (9–10). Addition of CN^- to a solution of $[Tl(dota)]^-$ resulted in the emergence of a new signal at δ = 2463 ppm ($w_{1/2}$ ~ 2500 Hz) whose chemical shift was almost identical to that of the $[Tl(edta)(CN)]^{2-}$ complex (δ = 2460 ppm).[27] The intensity ratio of the signals assigned to $[Tl(dota)]^-$ and $[Tl(dota)(CN)]^{2-}$ allowed us to estimate a stability constant of ~10 for the mixed ligand complex. However, in order to get a more reliable equilibrium constant, pH-dependent ^{205}Tl-NMR spectra were recorded. The pH- dependence of the intensity ratio of the two signals indicated that the formation of the mixed ligand complex was depressed by the protonation of cyanide to form HCN (Figure **4.1.2.**2). The following simultaneous equilibria were considered:

$$[Tl(dota)]^- + CN^- \rightleftharpoons [Tl(dota)(CN)]^{2-} \qquad (\mathbf{4.1.2.}3)$$

$$K_{mix} = [Tl(dota)CN^{2-}] / [CN^-][Tl(dota)^-] \qquad (\mathbf{4.1.2.}4)$$

$$H^+ + CN^- \rightleftharpoons HCN \qquad (\mathbf{4.1.2.}5)$$

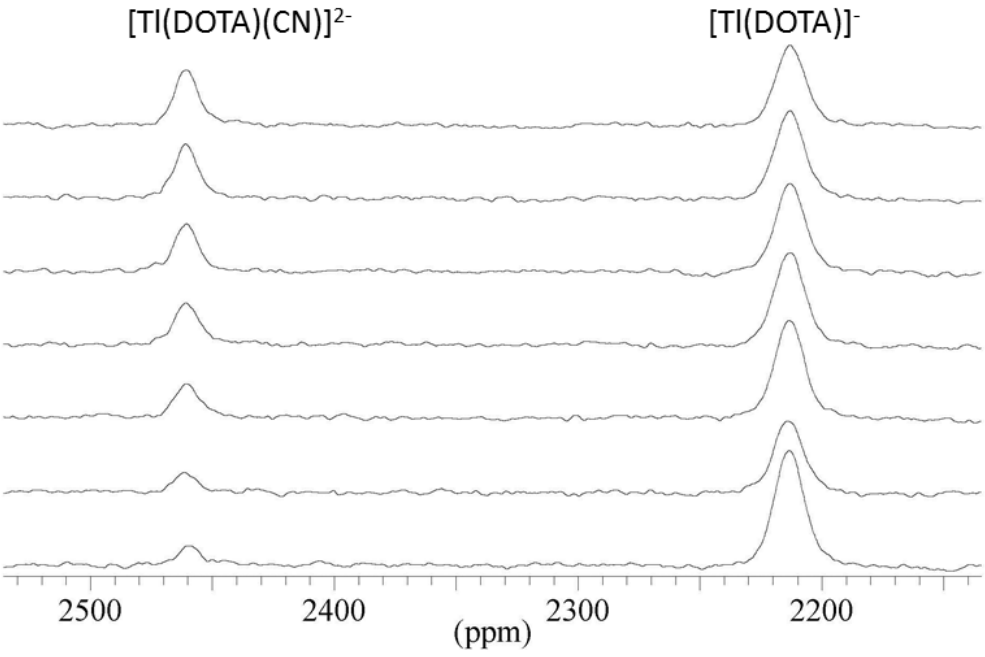

Figure 4.1.2.2 207.1 MHz ^{205}Tl-NMR spectra of samples with $c_{Tl(dota)}$ = 25 mM, c_{CN^-} = 100 mM at different pH values (from top to bottom): 10,62; 10.09; 9.76; 9.58; 9.40; 9.21 and 9.00

Using the mass balance equations for the components of the equilibrium system and $K_{HCN} = 10^{9.09}$ (I = 1 M)[104] we obtained K_{mix} = 6.0 $\pm$ 0.8, a value that is eight orders of magnitude lower than that of [Tl(edta)(CN)$^{2-}$] ($K_{mix} = 10^{8.7}$). This difference is in line with a very tight wrapping of Tl^{3+} by the dota^{4-} ligand. It is worth mentioning that our attempts to measure the ^{205}Tl-^{13}C coupling constant (expected to be similarly large as the $^{1}J_{205Tl\text{-}13C}$ = 10.5 kHz for [Tl(edta)(CN)]$^{2-}$)[24], by ^{205}Tl-NMR using ^{13}C-enriched NaCN failed which is likely related to the

fast cyanide exchange at high pH values required for the formation of the mixed ligand complex.

4.1.3. Studies on the stability and kinetic inertness of $[Tl(dota)]^-$ by UV-vis Spectroscopy

The stability constant of $[Tl(edta)]^-$ has been determined by a competition method using large excess of both halide ligands and H^+.[105] In case of $[Tl(dota)]^-$ an even greater stability is expected furthermore the macrocyclic complex forms very slowly in acidic solutions, which prevents the use of direct potentiometry for stability constant determination. Instead, we have used a competition method in which both a halide, namely the bromide, and H^+ compete for Tl^{3+} and $dota^{4-}$, respectively, according to the following equilibrium characterized by the equilibrium constant, K_{comp}:

$$(n\text{-}1)H^+ + [HTl(dota)] + 4\ Br^- \rightleftharpoons TlBr_4^- + H_ndota^{(4-n)-} \quad (\mathbf{4.1.3.}1)$$

$$K_{comp} = [TlBr_4^-][H_ndota^{(4-n)-}]/[HTl(dota)][H^+]^{n-1}[Br^-]^4 \quad (\mathbf{4.1.3.}2)$$

Tl^{3+} behaves as a "*soft*" acid according to the classification of Pearson, as the stability of halide complexes increases from the light halide ions to the heavy ones. Therefore, iodide would be the strongest competing agent for Tl^{3+}.

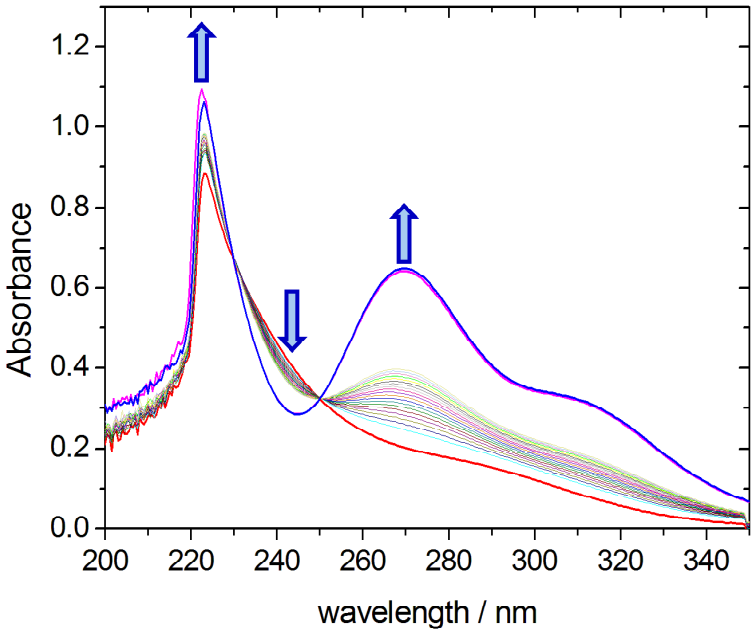

Figure 4.1.3.1 Time dependence of UV-spectra attributed to the ligand-exchange reaction between [HTl(dota)] and Br^- in 1M $HClO_4$: [HTl(dota)] (red, recorded at t_0) is slowly converted to $[Tl(Br)_4^-]$ (blue, recorded at 450 hours; the absorbance value and the shape of the spectrum are in accordance with separate measurements of $[TlBr_4]^-$). Intermediate spectra were recorded at 1 hour intervals for 19 hours. Conversion is ~99% at 240 h (magenta).

However one has to consider redox reactions, i.e. Tl^{3+} can oxidize iodide to iodine while Tl^+ is formed (TlI_4^- is the only TlI_n^{+3-n} species detected in solution at high I^-/ Tl^{3+} ratios).[3] Preliminary experiments have confirmed the immediate formation of iodine, and therefore we have selected Br^- for the competition reactions.

Knowing the kinetic inertness of [M(dota)] complexes, suitable thermodynamic data can only be extracted from properly equilibrated competition systems. Thus, batch samples containing 0.5 mM $Tl(dota)^-$, 0.5 M NaBr were prepared, varying the concentration of the acid in the range of 0.1, 0.3, 0.5, 0.8 and 1M of $HClO_4$ and keeping the total perchlorate concentration constant (at 1M with $(Na^+ + H^+)ClO_4^-$). The dissociation of the complex, i.e. the formation of $[TlBr_4]^-$ was followed over time recording spectra in the 200-350 nm range until the expected equilibration of the system (Figure **4.1.3.**1).

The spectra shown in Figure **4.1.3.**1 clearly show isosbestic point(s), which is in agreement with the presence of two species ([HTl(dota)] and $[Tl(Br)_4^-]$) in equilibrium with measurable absorbance during the 240 hours experimental time in the system, in accordance with the equation **4.1.3.**1. However, the reaction is substantially slower in the less acidic samples, where the isosbestic points were not observed. This indicates that some kind of parallel side reaction is occurring under these conditions. This may be a slow redox reaction involving bromide ions and the Tl^{3+} ion in an out-of-cage intermediate in which the metal ion is coordinated only by carboxylate groups (as in the formation/dissociation intermediate observed for other dota complexes). We invested a high amount of time and energy trying to avoid this complication (exclusion of air from samples with argon, increasing temperature to shorten the equilibration time by conventional means and by using a microwave reactor) without any success in measuring the equilibrium constant defined by equation **4.1.3.**2.

Finally we decided to only use spectra recorded at low conversion to evaluate the kinetics of our Tl-macrocyclic complex by means of the

initial rate method. Assuming that $[Tl(dota)]^-$ dissociates similarly to $[Gd(dota)]^-$,[73c] the following equations may be used to evaluate the kinetic data:

$$-d[Tl(dota)]_t/dt = k_{obs}[HTl(dota)]_t \qquad (\mathbf{4.1.3.}3)$$

$$k_{obs} = k_0 + k_1[H^+] + k_2[H^+]^2 \qquad (\mathbf{4.1.3.}4)$$

where k_{obs} is the observed pseudo first-order reaction rate constant, k_0 is the rate constant of spontaneous (or water assisted) dissociation of the monoprotonated complex, k_1 and k_2 are the constants of proton-assisted dissociation. The experimental results are shown on Figure **4.1.3.**2. Curve fitting gives $k_0 = 0$ (fixed to 0 as the fitting of the dissociation kinetic data in a trial returned a small negative value with large error), $k_1 = (9\pm7)\times10^{-7}$ $s^{-1}M^{-1}$ and $k_2 = (5\pm0.8)\times10^{-6}$ $s^{-1}M^{-2}$ values. The data shows quadratic dependence of k_{obs} on acidity with no detectable spontaneous dissociation, which is not surprising because spontaneous dissociation of the monoprotonated complex is expected to occur slower by several orders of magnitude, than the acid-catalyzed dissociation (which is the dominant reaction pathway in the acid concentration range applied in the current study). The k_1 value also has a large uncertainty, and may be a calculation artifact caused by the limited number of data points and their inaccuracy in the lower c_{H+} range related to the above-mentioned side reactions during the very slow competition reaction. This kind of rate law is in accordance with the related literature of dota-complexes, i.e. the dissociation is a dominantly proton-assisted process. (We have found some minor spectral changes that might be related to some interaction

between [HTl(dota)] and the Br^- ion, but we could not quantitatively measure this probably small contribution to the dissociation kinetics).

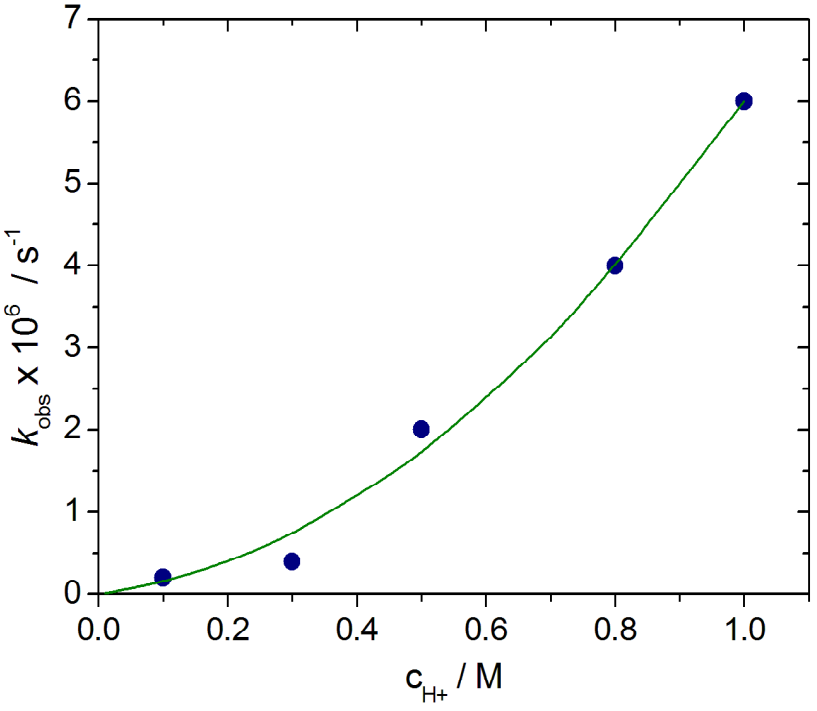

Figure 4.1.3.2 Plot of k_{obs} vs. acid concentration in Tl(III) - $dota^{4-}$ - H^+ - Br^- system

Using the $k_{obs} = k_1[H^+] + k_2[H^+]^2$ rate law one can calculate the half life of the complex at different pH values. Half-life of $[Tl(dota)]^-$ is 32 h in 1 M $HClO_4$ and approximated to $5 \cdot 10^9$ h at pH = 7.4. The latter value indicates that the dissociation of $[Tl(dota)]^-$ at physiological pH is negligible. To our surprise however, the $[^{201}Tl(dota)]^-$ complex was found recently to decompose in vivo.[104] Our data suggests that this phenomenon is more likely to be caused by the bioreduction of Tl(III) in the samples

rather than the dissociation of the $[Tl(dota)]^-$ complex. Tl^+ (showing similarity to K^+ both in size and complexation properties) likely forms a weak and labile complex with DOTA, making the dissociation of the reduced radioisotope from the complex easy.

4.1.4. Additional solution structure data obtained by ^1H and ^{13}C-NMR spectroscopy

The ^1H-NMR spectrum of $[Tl(dota)]^-$ presents six broad signals at room temperature: one doublet can be assigned to the protons of the acetate methylene groups and two doublets to those of the ring ($^3J_{^1H\text{-}^{205}Tl}$ scalar coupling splits these signals into doublets). The broadness of these signals is related to exchange processes occurring in solution. Based on the composition of the complex and that of the solution, the exchange is attributed to the intramolecular rearrangement of the complex. At higher temperatures the signals sharpen and their structure becomes visible as a consequence of the acceleration of the exchange processes. This is also supported by ^{13}C-NMR spectra, which at high temperatures show two signals in the aliphatic region: a singlet assignable to the acetate methylene carbons and a ^{205}Tl coupled doublet of the ring carbons (Figure **4.1.4.**1). The carbon nuclei of the methylene groups of the pendant arms do not show ^{205}Tl–coupling. This is likely caused by the combined effect of a two-bond coupling (through the nitrogen) and a three-bond coupling (through the carboxylate oxygen). These couplings may possess differing signs that presumably cancel out.

The ^1H- and ^{13}C-NMR spectra recorded at low temperature (272 K) are relatively well resolved, and could be fully assigned with the aid of

the homonuclear ^{1}H-^{1}H COSY and heteronuclear ^{1}H-^{13}C HSQC spectra (Figure **4.1.4.**2, see Chart **4.1.4**.1 for labeling). At this temperature the ring carbon doublet splits into two, indicating the presence of two different chemical environments for the carbon nuclei of the macrocyclic moiety.

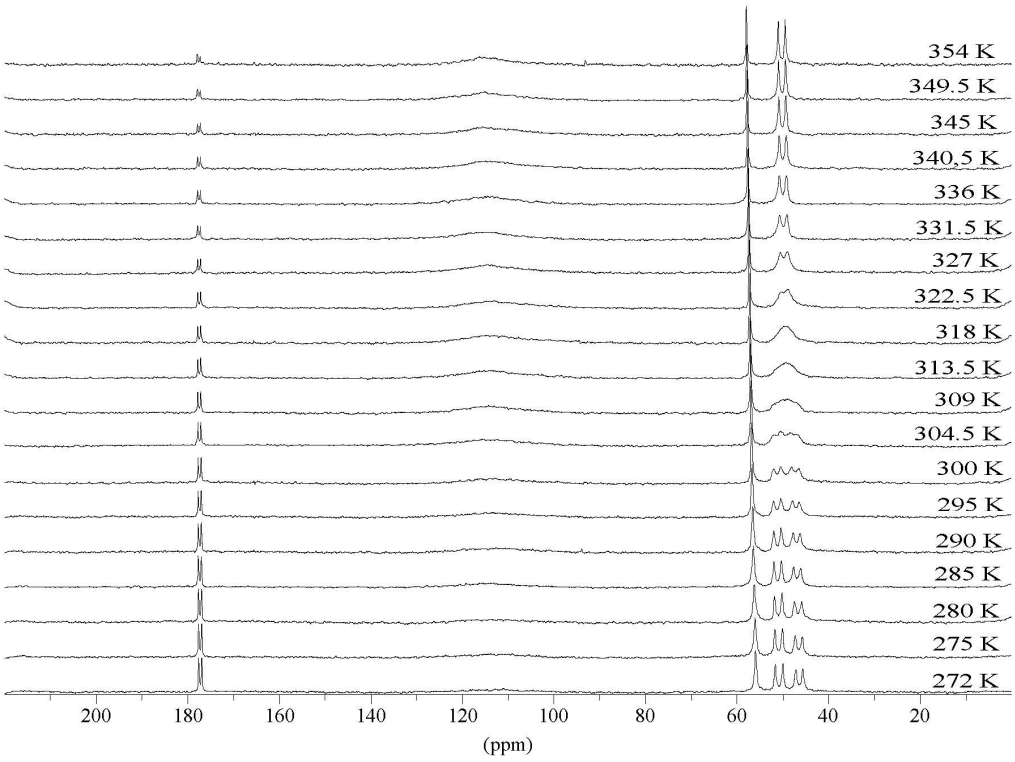

Figure 4.1.4.1 100 MHz ^{13}C-NMR spectra of a 0.1 M Na[Tl(dota)] solution in D_2O recorded at different temperatures in D_2O (pH = 4)

The spectrum shows four signals: the ^{205}Tl-coupled doublet ($^{2}J_{^{205}Tl-^{13}C}$ = 64 Hz) of the carboxylate (-C=O) groups at δ=179.7 ppm (C1), a singlet due to the -CH_2- groups of the acetate pendant arms at 58.8 ppm (C2), and two ^{205}Tl-coupled doublets of the non-equivalent carbon

atoms of the macrocycle ring centered at δ=49.2 ($^2J_{^{205}Tl-^{13}C}$ = 156 Hz) and 53.6 ($^2J_{^{205}Tl-^{13}C}$ = 161 Hz) ppm. This pattern points to a C_4 symmetry of the $[Tl(dota)]^-$ complex at low temperatures, while the spectra at temperatures higher than

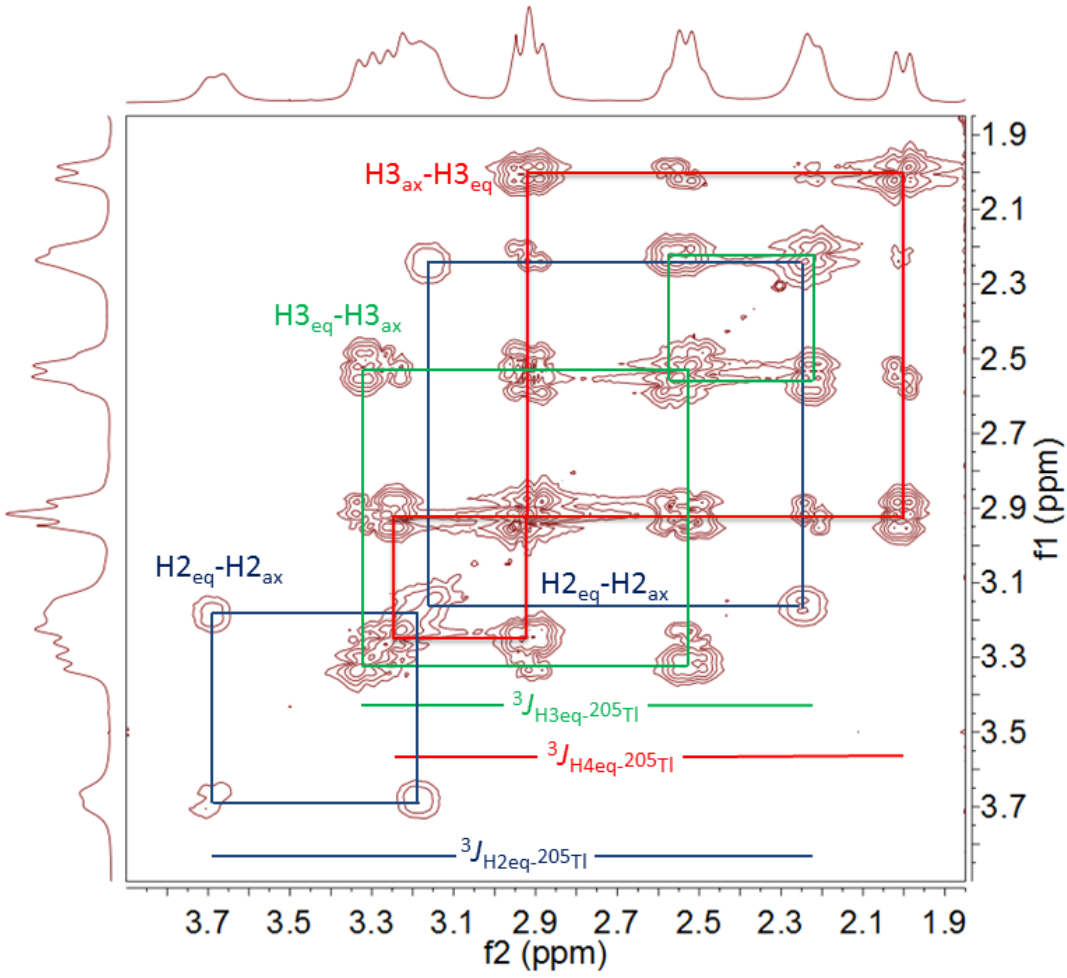

Figure 4.1.4.2 400 MHz ^1H-^1H COSY spectrum of 0.1 M $[Tl(dota)]^-$ recorded in D_2O solution ($pD_{reading}$ = 4) at 272.5 K (see Chart **4.1.4.1** for labelling)

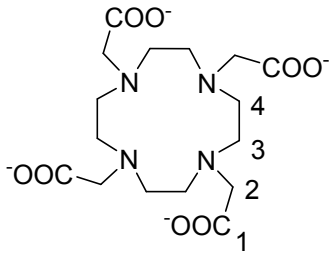

Chart 4.1.4.1 Ligand H_4dota and the numbering scheme used for NMR spectral assignment

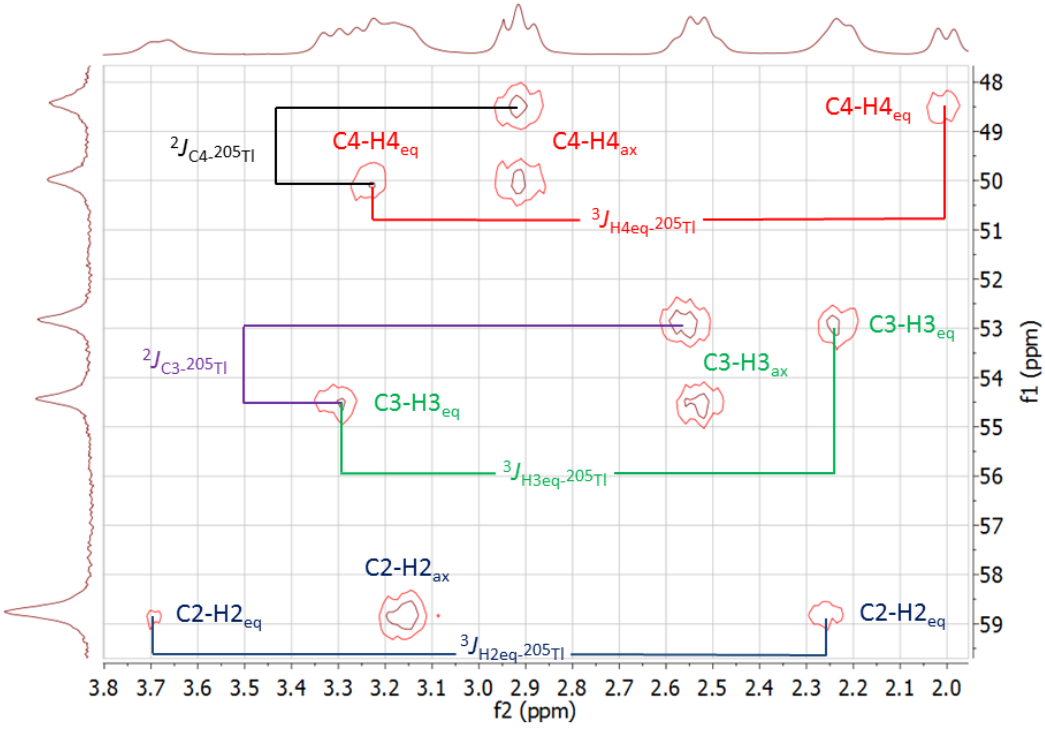

Figure 4.1.4.3 400 MHz ^{1}H-^{13}C HSQC spectrum of 0.1 M $[Tl(dota)]^-$ at 272.5 K

320 K can be interpreted as an effective C_{4v} symmetry. The ^{1}H-^{13}C HSQC spectrum (Figure **4.1.4.**1) shows that each of the 3 carbon nuclei in the aliphatic region is coupled with 4 proton signals, two of them showing very small chemical shift differences.

This is clearly observed for the proton nuclei of the $–CH_2–$ groups of the acetate arms (H2). For these protons one expects an AB spin system with a $^{2}J_{ax\text{-}eq}$ of ~16 Hz. However, the coordination of the ligand to the Tl^{3+} ion creates an AB-X system, which splits each of the components of the AB spin systems into doublets due to the $^{3}J_{^{1}H\text{-}^{205}Tl}$ coupling.

The ^{1}H–^{1}H COSY spectrum relates the signals at 3.19 ppm and 3.68, and those at 3.16 and 2.24 ppm, while no cross-peak is observed relating the signals at 3.68 and 2.24 ppm. All these four signals are however correlated to the carbon atom of the acetate arms in the HSQC spectrum. Thus, the signals at 3.68 and 2.24 ppm are attributed to a single proton nucleus whose resonance is split by the coupling to ^{205}Tl. An analogous reasoning allowed us to assign the proton signals of the macrocyclic fragment (Table **4.1.4.**1). Furthermore, the spin pattern of the signals allowed us to discriminate between axial (ax) and equatorial (eq) proton nuclei. Indeed, the different H-C-C-H dihedral angles relating axial and equatorial protons with the protons at a three bond distance result in different coupling patterns, as expected by the Karplus relationship.[106,107] As a result, the equatorial protons provide small ^{3}J coupling constants, so that their coupling patterns are dominated by the strong $^{2}J_{eq\text{-}ax}$ coupling (~16 Hz). This is for instance the case of the signal at 2.00 ppm, which is observed as a pseudo-doublet. On the contrary, axial protons give two strong couplings ($^{2}J_{ax\text{-}eq}$ and $^{3}J_{ax\text{-}ax}$) and a weak one

($^3J_{ax\text{-}eq}$), and they are observed as pseudo-triplets (see for instance the signal at 2.91 ppm, Figure **4.1.4.**3).

Table 4.1.4.1 NMR spectral data of $[Tl(dota)]^-$

^1H	δ (ppm)	$^3J_{^1H\text{-}^{205}Tl}$ (Hz)	^{13}C	δ (ppm)	$^2J_{^{13}C\text{-}^{205}Tl}$ (Hz)	$\delta^{cald}{}_{TSAP}$ [b]	$\delta^{cald}{}_{SAP}$ [c]
$H2_{ax}$	3.19 / 3.16	11	C1	179.7	64	179.7	178.2
$H2_{eq}$	3.68[d] / 2.24	574	C2	58.8	[a]	59.2	66.7
$H3_{ax}$	2.55 / 2.52	12	C3	53.6	161	51.8	56.9
$H3_{eq}$	3.32 / 2.23	441	C4	49.2	156	48.4	55.2
$H4_{ax}$	2.91	< 5					
$H4_{eq}$	3.24 / 2.00[f]	499					

[a] Not observed. [b] Chemical shifts of the TSAP' isomer calculated at the B3LYP/CRENBL/6-311+G(d,p) level using the GIAO method. [c] Chemical shifts of the SAP' isomer calculated at the B3LYP/CRENBL/6-311+G(d,p) level using the GIAO method. [d] $^2J_{2eq\text{-}2ax}$ = 13.5 Hz. [e] $^2J_{3eq\text{-}3ax}$ = 14.5 Hz [f] $^2J_{4eq\text{-}4ax}$ = 14.0 Hz.

The $^3J_{^1H\text{-}^{205}Tl}$ coupling constants obtained from the analysis of the NMR spectra (Table **4.1.4.**1) indicate that the equatorial protons provide coupling constants of ca. 440-575 Hz, while the coupling constants involving axial protons are rather small (< 15 Hz). These coupling constants are very similar to the average coupling constant estimated from the splitting of the ^{205}Tl NMR spectrum recorded at low temperature

(~500 Hz, see above), which confirms the assignments given in Table **4.1.4.**1. An inspection of the X-ray structure of $[Tl(dota)]^-$ shows that the equatorial protons provide average Tl-N-C-H_{eq} dihedral angles of 160.4-162.9º, while the corresponding values for axial protons Tl-N-C-H_{ax} take values of ca. 80-82º. These results indicate that the $^3J_{^1H-^{205}Tl}$ coupling constants follow the empirical relationship of Karplus ($^3J = A\text{-}B\cos\phi + C\cos 2\phi$, where ϕ is the dihedral angle and A, B and C are empirical constants). A similar Karplus-like dependence was also observed for the spin density distributions in the paramagnetic $[Gd(dota)(H_2O)]^-$ complex and related systems.[108]

4.1.5. Solution dynamics study with ^{13}C-NMR

The multinuclear NMR study described in the previous sections indicate an octadentate binding of the ligand to the Tl^{3+} ion in $[Tl(dota)]^-$. Furthermore, the X-ray structure suggests that this complex might adopt a TSAP' structure in solution. In order to confirm this hypothesis we performed theoretical calculations in aqueous solution at the B3LYP/CRENBL/6-311+G(d,p) level. Our calculations provide two energy minima that correspond to the expected SAP' and TSAP' isomers of the complex (Figure **4.1.5.**1). A comparison of the experimental (X-ray) and calculated structure of the TSAP' isomer indicates that our calculations provide molecular geometries in good agreement with the reference crystallographic data (Table **4.1.1.**1). The main discrepancy between the experimental and calculated structures is the overestimation of the Tl-N distance by ca. 0.08 Å in the latter.

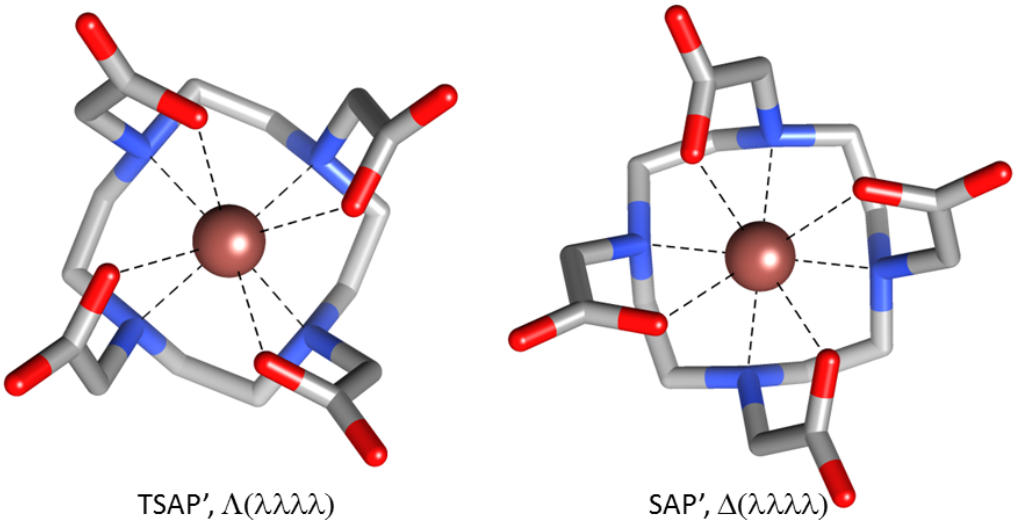

Figure 4.1.5.1 Geometries of the SAP' and TSAP' isomers of $[Tl(dota)]^-$ obtained from geometry optimizations in aqueous solution at the B3LYP/CRENBL/6-311+G(d,p) level. Hydrogen atoms are omitted for simplicity. Bond distances: Tl-N = 2.537 (TSAP') and 2.528 Å (SAP'); Tl-O: 2.354 (TSAP') and 2.341 Å (SAP')

According to our calculations the TSAP' isomer is more stable than the SAP' one by 15.2 kJ mol^{-1}, which is in line with the structure observed in the solid state. In order to confirm that $[Tl(dota)]^-$ adopts a TSAP' structure in solution we calculated the ^{13}C-NMR chemical shifts of the SAP' and TSAP' isomers at the B3LYP/CRENBL/6-311+G(d,p) level. It has been shown that the magnetic shieldings calculated with the use of ECPs are not gauge invariant, which means that magnetic shieldings calculated with different origins are different. However, the errors introduced by this violation of the gauge invariance have been shown to amount to few ppm, and therefore ^{13}C-NMR shifts can be

calculated by this method with reasonably good accuracy.[109,110] The ^{13}C-NMR shifts calculated for the TSAP' isomer are in very good agreement with the experimental data, with absolute deviations < 1.8 ppm, while much larger deviations between the experimental and calculated data are obtained for the SAP' isomer (up to 6.8 ppm, see Table **4.1.4.**1). Thus, our calculations confirm that the $[Tl(dota)]^-$ presents a TSAP' structure in aqueous solution.

The increase of the symmetry observed in the ^{13}C-NMR spectra upon increasing the temperature can be explained by the higher rate of the chemical exchange between the two different chemical environments of the ring carbon atoms. Indeed, the doublet signals due to the carbon nuclei of the macrocyclic fragment are clearly separated at 272 K indicating a "slow exchange regime" (Figure **4.1.4.**1). The signals gradually broaden as the temperature increases, and they are hardly visible in the spectra recorded in the temperature range 300-320 K. The temperature of coalescence is ca. 315 K. The time averaged signal (a Tl-coupled doublet) sharpens above 325 K as expected for a two site exchange system being in "fast exchange regime". It is worth noting however that the other two signals, i.e. the signals of the acetate arms, behave differently from the ring carbon signals. The half-widths for both signals are changing with temperature. However, the signal of aliphatic carbon atoms of the acetate arms becomes sharper with increasing temperature, which is typical of systems in "fast exchange" at the actual NMR time scale. One would expect splitting of the acetate peak into two signals below 272 K, due to a slow isomerisation process between two species with lower symmetry, as observed earlier for LnDOTA-like complexes. However, we could not cool down the sample without

freezing in order to find experimental evidence for the hypothesis. Thus, we could not measure the chemical shift difference for the two sites, and the actual NMR time scale for those nuclei is not known. The doublet signal of the carbonyl-carbon atoms changes similarly to the signal of the aliphatic carbon atoms at low temperatures (i.e. sharpening in the range of 272-300 K), but above 300 K substantial broadening can be observed. The actual NMR time scales of the signals due to the pendant arms are likely defined by the spin-spin coupling constants $^{3}J(^{13}C\text{-}^{205}Tl)$. The signal due to the carbonyl groups is in the slow exchange regime at low temperatures, and thus they broaden as the temperature increases. The signal due to the $-CH_2-$ carbon nuclei of the pendant arms is however in the fast exchange regime at low temperatures, presumably due to a smaller $^{3}J(^{13}C\text{-}^{205}Tl)$ coupling.

The $[Tl(dota)]^-$ complex exists in solution as a racemic mixture of the TSAP' $\Lambda(\lambda\lambda\lambda\lambda)/\Delta(\delta\delta\delta\delta)$ enantiomeric pair, while no significant populations of the SAP' isomers could be detected by NMR spectroscopy. Thus, the exchange process revealed by the ^{13}C-NMR data can be attributed to a $\Lambda(\lambda\lambda\lambda\lambda) \leftrightarrow \Delta(\delta\delta\delta\delta)$ interconversion, which represents a simple case of a two-site exchange between equally populated sites. This process involves both the inversion of the macrocyclic unit $[(\lambda\lambda\lambda\lambda) \leftrightarrow (\delta\delta\delta\delta)]$ and the rotation of the four acetate pendant arms $[\Lambda \leftrightarrow \Delta]$, as described previously in detail for Ln^{3+} dota-like complexes.[111]

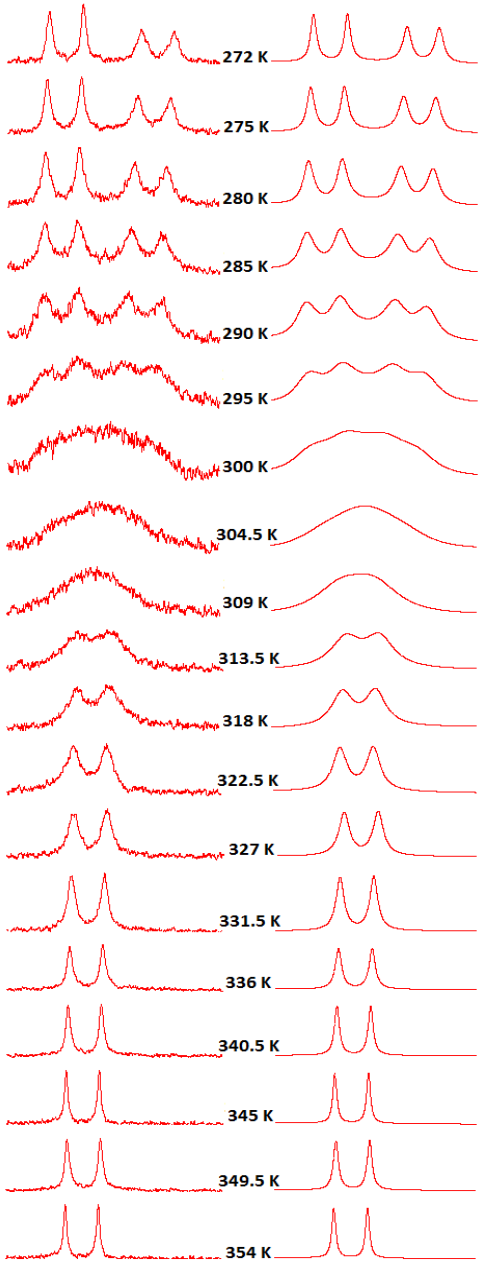

Figure 4.1.5.2 Experimental (left) and simulated (right) ^{13}C-NMR spectra of [Tl(dota)]$^{-}$ at varying temperatures

Since the temperature dependence of the signals at 53.6 and 49.2 ppm covers both the fast exchange and the slow exchange regimes, we used these resonances to perform a quantitative band-shape analysis of the exchange process, which provides the exchange rates k_{exch} at every temperature. The agreement between the experimental and simulated spectra is excellent (Figure **4.1.5.**2).

The temperature dependence of the evaluated time constants was subsequently used to obtain the activation parameters for the exchange process using the Eyring-Polányi equation. The results are compared to those obtained for related dota^{4-} complexes in Table **4.1.5.**1.

Table 4.1.5.1 Activation parameters obtained for the Λ(λλλλ) ↔ Δ(δδδδ) interconversion in [Tl(dota)]$^-$ and related systems

		$\Delta H^{\neq}$ (kJ mol^{-1})	$\Delta S^{\neq}$ (J K^{-1} mol^{-1})	$\Delta G^{\neq}_{298}$ (kJ mol^{-1})
[Tl(dota)]$^-$	Exp.	66 ± 2	+23 ± 6	59 ± 2
	Calcd.	73.2	+19.2	67.5
[Bi(dota)]$^-$	Exp.	40	-76 ± 15	63
[Lu(dota)]$^-$	Exp.	101	+116	66

[a] Values obtained for the arm-rotation process with DFT calculations in aqueous solution at the B3LYP/CRENBL/6-31+G(d,p) level.

The activation enthalpy ($\Delta H^{\neq}$) determined for [Tl(dota)]$^-$ falls between the values reported for [Bi(dota)]$^-$ and [Lu(dota)]$^-$. However, the different signals of the activation entropy obtained for the latter two complexes and the small positive $\Delta S^{\neq}$ value determined for [Tl(dota)]$^-$ result in relatively similar activation free energies at 298 K ($\Delta G^{\neq}_{298}$). The

[Lu(dota)]$^-$ complex exists in solution as a mixture of the eight-coordinate TSAP' isomer and the nine-coordinate SAP form, and activation parameters for both the ring-inversion and arm-rotation processes could be obtained.[59b] Thus, the large positive activation energy obtained for this complex might be related to the expulsion of the coordinated water molecule in the transition state responsible for the $\Lambda(\lambda\lambda\lambda\lambda) \leftrightarrow \Delta(\delta\delta\delta\delta)$ interconversion. For [Tl(dota)]$^-$ $\Delta S^{\neq}$ takes a relatively small positive value, which is likely related to the rearrangement of the hydration shell during the interconversion process.

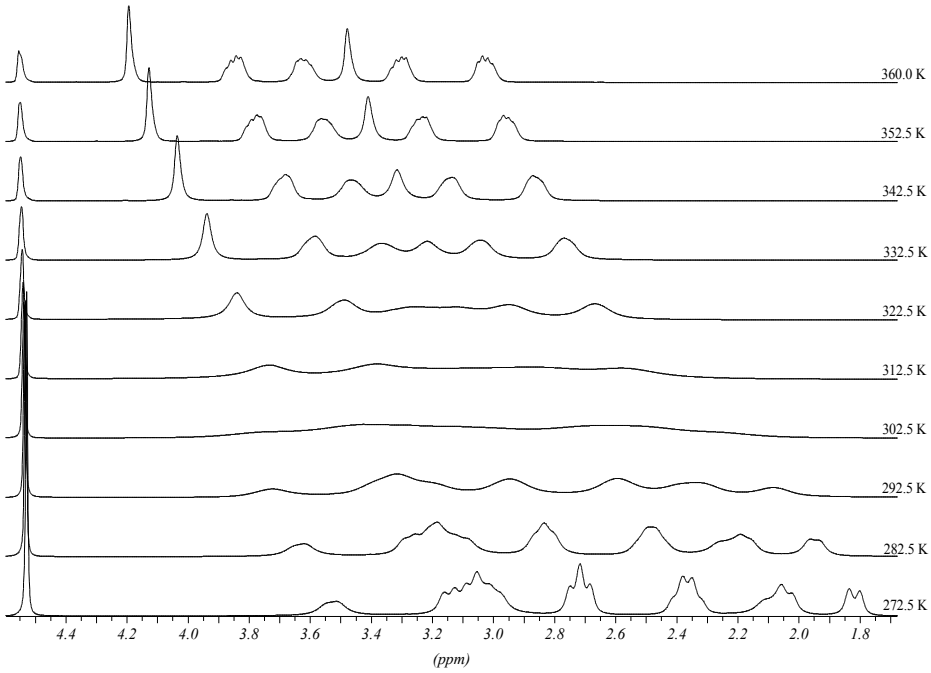

Figure 4.1.5.3 ^{1}H-NMR spectra of 0.1 M [Tl(dota)]$^-$ at varying temperatures

To obtain a more detailed information of the mechanism responsible for the enantiomerization process in $[Tl(dota)]^-$, we performed a computational investigation of the ring inversion and arm rotation processes.

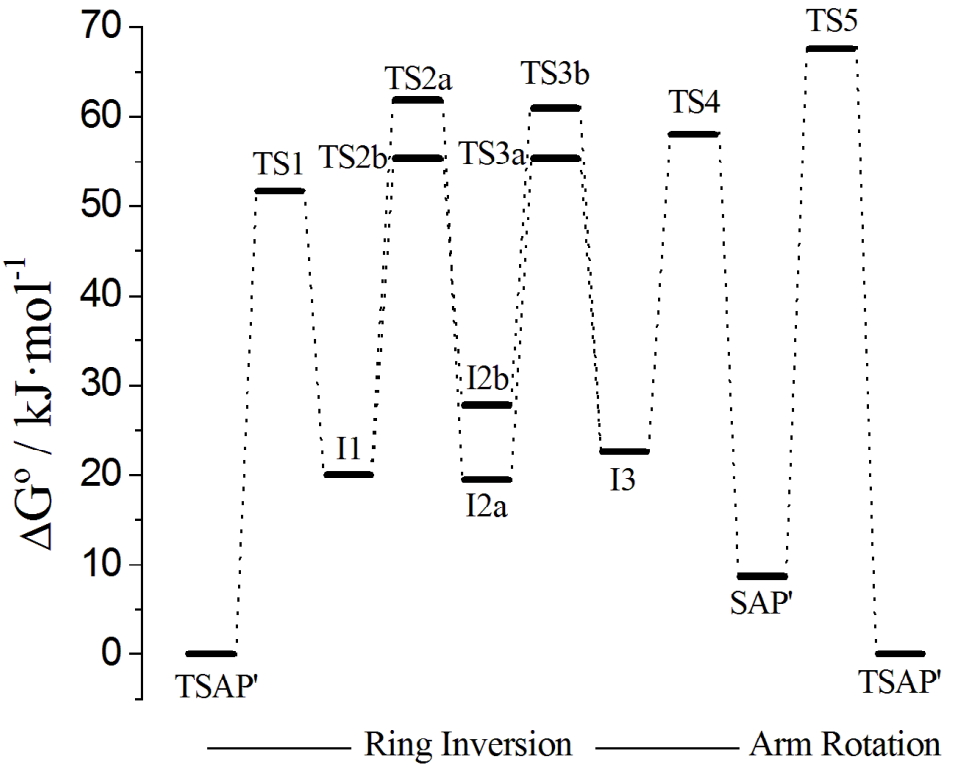

Figure 4.1.5.4 Relative free energies of minima, intermediates (labeled as "I") and transition states (labeled as "TS") involved in the Λ(λλλλ) ↔ Δ(δδδδ) interconversion process of $[Tl(dota)]^-$ calculated in aqueous solution at the B3LYP/CRENBL/6-31+G(d,p) level

According to our calculations performed in aqueous solution at the B3LYP/CRENBL/6-31+G(d,p) level the inversion of the macrocyclic ring is a four-step process involving the stepwise inversion each of the

four five-membered chelate rings formed by the coordination of the macrocyclic moiety. In each of these steps one of the chelate rings changes its configuration from δ to λ (or vice versa) through a transition state in which the H-C-C-H units adopt a nearly eclipsed conformation. Similar four-step processes have been obtained previously using HF and DFT calculations for different Ln^{3+} complexes with cyclen-based ligands.[112] Due to the symmetry properties of the $[Tl(dota)]^-$ complex (C_4 point group), two different routes are possible for the inversion of the second and third chelate rings (Figure **4.1.5.**4). As once the first chelate is inverted, the second step may proceed via inversion of a chelate ring either in opposite (TS2a & TS3a) or adjacent (TS2b & TS3b) position at the macrocyclic ring with respect to the former. According to our calculations the lowest-energy pathway corresponds to that proceeding through TS3b, which provides an activation Gibbs free energy for the ring-inversion process of $\Delta G^{\neq} = 60.8$ kJ mol^{-1} at 298 K.

Contrary to the ring-inversion process, the arm rotation pathway is a single-step process involving the simultaneous rotation of the four pendant arms of the ligand. The structure of the TS (TS5, Figure **4.1.5.**4) is quite distorted, with four different Tl-N distances in the range 2.50-2.75 Å and four Tl-O distances ranging between 2.30 and 2.37 Å. The activation free energy for the arm rotation process amounts to $\Delta G^{\neq}_{298} =$ 67.5 kJ mol^{-1}, and thus the arm-rotation process likely represents the rate determining step for the Λ(λλλλ) ↔ Δ(δδδδ) interconversion in $[Tl(dota)]^-$. The $\Delta H^{\neq}$ and $\Delta S^{\neq}$ values calculated for the arm rotation pathway (Table **4.1.5.**1) show a very good agreement with the experimental values, which provides additional support for this

hypothesis. In contrast, the ring inversion path provides negligible activation entropy.

4.2. Characterization of [Tl(*c*do2a)]$^{+}$ and its iodido mixed-ligand complex

4.2.1. Background of ligand choice

Although [Tl(dota)]$^{-}$ has proven to be quite robust, it lacks the free metal coordination site needed for binding additional anions. Logic dictates and experience has shown that ligands with fewer pendant donor sites should leave the encapsulated metal more accessible to water molecule(s) or additional small anion(s). To this end, the iodide-binding ability of various Tl(III)-complexes was investigated by ^{205}Tl-NMR, using a number of macrocyclic (and one mesocyclic) ligands. The ligands investigated are, in descending order of the number of donor sites: do3a (1,4,7,10-tetraazacyclododecane-1,4,7-triacetic acid), pcta (3,6,9,15-tetraazabicyclo [9.3.1]pentadeca-1(15),11,13-triene-3,6,9-triacetic acid), aazta (2,2'-(1,4-bis(carboxymethyl)-6-methyl-1,4-diazepan-6-ylazanediyl)diacetic acid), *cys*- and *trans*-do2a (1,4,7,10-tetraazacyclododecane-1,4-diacetic acid and 1,4,7,10-tetraazacyclododecane-1,7-diacetic acid) and do1a (1,4,7,10-tetraazacyclododecane-1-acetic acid). To much of our surprise only one of the ligands, *c*do2a was found to bind iodide ions in its Tl(III)-complex. This fact is especially interesting when DFT calculations performed for both do2a isomers are taken into consideration: not only is [Tl(*t*do2a)]$^{+}$ expected to also form a ternary complex with iodide ions, it was also

found to be energetically more favourable than that of $[Tl(cdo2a)]^+$. The details on why this is not the case are still unknown at this time, we speculate that steric hindrance may be quite different in the two complexes.

4.2.2. Dissociation kinetics of $[Tl(cdo2a)]^+$

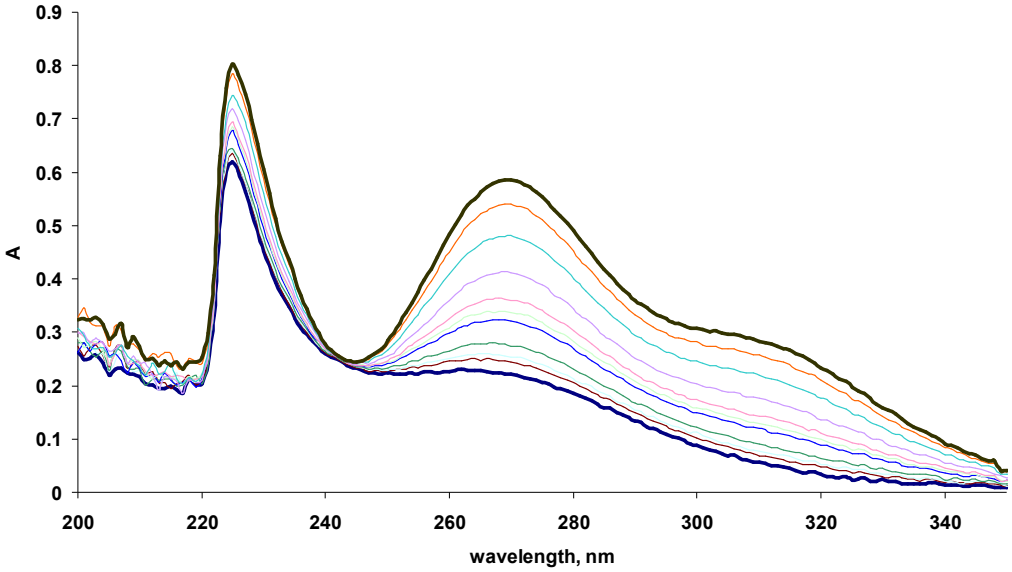

Figure 4.2.2.1 Time dependence of UV-spectra attributed to the ligand-exchange reaction between $[Tl(cdo2a)]^+$ and Br^- in 1M $HClO_4$: $[Tl(cdo2a)Br]$ (bottom black, recorded at t_0) is slowly converted to $[Tl(Br)_4^-]$ (top black, recorded at 15 hours; the absorbance value and the shape of the spectrum are in accordance with separate measurements of $[TlBr_4]^-$)

The double competition method described earlier in case of $[Tl(dota)]^-$ was used to also determine the dissociation properties of $[Tl(cdo2a)]^+$, with the latter showing some similarity to the former (see Figure **4.2.2.**1). The initial absorbance is greater, likely as a consequence of [Tl(*c*do2a)Br] forming. The largest difference is the increased dissociation rate (obtained in the same manner as for $[Tl(dota)]^-$), reaching total Tl(III)-displacement in 1M $HClO_4$ overnight, as less donor groups make the complex less compact and the metal center more accessible.

4.2.3. Acid-base properties of $[Tl(cdo2a)]^+$

The parent complex can form mixed hydroxo complexes according to the following equations:

$$[Tl(cdo2a)]^+ + H_2O \rightleftharpoons [Tl(cdo2a)OH] + H^+ \qquad (\mathbf{4.2.3.}1)$$

$$[Tl(cdo2a)OH] + H_2O \rightleftharpoons [Tl(cdo2a)(OH)_2]^- + H^+ \qquad (\mathbf{4.2.3.}2)$$

The stability constants of [Tl(*c*do2a)OH] and $[Tl(cdo2a)(OH)_2]^-$ were determined via pH- potentiometry and were found to be $lgK^{OH}_{[Tl(cdo2a)]} = -7.37(8)$ and $lgK^{OH}_{[Tl(cdo2a)OH]} = -11.10(9)$. With two less donor sites than in dota, this complex may possess up to two coordinated water molecules, however the significant difference between the two values indicates that the complex most likely has only one and the second coordinated OH^- most likely replaces a carboxylate moiety.

4.2.4. Investigation of the iodido-mixed ligand complex [Tl(*c*do2a)I]

Formation of the mixed iodido complex can be described by the next equilibrium:

$$[Tl(cdo2a)]^{+} + I^{-} \rightleftharpoons [Tl(cdo2a)I] \qquad (\mathbf{4.2.4.}1)$$

To determine the stability of the [Tl(*c*do2a)I] mixed-ligand complex, shown in eq. **4.2.4.**1, potentiometric and NMR titrations were carried out, shown in Figures **4.2.4.**1 and **4.2.4.**2. The effect of OH^{-}–competition was avoided by keeping the pH in a range of 3–4. Potentiometric titrations were performed on samples containing 1 mM $[Tl(cdo2a)]^{+}$ at pH = 4 in 1 M $NaClO_4$. ^{205}Tl-NMR of $[Tl(cdo2a)]^{+}$ shows a signal at δ = 2500 ppm, with a half-width of $w_{½}$ = 5500 Hz, similar in chemical shift, but rather broad compared to $[Tl(dota)]^{-}$ ($w_{½}$ = 2200 Hz). This may be attributed to lower overall rigidity and compactness. The signal of [Tl(*c*do2a)I] appears at δ = 1230 ppm (more than 1200 ppm downfield). Using the same principles and methods as for $[Tl(dota)]^{-}$ the formation constant of $lgK^{I}_{[Tl(cdo2a)]}$ = 4.1±0.1 was obtained, making this ternary complex somewhat less stable than $[Tl(edta)I]^{2-}$. This is to be expected of macrocyclic complexes, as the coordinated metal ion is much less accessible than with open-chain ligands. Even so, [Tl(*c*do2a)I] is relatively stable as mixed ligand complexes go.

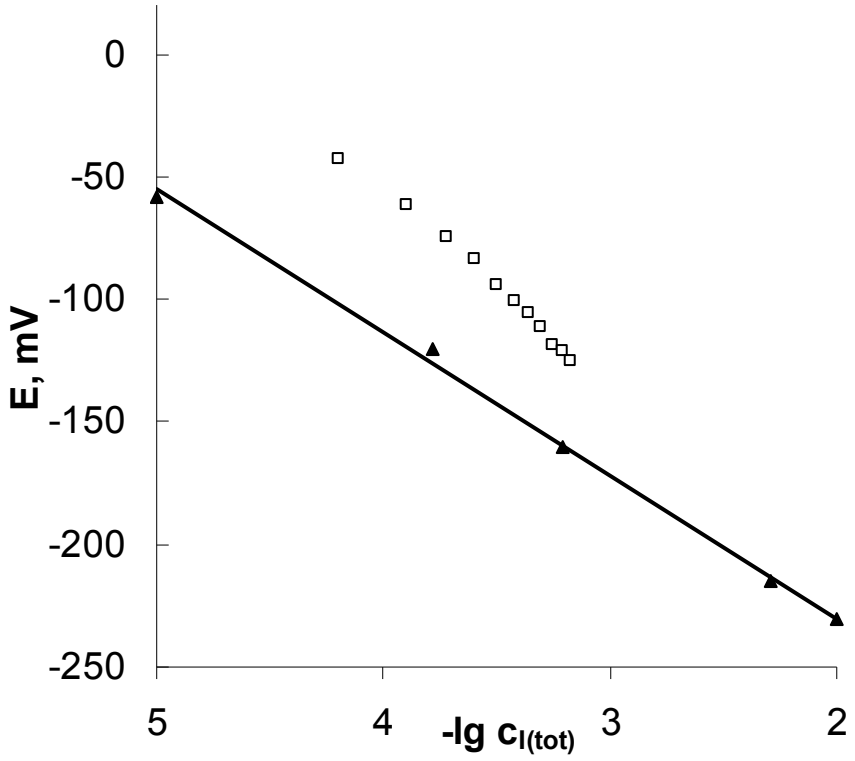

Figure 4.2.4.1 Potentiometric titration curve of $[Tl(cdo2a)]^+$ (hollow squares) and calibration points (black triangles) using iodide-selective electrode. 1 mM $[Tl(cdo2a)]^+$ at pH = 4 in 1 M $NaClO_4$

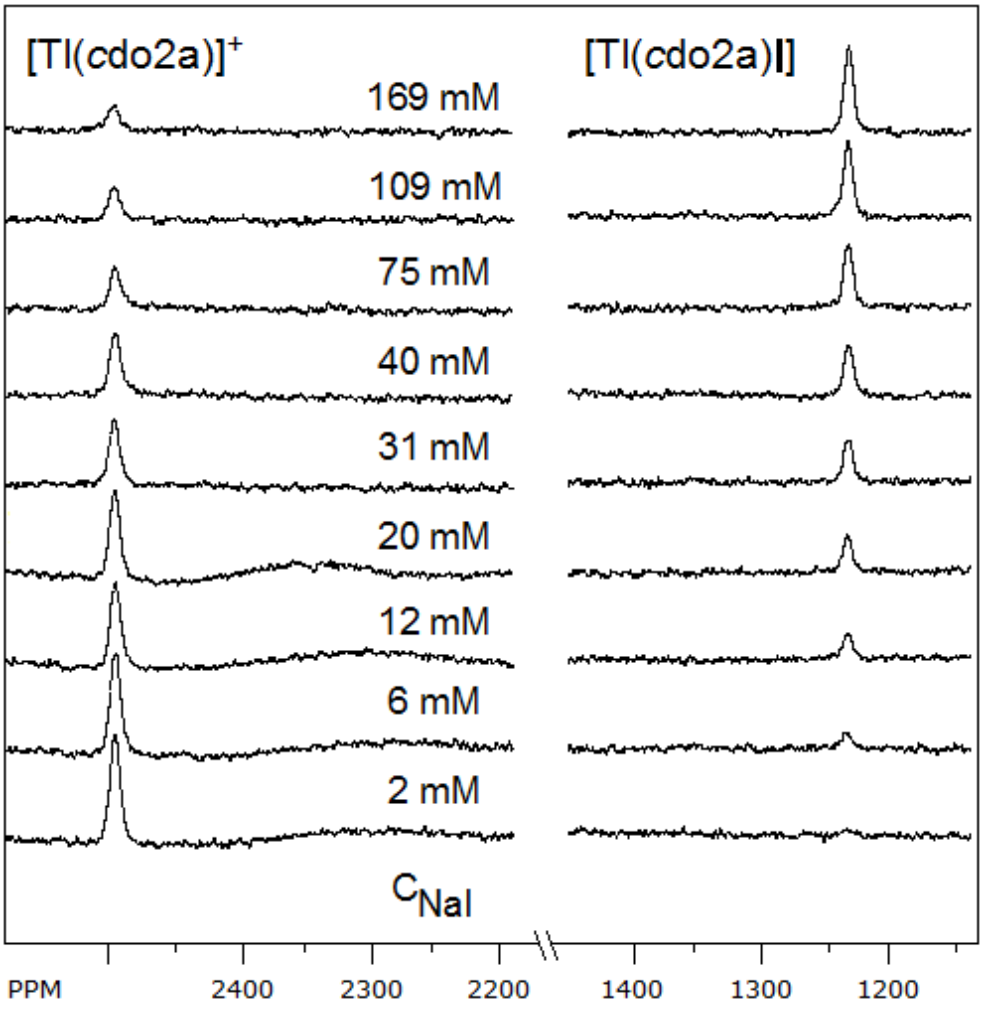

Figure 4.2.4.2 ^{205}Tl NMR titration of 9 mM [Tl(*c*do2a)]$^{+}$ with 1.107 M NaI at pH = 4. I = 1 M $NaClO_4$

4.2.5. Comparison with a rigidified open-chain complex [Tl(cdtabba)]$^{+}$

Although the investigation of Tl(III)-complexes of open-chain ligands was not the primary goal of this work, it is worth comparing

properties of $[Tl(cdo2a)]^+$ to one. The acid-base properties and stability constant of such a mixed-ligand complex with a bisamide cdta-derivative, cdtabba (2,2'-(cyclohexane-1,2-diylbis((2-(butylamino)-2-oxoethyl)azanediyl))-diacetic acid) were determined in the same fashion via potentiometry (see Fig. **4.2.5.**1).

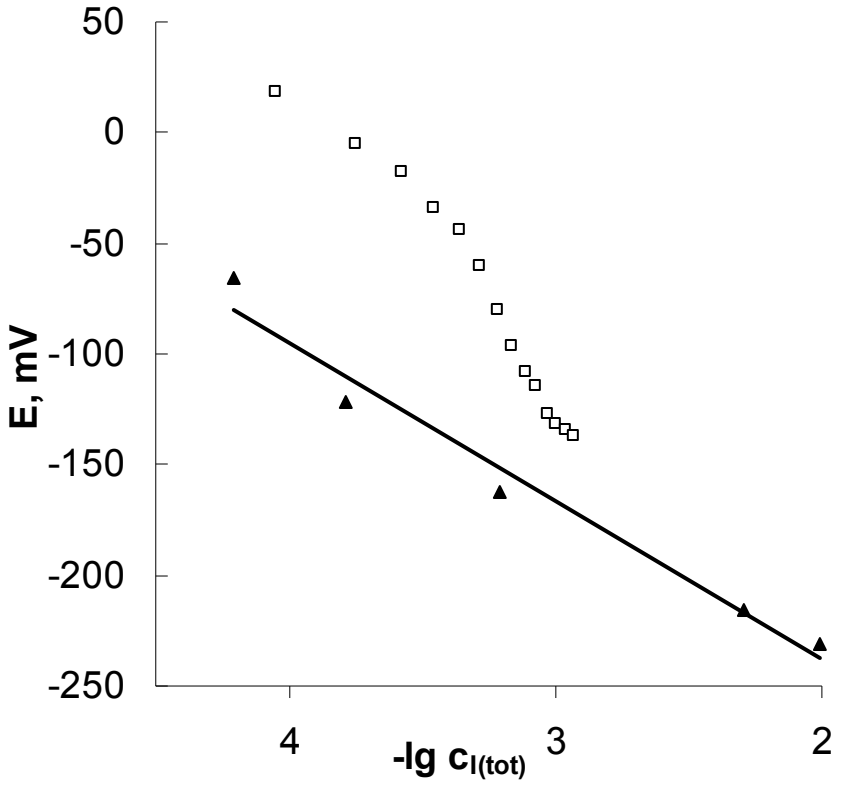

Figure 4.2.5.1 Potentiometric titration curve of $[Tl(cdtabba)]^+$ (hollow squares) and calibration points (black triangles) using iodide-selective electrode. 1 mM $[Tl(cdtabba)]^+$ at pH = 4 in 1 M $NaClO_4$

The complex itself is somewhat similar to $[Tl(cdo2a)]^+$ as the ligand possesses the same number and type of donor atoms, but is made rigid

(compared to edta) by having a cyclohexane backbone instead of being macrocyclic and has one carboxylate on each nitrogen replaced with a butylamide group. This ligand was shown to form quite inert complexes with e.g. Mn^{2+}.

$$[Tl(cdtabba)] + H_2O \rightleftharpoons [Tl(cdtabba)OH]^- + H^+ \quad (\mathbf{4.2.5.}1)$$

$$[Tl(cdtabba)OH]^- + H_2O \rightleftharpoons [Tl(cdtabba)(OH)_2]^{2-} + H^+ \quad (\mathbf{4.2.5.}2)$$

$$[Tl(cdtabba)] + I^- \rightleftharpoons [Tl(cdtabba)I]^- \quad (\mathbf{4.2.5.}3)$$

The obtained equilibrium constants for equations **4.2.5.**1 – **4.2.5.**3 are as follows: $lgK^{OH}_{[Tl(cdtabba)]}$ = -6.04(3), $lgK^{OH}_{[Tl(cdtabba)OH]}$ = -8.80(4) and $lgK^{I}_{[Tl(cdtabba)]}$ = 5.73±0.79, respectively. The complex is more acidic overall, but the most interesting finding is that its iodido-mixed ligand complex is almost two orders more stable than [Tl(*c*do2a)I]. ^{205}Tl NMR spectra have also been recorded both in the presence and absence of iodide (see Fig. **4.2.5.**2), although no NMR titration has been performed. The parent complex shows a broad ($w_{½}$= 9500 Hz) peak at δ = 2325 ppm, while the ternary complex produces two peaks at δ = 928 and 879 ppm ($w_{½}$= 2200 Hz). We have yet to interpret this phenomenon, although the ligand does contain two adjacent stereocenter carbon atoms in its backbone which likely play an important role in it.

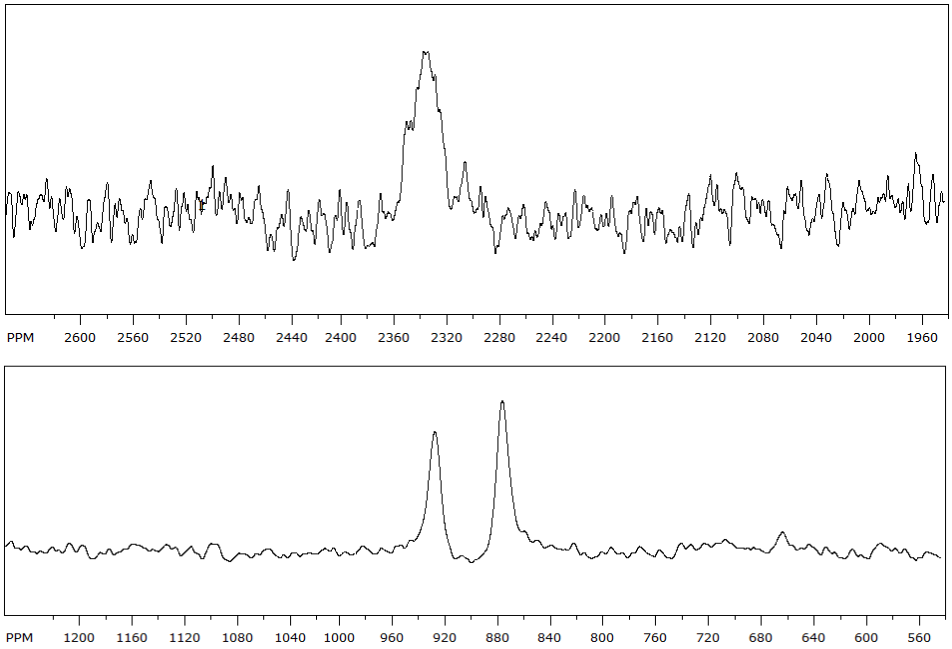

Figure 4.2.5.2 144.28 MHz ^{205}Tl NMR spectra of 10 mM $[Tl(cdtabba)]^+$ (above) and 10 mM [Tl(cdtabba)I] (below) at pH = 4, in 1 M $NaClO_4$

Although stability is a key point in any applications of metal complexes in medicine, it must be remembered that in vivo applications also require the compounds in question to be quite inert for all imaging modalities, targeted or otherwise. In nuclear medicine, tracers are usually employed in nanomolar concentrations, meaning that most of the naturally occurring potentially competing species in the body are usually in gross excess to the radioisotope (and carrier). This is a minor problem when the radionuclide is covalently bound in a molecule, but will almost always shift the equilibria of coordination compounds towards complete dissociation. Even if a compound in question is unreactive to everything found in bodily fluids, spontaneous dissociation can still become a key

factor. Therefore kinetic inertness becomes a necessity, perhaps even outweighing stability. We currently do not possess kinetic data on either complex, but suspect that they are likely too labile for medical applications, as we know from ligand exchange reactions on Tl(edta)X mixed halide complexes published earlier.[27] The open-chain derivative [Tl(cdtabba)I] is presumably the less inert out of the two, despite its increased stability. Experiments for gathering such kinetic data may be conducted via multinuclear NMR (^{1}H, ^{13}C, ^{205}Tl, or even ^{127}I) or by following the decay of radioactive iodide in case of highly dilute solutions. The complexes presented herein may be regarded as the first step, as there are ways to increase inertness through ligand design and/or modification. Preparation of ligands tuned for medical use as highly inert complexes is a top current focus of research in the fields of imaging and coordination chemistry including our research group,[113] having attained considerable knowledge and experience in it. At the time of this work the data on the aforementioned two complexes is yet to be published.

4.3. Study of the ternary complex formation between [Al(nota)] and F^{+}

As indicated earlier,[80,81] [Al(nota)] is known to be capable of carrying the radioactive ^{18}F-isotope that has a key role in PET investigations. Laverman and his coworkers developed a method for radiolabeling the Al(III) complex of an Octreotide derivative of nota, in which an acetate arm has been modified (amidated) to link the peptide[114]. This method uses high temperature (100 °C for 10–15 min) for the complexation in acetate buffer, since the formation rate of [Al(nota)] is

relatively low under these conditions. The radiolabeled compound ([Al(^{18}F)(nota)-octreotide]) was found to be intact in human serum after 4 h and no in vivo dissociation was detectable in mice after 30 min. In fact, this procedure provides a promising agent for PET investigations, but no information on the thermodynamic stability or kinetic inertness of the Al(III)-F-nota ternary complex is available so far. Such data would be highly useful in predicting its in vivo behavior. Attempts were made to follow the formation of the mixed ligand complex between [Al(nota)] and F^-, using both direct potentiometric titration and ‘‘out of cell’’ technique by fluoride selective electrode and by ^{19}F NMR. In all cases, the potentials recorded by F^--selective electrode in the presence and absence of (pre-prepared) [Al(nota)] complex were identical, indicating that the expected complex formation does not occur under these circumstances (25 °C, 0.15 M NaCl). An obvious explanation of this phenomenon can be the high rigidity of [Al(nota)]. Since the coordination sphere of the Al(III) ion is saturated with the donor atoms of nota, coordination of one further F^- ion to the inner sphere requires the dissociation of a carboxylic oxygen, which is an extremely slow process as proven by kinetic experiments in HCl. Therefore, in order to reach equilibrium, the samples were heated for 10 min at 100 °C as described in the literature, and their ^{19}F NMR spectra were recorded after cooling to room-temperature. Only the signal of free F^- was detectable after this treatment which means no detectable formation of the ternary complex, i.e. the formation is quite slow even at 100 °C. It should be noted, that the behavior of $[Al(edta)F]^{2-}$ could easily be followed by fluoride selective electrode.[115]

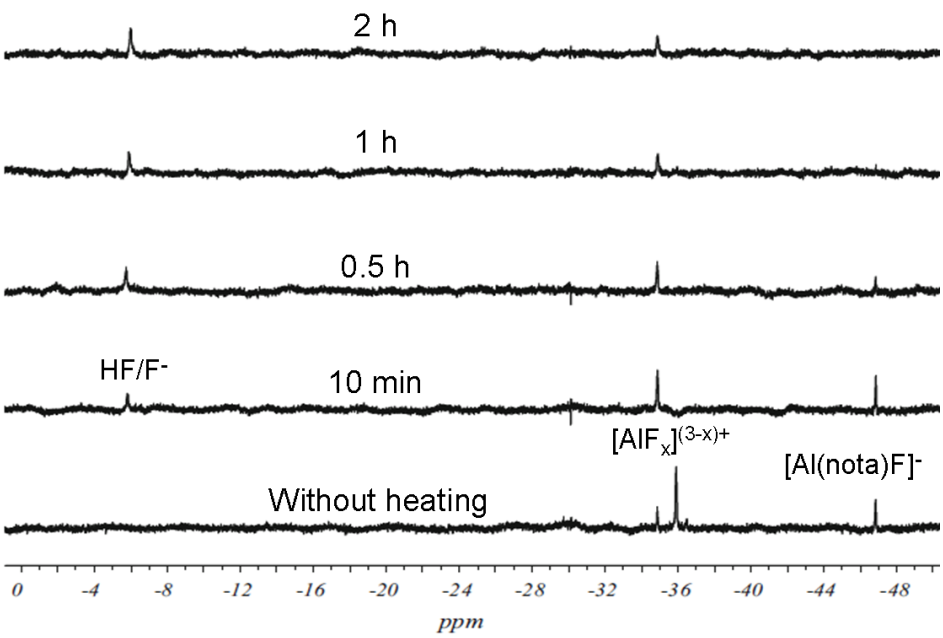

Figure 4.3.1 376.5 MHz ^{19}F-NMR spectra of samples containing Al(III), nota and F^- in equimolar amounts (4 mM of each) after heating in pH = 4 acetate buffer for varying times at 100 °C

Figure **4.3.**1 shows the dependence of ^{19}F-NMR spectra in samples with equimolar Al(III), nota and fluoride (4 mM each) on heating time, recorded 24 h afterwards. In the sample without heating there is a new signal, most likely the signal of the ternary complex at –47 ppm among the signals of Al(III) fluorido complexes (–35 to –36 ppm)[116]. In the sample heated for 10 min, the signal of the free F^- ion appears and the signals of Al(III) fluorido complexes decrease, together with a slight increase in intensity of the mixed ligand complex. Further treatment of the samples causes complete decomposition of the mixed ligand complex to parent AlF_2^+ complex and F^- ion, shown by the signals at –35 ppm and –5 ppm, respectively. (The signal at –5 ppm is the time averaged signal of F^- and HF).

The formation of $[Al(nota)(F)]^-$ was almost 100 % in 50 % ethanol after 15 min of heating according to the ^{19}F-NMR spectrum (Fig. **4.3.**2). The chemical shift was -48 ppm, slightly different from the –47 ppm measured in water likely due to a solvent effect. The role of ethanol could be related to the decreased basicity of the ring nitrogen donor atoms in nota,[117] resulting in faster complex formation due to weaker competition between the H^+ ion and Al(III) for the donor atoms of the macrocycle.

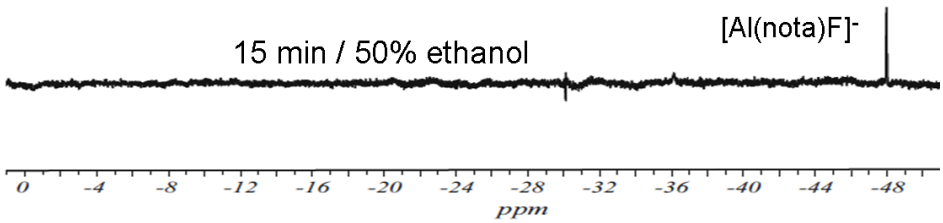

Figure 4.3.2 376.5 MHz ^{19}F-NMR spectra of samples containing Al(III), nota and F^- in equimolar amounts (4 mM each) after heating in pH = 4 acetate buffer for varying times at 100 °C

A detailed study of formation kinetics for metal-macrocyclic complexes in mixed solvents is in progress in our laboratory. Preliminary results show that complex formation kinetics are fairly complicated in the Al(III)–nota–H^+–F^- four-component system, further experiments should be performed to describe and understand the formation kinetics of the mixed ligand complex.

4.4. Characterization of $[Tl_2\{B\text{-}\beta\text{-}SiW_8O_{30}(OH)\}_2]^{12-}$, a newly synthesised thallium-containing polyoxometallate

Although thallium(I) salts of conventional di-, para- and metatungstates have been prepared by usual methods ($Tl_2O{\cdot}WO_3$, $Tl_2O{\cdot}2WO_3$, $5Tl_2O{\cdot}12WO_3$, $Tl_2W_4O_{13}$ and $Tl_{0.3}WO_3$), [118, 119] these compounds are tungsten oxides with an extended structure and to date no structurally characterized discrete Tl-containing polyanions have been reported. In this work we also present data on the synthesis and solution characterization of the novel, thallium(III)-containing 16-tungsto-2-silicate $[Tl_2\{B\text{-}\beta\text{-}SiW_8O_{30}(OH)\}_2]^{12-}$, which represents the first structurally characterized discrete thallium-containing metal-oxide. In the polyanion, two octahedrally coordinated Tl^{3+} ions are sandwiched between two lacunary $\{B\text{-}\beta\text{-}SiW_8\}$ Keggin-type fragments (Fig. **4.4.1.**1).

4.4.1. X-ray crystal structure

Single crystal X-ray analysis revealed that the compound crystallizes in a monoclinic crystal system with space group $P2_1/m$. The $[Tl_2\{B\text{-}\beta\text{-}SiW_8O_{30}(OH)\}_2]^{12-}$ architecture presents a polyanion with idealized C_{2h} symmetry, which consists of two thallium(III) centers and two $\{B\text{-}\beta\text{-}SiW_8O_{31}\}$ POM units. The $\{B\text{-}\beta\text{-}SiW_8O_{31}\}$ units were formed from the $[\gamma\text{-}SiW_{10}O_{36}]^{8-}$ precursor by rotational isomerization and loss of tungsten. The first POM comprising a $\{B\text{-}\beta\text{-}SiW_8O_{31}\}$ unit was reported in 2005. [120] The $\{M_2(B\text{-}\beta\text{-}SiW_8O_{31})_2\}$ structure type has been seen before.[121] The two equivalent thallium(III) centers in the polyanion are both six-coordinated, and each thallium ion is coordinated to two $\{B\text{-}\beta\text{-}$

$SiW_8O_{31}\}$ lacunary POM fragments via four terminal O atoms of the two complete tungsten-oxo triads and two terminal O atoms of two $\{SiO_4\}$ hetero groups. The Tl-O bond length ranges from 2.156(1) to 2.238(1) Å, and the distance between both thallium atoms is 3.338(1) Å. Bond valence sum (BVS) calculations[122] confirm that the oxidation state of the two thallium centers is +3. As based on elemental analysis, the polyanion is diprotonated and BVS as well as DFT (*vide infra*) suggest that they are located on the two μ_3-O atoms.

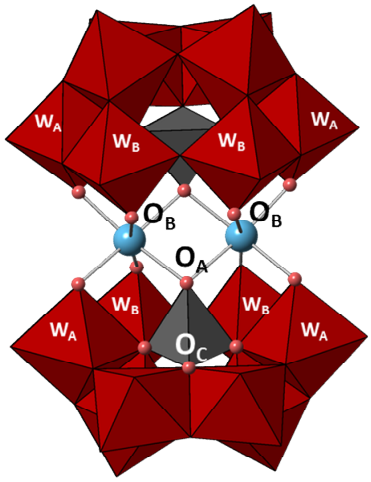

Figure 4.4.1.1 Polyhedral representation of $[Tl_2\{B\text{-}\beta\text{-}SiW_8O_{30}(OH)\}_2]^{12-}$ (1). Color legend: WO_6 (dark red) octahedra, SiO_4 (dark grey) tetrahedra, Tl (light blue), O (light red). The most basic types of oxygens are labeled as O_A, O_B and O_C. The tungsten atoms W_A and W_B have different $^{203/205}Tl$–^{183}W spin-spin coupling constants

Preliminary DFT calculations were performed in order to evaluate the most probable protonation sites and proton distribution in aqueous solution. The structure was optimized initially for the non-protonated anion $[Tl_2\{B\text{-}\beta\text{-}SiW_8O_{31})\}_2]^{14-}$ and the most characteristic X-ray bond

distances were rather well reproduced: Tl-O(Si) 2.28 Å, W-O(Si) 2.25 - 2.43 Å, W-O(Tl) ca 1.81 Å, and Tl···Tl 3.37 Å.

4.4.2. Solution structure study

$[Tl_2\{B\text{-}\beta\text{-}SiW_8O_{30}(OH)\}_2]^{12-}$ is sufficiently soluble in water to record ^{205}Tl and ^{203}Tl NMR spectra of reasonable quality (Figure **4.4.2.**1). Both isotopes have a spin of 1/2, and a natural abundance of 70.5 % and 29.5%, respectively. At first sight, both spectra appear as pseudo-triplets, attributed to the spin-spin coupling between two sterically identical Tl-atoms. The central peaks are assigned to polyanions with homonuclear ^{205}Tl-^{205}Tl or ^{203}Tl-^{203}Tl coupling, whereas the satellite peaks belong to heteronuclear ^{205}Tl-^{203}Tl coupled polyanions, respectively. The peak intensities of the pseudo-triplets agree very well with the expected ones from the isotope ratios, 29.5/2 : 70.5 : 29.5/2 (^{205}Tl NMR), and 70.5/2 : 29.5 : 70.5/2 (^{203}Tl NMR), see SI for details. This finding is in full agreement with the solid-state structure having two Tl-atoms in identical positions, and it proves unequivocally that the dimeric structure is preserved in solution. The chemical shift difference between the satellite peaks represents the coupling constant, $^2J(^{205}Tl\text{-}^{203}Tl)$ = 2670 Hz. Interestingly, a closer look at the spectra indicates further fine structure of the recorded peaks caused by spin-spin coupling with ^{183}W atoms (14.3%). The two different values for $^2J(^{203}Tl\text{-}^{183}W)$ are ca. 470 and 350 Hz, respectively, and the corresponding values for $^2J(^{205}Tl\text{-}^{183}W)$ are ca 1% larger (see Figure **4.4.2.**1 caption for details). These values can be rationalized by coupling to two structurally inequivalent types of tungsten being two bonds away from the thallium centers. These couplings may

actually be averaged effects of two types of ^{183}W centers (W_A, W_B) with similar chemical environments. The Tl···W distances are 3.64 and 3.65 Å for W_A, and 3.72 and 3.73 Å for W_B, respectively.

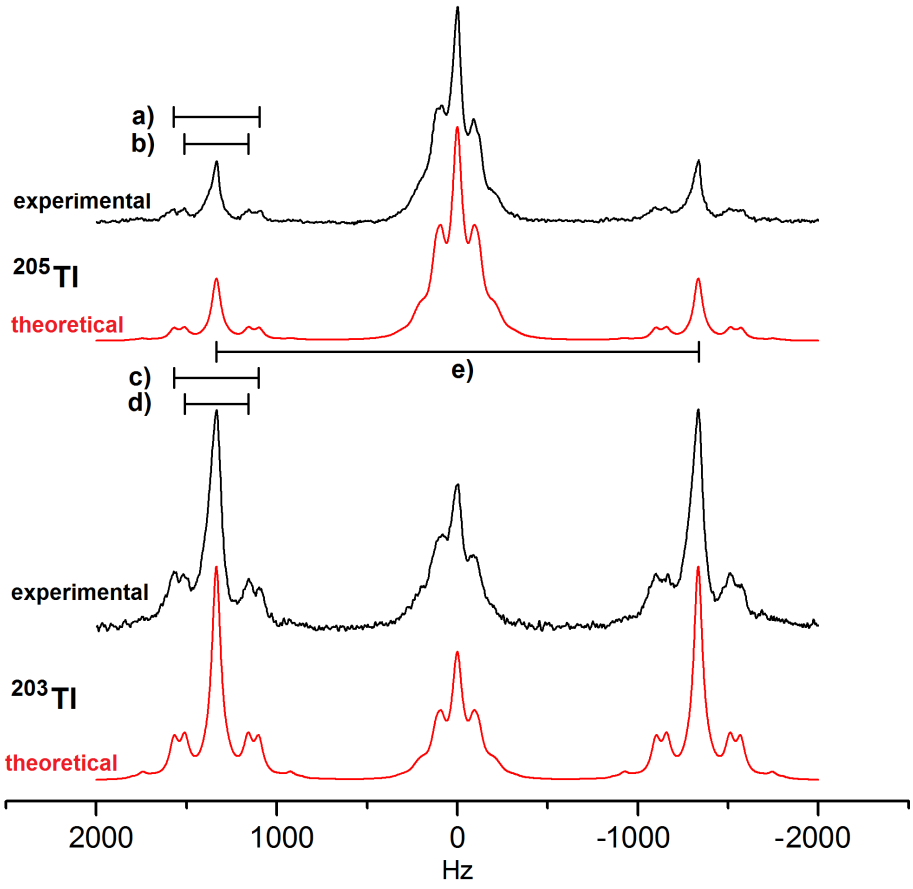

Figure 4.4.2.1 Experimental (black) and theoretically simulated (red) 144.26 MHz ^{205}Tl (top) and 142.86 MHz ^{203}Tl NMR (bottom) spectra of $[Tl_2\{B\text{-}\beta\text{-}SiW_8O_{30}(OH)\}_2]^{12-}$, ~6 mM in 0.04 M acetic acid/sodium acetate buffer, pH = 4.1. Coupling constants shown: a) $^2J(^{205}Tl\text{-}^{183}W_A)$ ca. 475 Hz, b) $^2J(^{205}Tl\text{-}^{183}W_B)$ ca. 354 Hz, c) $^2J(^{203}Tl\text{-}^{183}W_A)$ ca. 470 Hz, d) $^2J(^{203}Tl\text{-}^{183}W_B)$ ca. 350 Hz and e) $^2J(^{205}Tl\text{-}^{203}Tl) = {}^2J(^{203}Tl\text{-}^{205}Tl)$ ca. 2700 Hz (same value in both spectra)

However, the relatively broad spectral lines prohibit such a detailed investigation. The ^{1}H couplings do not play a role because of fast exchange, and the effects of ^{29}Si (I = 1/2, 4.7%) and ^{17}O (I = 5/2, 0.037 %) are also not detectable.

4.4.2.1. Simulation of Tl NMR spectra

We have also simulated the Tl NMR spectra considering the symmetry, the relative positions of the Tl and W atoms, the natural abundance of the NMR-active nuclei and the spin-spin coupling constants measured experimentally. The experimentally obtained NMR spectra are superpositions of several spectra with different combinations of NMR-active nuclei. The NMR model used for simulation is based on the solid-state structure of the polyanion**.** Three (I = 1/2) isotopes, ^{203}Tl, ^{205}Tl and ^{183}W (natural abundances 0.295, 0.705, and 0.143, respectively), and geminal spin-spin couplings are taken into consideration. The two Tl atoms in the polyanion are sterically identical with C_{2h} symmetry**.** One Tl may be coupled with the other Tl and at most four W nuclei (of two different types: two W_A and two W_B). The three identified independent coupling constant values are $^{2}J(^{203}Tl, ^{205}Tl)$ = 2670 Hz, $^{2}J(^{203}Tl, ^{183}W_A)$ = 470 Hz, and $^{2}J(^{203}Tl, ^{183}W_B)$ = 350 Hz. The four other coupling constants ($^{2}J(^{205}Tl\text{-}^{183}W_A)$, $^{2}J(^{205}Tl\text{-}^{183}W_B)$, $^{2}J(^{203}Tl\text{-}^{203}Tl)$ and $^{2}J(^{205}Tl\text{-}^{205}Tl)$) used differ only by 1%, because the magnetogyric ratio, which they are proportionate to, is 1% higher for ^{205}Tl than for ^{203}Tl. If the natural abundance of the observed isotope equals **p** (p = 0.295 or p = 0.705), then the ratio of polyanions containing **2, 1** and **0** observed Tl-isotopes is defined by the binomial distribution and their NMR signal intensity ratio can be calculated by multiplying with said numbers: $\boldsymbol{2}\cdot p^2 : \boldsymbol{1}\cdot 2\cdot p\cdot(1\text{-}p) :$

0$\cdot(1\text{-}p)^2$ = **p : (1-p) : 0**. The polyanions with two observed Tl isotopes or two different Tl isotopes produce different NMR signals, which are separated because of $^2J(Tl\text{-}Tl) >> {}^2J(Tl\text{-}^{183}W)$.

In the multiplets assigned to heteronuclear Tl-Tl coupling (satellite signals) all couplings are first-order and the Tl-Tl coupling produces a symmetric doublet. The ^{183}W-couplings are more complicated, owing to the two different coupling constants. For each satellite, coupling of 1, 2, 3, or 4 ^{183}W nuclei results in 4, 9, 12, or 9 peaks, respectively. If p = 0.143, then the intensity of the satellite is shared among polyanions containing 0, 1, 2, 3, and 4 ^{183}W couplings with probabilities of $(1\text{-}p)^4$, $4\cdot p\cdot(1\text{-}p)^3$, $6\cdot p^2\cdot(1\text{-}p)^2$, $4\cdot p^3\cdot(1\text{-}p)$, p^4 (0.54, 0.36, 0.09, 0.01 and 0.0004) respectively, according to the binomial distribution (see Table **4.4.2.1.**1). The central peak will rise to 58.5 % intensity, caused by splitting, the following four observable signals will be 9.2% each and the intensity left for all other signals is <5%. The coupling constants can be obtained from the satellite peaks.

In multiplets assigned to homonuclear Tl-Tl coupling (central signals) without ^{183}W coupling, the two Tl nuclei are magnetically equivalent (A_2 spin system) providing a singlet signal with a chemical shift δ = 2206 ppm. The ^{183}W coupling causes magnetic non-equivalence of the two Tl centers, so the simple first-order coupling cannot be used any further. Formulae used in the case of ABX (more precisely AA'X in our case) spin systems are known.[123] Tungsten is only coupled to one of the two thalliums (**A**-A'-X), resulting in J(A',X) = 0 for the other one and resulting in 4 doublets. The distance between two doublets is greater than 5400 Hz and their intensity is at most 0.4% of all others, making them unobservable (lost in the noise). The distance of the other two doublets is

half the coupling constant (ca. 240 or 180 Hz) and they are split by only ca. 11 Hz or 6 Hz, meaning that they are not sufficiently separated to be observable.

Table 4.4.2.1.1 Breakdown of the spin systems and their contribution to the intensity pattern observed in the Tl NMR spectra of $[Tl_2\{B\text{-}\beta\text{-}SiW_8O_{30}(OH)\}_2]^{12-}$

Central peaks (Homonuclear Tl-Tl coupling)		***No. of coupled ^{183}W nuclei***	Satellite peaks (Heteronuclear Tl-Tl coupling)	
No. of spin systems	Intensity contribution		No. of spin systems	Intensity contribution
1	**29.15%**	**0**	1	**54.0%**
2	38.85%	**1**	2	36.0%
6	22.65%	**2**	3	9.0%
8	7.55%	**3**	2	1.0%
11	1.57%	**4**	1	0.04%
8	0.21%	**5**		
6	0.017%	**6**		
6	0.00083%	**7**		
1	0.000017%	**8**		

Four similar doublets appear when considering both coupling constants. The coupling of two ^{183}W centers requires numerical solution of six different spin systems (34 observable peaks). Fortunately, simulation with first-order couplings and constants of $^2J(Tl\text{-}^{183}W_A)/2$ and $^2J(Tl\text{-}^{183}W_B)/2$ produces an almost identical spectrum at the used line-width of 60 Hz; i.e. this simplification could be used for polyanions with 3, 4, 5, 6, 7, 8 ^{183}W

isotopes, having almost negligible contributions. The intensity of the central multiplet is shared between polyanions containing 0, 1, 2, 3, …, 8 ^{183}W couplings with probabilities of $(1\text{-}p)^8$, $8 \cdot p \cdot (1\text{-}p)^7$, …, p^8 (0.292, 0.389, 0.227, 0.076, 0.016, …, 1.7×10^{-7}), respectively, according to the binomial distribution (see Table **4.4.2.1.**1). Summing up the intensities of close signals raises that of the central signal to 41.1 %, the next 4 signals will be 11.2 % each (however, their separation is only 30 Hz per pair), and finally "shoulders" with 6.1 % intensity each appear on both sides. In order to visualize the complexity of the numerous spin systems**,** we have simulated both the ^{205}Tl and ^{203}Tl NMR spectra using Lorentzians with 5 Hz linewidth and plotted them together with the experimental spectra (Figure **4.4.2.1.**1). The similarity in shape and positions of peak maxima is obvious.

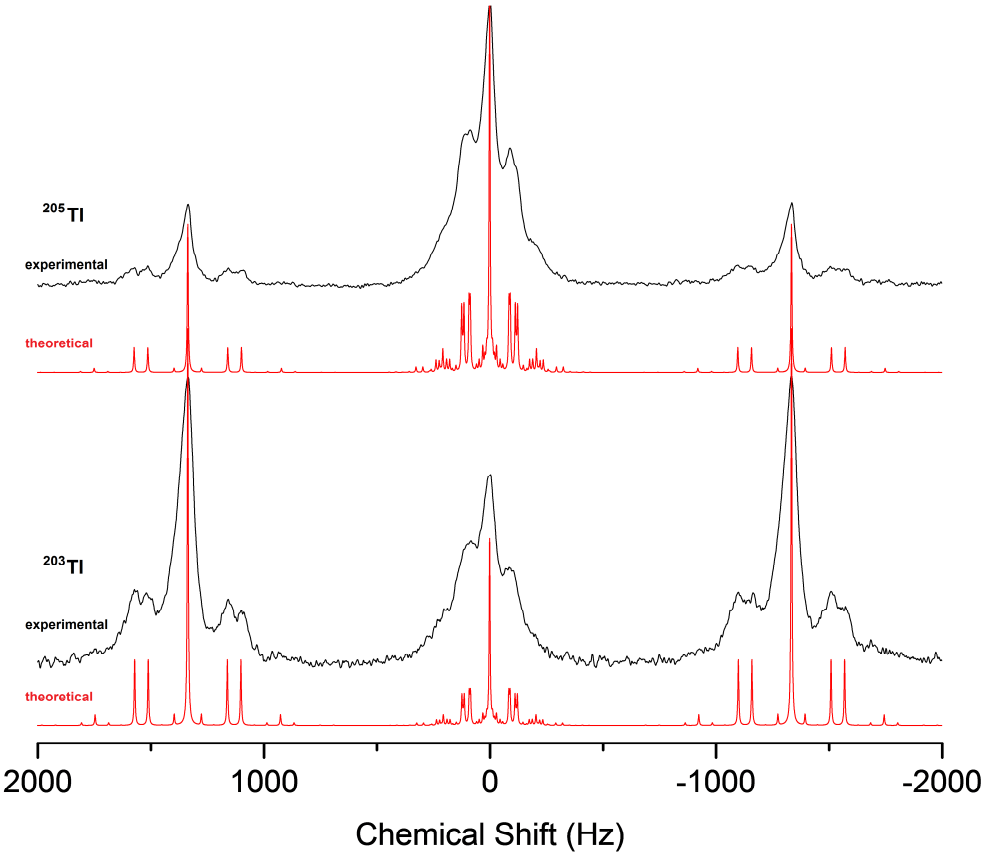

Figure 4.4.2.1.1 Experimental (black) and theoretical (simulated with 5 Hz line-width, red) 144.28 MHz ^{205}Tl and 142.88 MHz ^{203}Tl spectra of $[Tl_2\{B\text{-}\beta\text{-}SiW_8O_{30}(OH)\}_2]^{12-}$. Calculations were performed with a home-made MATLAB program and a few spin systems were simulated with WINDNMR

The chemical shift value of ca. 2206 ppm (the position of the centralpeaks, referenced to infinitely diluted $TlClO_4$ as 0 ppm) is consistent with a +3 oxidation state for the thallium atoms being six-coordinated to O atoms in an octahedral geometry in water. [124 ,27]

Comparing the $^{2}J(^{205}Tl\text{-}^{203}Tl)$ = 2670 Hz coupling constant to literature values is difficult, as published constants are mostly based on organothallium compounds in nonaqueous solvents. The $^{2}J(^{205}Tl\text{-}^{203}Tl)$ = 2560 Hz coupling constant for $(TlOEt)_4$ is very similar to ours,[125] but values ranging from 1920 to 19835 Hz for thallium-metal carbonyls have also been reported.[126]

4.4.3. Solution behavior and overall robustness

The solution properties of the polyanion were also studied by electrospray-ionization mass spectrometry (ESI-MS) by the group in Bremen, which has proven to be a valuable analytical technique for studying POM structures.[127] The major peaks observed in the solution MS show a series of envelopes related to various species with different numbers of associated potassiums and protons. For example, the highest intensity peak centered at m/z of 886.34 can be assigned to the -5 charged dehydrated species $[K_2HTl_2(SiW_8O_{29})(SiW_8O_{30})]^{5-}$, which indicates that complete dehydration has taken place during the ionization process. The other main peaks and assignments are summarized in the inset of Figure **4.4.3.**1.

Both ESI-MS and Tl NMR suggest that the polyanion maintains its integrity in aqueous solution. Nevertheless, this solution stability is very interesting. In order to avoid hydrolysis of "soft" thallium(III) ions in aqueous solution, one usually needs either very strong soft ligands or strongly chelating organic ligands, as previously discussed. The two {*B*-*β*-SiW_8O_{31}} lacunary POM units with five terminal oxo-groups each appear to be excellent polydentate ligands for Tl^{3+} ions. The Si-O sites

behave as μ_3-O atoms, and the other O-donors bind each thallium center inside four six-membered chelate rings.

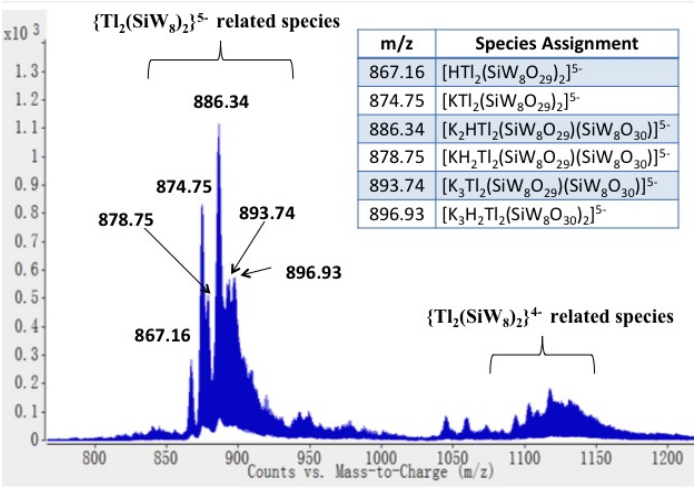

m/z	Species Assignment
867.16	$[HTl_2(SiW_8O_{29})_2]^{5-}$
874.75	$[KTl_2(SiW_8O_{29})_2]^{5-}$
886.34	$[K_2HTl_2(SiW_8O_{29})(SiW_8O_{30})]^{5-}$
878.75	$[KH_2Tl_2(SiW_8O_{29})(SiW_8O_{30})]^{5-}$
893.74	$[K_3Tl_2(SiW_8O_{29})(SiW_8O_{30})]^{5-}$
896.93	$[K_3H_2Tl_2(SiW_8O_{30})_2]^{5-}$

Figure 4.4.3.1 Negative ion mass spectrum of $[Tl_2\{B\text{-}\beta\text{-}SiW_8O_{30}(OH)\}_2]^{12-}$ showing the different fragmented species and their assignments

This structure where the Tl-centers are "closely packed" is highly stable against dissociation into monomers, or losing Tl^{3+} in the form of insoluble Tl_2O_3. In order to gain information on the solution stability of the polyanion, an NMR sample was prepared by dissolving 19 mg (~3.8 μmol) of compound in 2 mL of water (the resulting pH was found to be 5.3). The pH was then set to 4 with a dilute sodium-acetate/acetic acid buffer, reaching a roughly tenfold excess of acetate to Tl(III). This dilute buffer was prepared from 8 mL of glacial acetic acid, 3.4 g of sodium-acetate dihydrate and 2 mL of water, then diluted 1:100. The broad Tl-signals recorded from the sample at initial pH 5.3 became sharper when

the pH was lowered to ca. 4, but no further spectral changes (including the appearance of $[Tl(Ac)_4]^-$) were observed afterwards. The sample was further titrated with the acetate buffer until 10:1 acetate:Tl(III) ratio was reached, with no visible change occurring even after several hours. Treating the polyanion as a M_2L_2 complex and using the known stability constant of $[Tl(Ac)_4]^-$ ($lg\beta_4$= 18.3) a minimal conditional stability was obtained for the formation process (see equations **4.4.3.**1 & **4.4.3.**2).

$$2\ Tl^{3+} + 2\ SiW_8O_{30}(OH)^{9-} \rightleftharpoons [Tl_2\{B\text{-}\beta\text{-}SiW_8O_{30}(OH)\}_2]^{12-} \quad (\mathbf{4.4.3.}1)$$

$$\beta_{Tl_2Si_2W_{16}} = \frac{\left[Tl_2\{B-\beta-SiW_8O_{30}(OH)\}_2^{12-}\right]}{\left[Tl^{3+}\right]^2 \times \left[SiW_8O_{30}(OH)^{9-}\right]^2} \quad (\mathbf{4.4.3.}2)$$

The estimated $lg\beta_{Tl2Si2W16} \geq 40$ is certainly quite high, but one must keep in mind that it is an estimate and that polytungstates often exhibit extremely slow kinetics. Nevertheless, it may be used to extrapolate some aspects of the compounds solution properties. A series of molar fraction calculations were performed using the constant, emulating a dilution series in silico to gain some insight into the polyanions resistance to dilution. In this case the only species present in the system that competes for thallium with the POM fragments is hydroxide. The distribution curves (see Fig. **4.4.3.**2) indicate that the compound only dissociates to an appreciable extent in sub-nanomolar concentrations. Again, this must be treated carefully (due to the possibility of slow equilibration), however it does support that the antibacterial effect (see **4.4.4**) is most likely produced by the intact polyanion, as opposed to thallium ions liberated from it.

A more concentrated sample was prepared dissolving 50 mg (~9.9 μmol) of the POM in 2 mL water in order to obtain a better signal-to-noise ratio and explore whether the previously observed spectral change could be attributed to acetate ions, or is simply a matter of pH. After carefully adjusting the pH from 5.2 to 2.3 with HNO_3, a signal identical to the previously obtained one was observed. The ^{203}Tl spectra were also obtained from this sample. Further spectra recorded at various pH values (adjusted by using 5 M perchloric acid and freshly crushed solid NaOH) in the range of 1.8 – 4.8 showed no change in the observed signal structure or coupling constants.

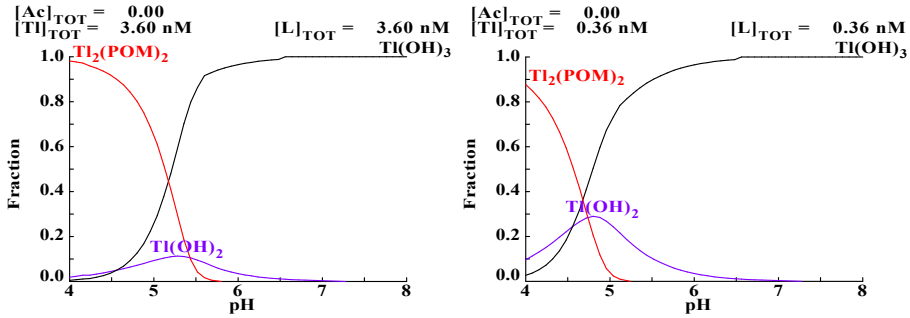

Figure 4.4.3.2 Distribution curves of $[Tl_2\{B\text{-}\beta\text{-}SiW_8O_{30}(OH)\}_2]^{12-}$ in dilute conditions

All samples were clear, colorless solutions that only showed signs of chemical change (as based on Tl NMR) after several months. The emerging new signals are close to the original ones (see Fig. **4.4.3.2**), but with a different structure. This, along with the absence of any visible precipitate, indicates that the decomposition products are still Tl^{3+}-

containing compounds, most likely other tungstosilicates with a single thallium center each.

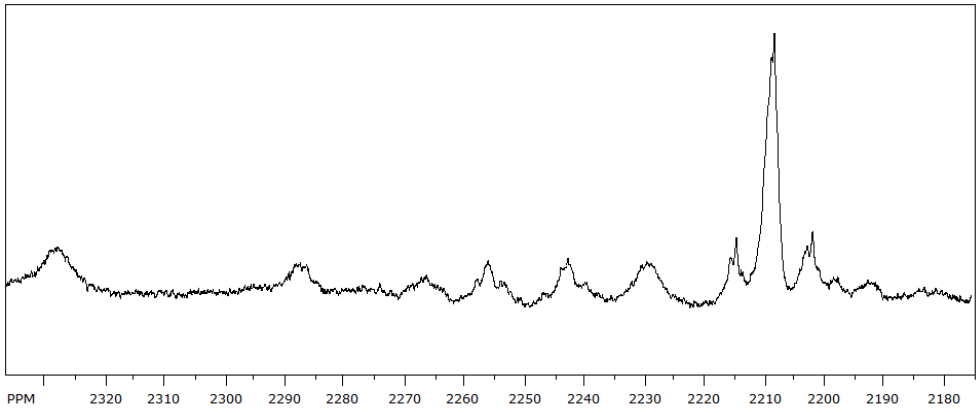

Figure 4.4.3.3 144.28 MHz ^{205}Tl and spectrum of 4.95 mM $[Tl_2\{B\text{-}\beta\text{-}SiW_8O_{30}(OH)\}_2]^{12-}$ at pH 2.3 after 6 months

4.4.4. Antibacterial activity

The antibacterial activity of the polyanion was also investigated at physiological pH by the group in Bremen. The minimum inhibitory concentration (MIC) is compared to that of thallium(III) nitrate and thallium(I) acetate the latter being a known inorganic antibiotic against Gram-negative bacteria.[128] Interestingly, both thallium salts show the same activity. In a phosphate buffer (0.5 M, pH 7), the Tl^{III} salt is not soluble, in contrast to the POM. The latter shows a high antibacterial activity against Gram-positive bacteria, especially *Bacillus aquimaris* and *Bacillus subtilis,* exhibiting a 32-fold increased sensitivity compared to the plain Tl^{I} and Tl^{III} salts. Studies on Gram-negative bacteria were also performed (Table **4.4.3.**1).

Table 4.4.3.1 Susceptibility of several Gram-positive and Gram-negative bacteria to 1 in MHB medium. The minimum inhibitory concentrations (MICs) were assayed in microtiter plates using a standard method.[129] The Mueller−Hinton−Bouillon (MHB) medium is used as a standard medium for MIC determination

MIC Determination (µg/mL)*	**Thallium(I) Acetate***		**Thallium(III) Nitrate***		**POM***	
	Buffer	**H_2O**	**Buffer**	**H_2O**	**Buffer**	**H_2O**
Gram-negative						
Escherichia coli DH5α	No Inhibition	No Inhibition	xx†	No Inhibition	80	80
P. syringae pv. Glycinea (PG4180)	5	5	xx	5	10	10
Gram-positive						
Bacillus subtilis	20	20	xx	20	0.625	1.25
Clavibacter michiganensis	2.5	2.5	xx	2.5	2.5	5
Bacillus aquimaris	10	10	xx	10	0.3125	10

* The MIC is calculated based on the Tl concentration present in each compound. For a valid comparison, the same concentration of Tl was used in all tested compounds (1.6 mg/ml). No activity was found by the POM precursor $K_8[\gamma\text{-}SiW_{10}O_{36}]$, which was used for the synthesis.

† Thallium(III) nitrate is not soluble in the sodium phosphate buffer used (0.5 M, pH 7).

The MIC values presented are promising, as the polyanion effects all tested organisms at similar –and in most cases, lower– Tl-concentrations than inorganic thallium salts. Considering the solution data obtained the inhibitory effect is unlikely to stem from the release of thallium from the POM, as the concentrations used in the biological study are several orders higher (μM) than those at which the POM would noticeably dissociate (nM).

4.5. Characterization of another novel Tl(III)-containing POM, $[Tl_2\{P_2W_{15}O_{57}\}_2]^{22-}$

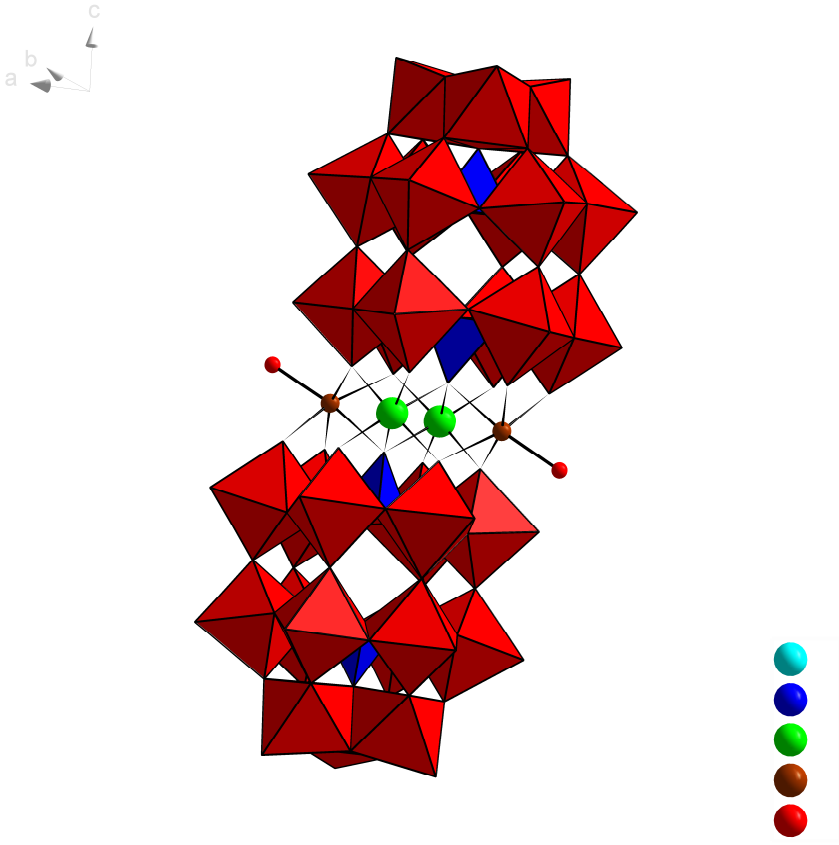

Figure 4.5.1 Polyhedral representation of $[Tl_2\{P_2W_{15}O_{57}\}_2]^{22-}$ (1). Color legend: WO_6 (red) octahedra, PO_4 (blue) tetrahedra, Tl (green), O (light red), Na (brown)

A similar compound to the one described above, $[Tl_2\{P_2W_{15}O_{57}\}_2]^{22-}$ was also synthesized in Bremen and is very similar to $[Tl_2\{B\text{-}\beta\text{-}SiW_8O_{30}(OH)\}_2]^{12-}$ with a few key differences. This polyanion has a different symmetry, being based on a lacunary Wells-Dawson structure and contains phosphate as a heterogroup instead of

silicate. Two thalliums are sandwiched between two POM fragments, similarly to $[Tl_2\{B\text{-}\beta\text{-}SiW_8O_{30}(OH)\}_2]^{12-}$. As ^{31}P is also a I = ½ nucleus but with 100% natural abundance, further peak splitting is to be expected and ^{31}P NMR becomes an additional tool to investigate it with. The ^{31}P NMR spectrum in Fig. **4.5.**2 was provided by our partners in Bremen.

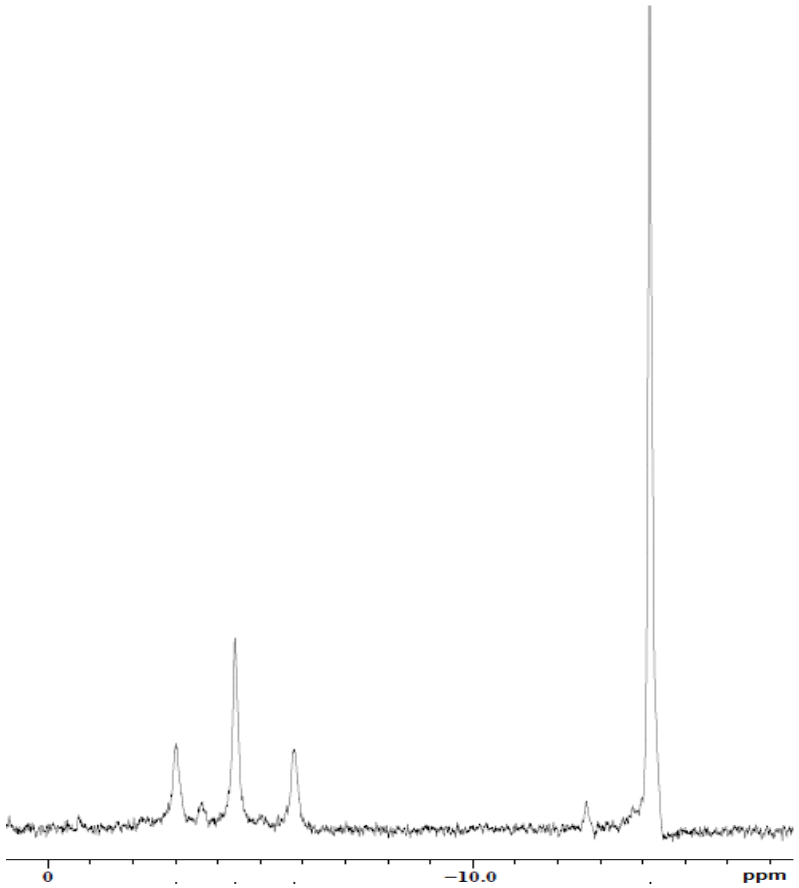

Figure 4.5.2 162.14 MHz ^{31}P NMR spectrum of 3.7 mM $[Tl_2\{P_2W_{15}O_{57}\}_2]^{22-}$ in 0.5 M phosphate buffer pH = 5.8**.**

Both ^{205} and ^{203}Tl NMR spectra were recorded from a sample made from 49 mg of the compound in 2.5 ml of water. The ^{31}P NMR shows a triplet

and a singlet peak, which can be assigned to the two phosphorous atoms that are coupled to both Tl-nuclei and the two that are isolated, respectively. The Tl NMR spectra however, show one major and one minor signal which do not synergize with the pattern seen in the ^{31}P NMR. Making the assumption that the major signal may be most likely attributed to the title ion, we have focused on interpreting it first. The following coupling constants were obtained or estimated: ^{2}J(P-Tl) ≈ 225 Hz (from the ^{31}P spectrum, $^{2}J(^{205}\text{Tl}\text{-}^{203}\text{Tl})$ ≈ 777 Hz, $^{2}J(\text{Tl}\text{-}^{183}\text{W})$ > 500 Hz. The spectra clearly exhibit different peak structures, indicating that the examined molecule does indeed contain two thallium nuclei within coupling distance, as in $[Tl_2\{B\text{-}\beta\text{-}SiW_8O_{30}(OH)\}_2]^{12-}$. In this case however, the satellite and central signals are much less separated and there are also two coupling ^{31}P nuclei introducing additional splitting and overlap. Even so, the same principles can be applied in this case as well.

The major signals in both ^{203} and ^{205}Tl NMR spectra were deconvoluted by treating each of them as a sum of constituent spectra belonging to molecules with only homo- or heteronuclear Tl-Tl coupling (somewhat akin to the evaluation of UV-vis spectra). The experimentally obtained spectra can be reconstructed per-point by adding these constituent spectra together in different proportions (determined by natural isotope abundances), as seen in Fig. **4.5.**4. The polyanion clearly retains its structure in solution, however we currently have no data on what the minor signal might be attributed to.

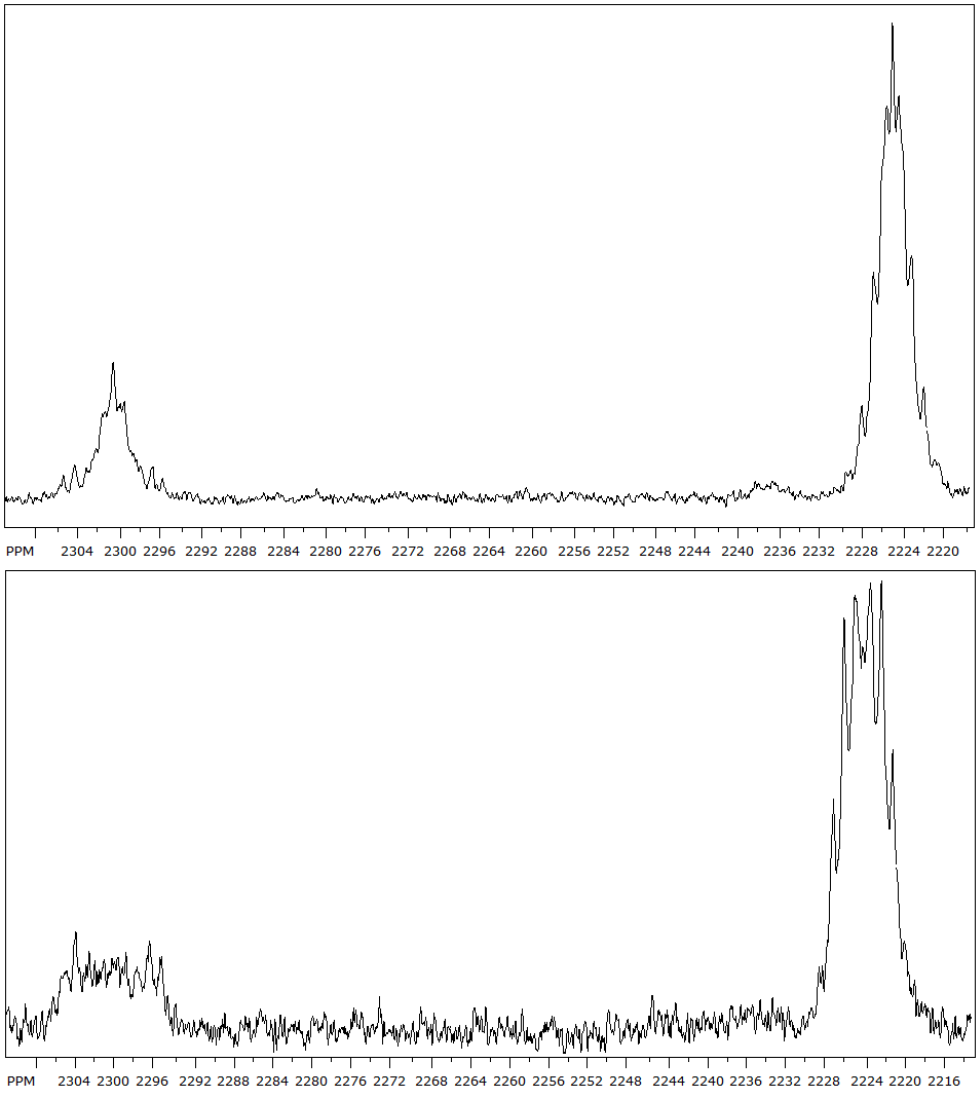

Figure 4.5.3 144.28 MHz ^{205}Tl NMR (above) and 142.86 MHz ^{203}Tl NMR (below) spectra of $[Tl_2\{P_2W_{15}O_{57}\}_2]^{22-}$ (below)

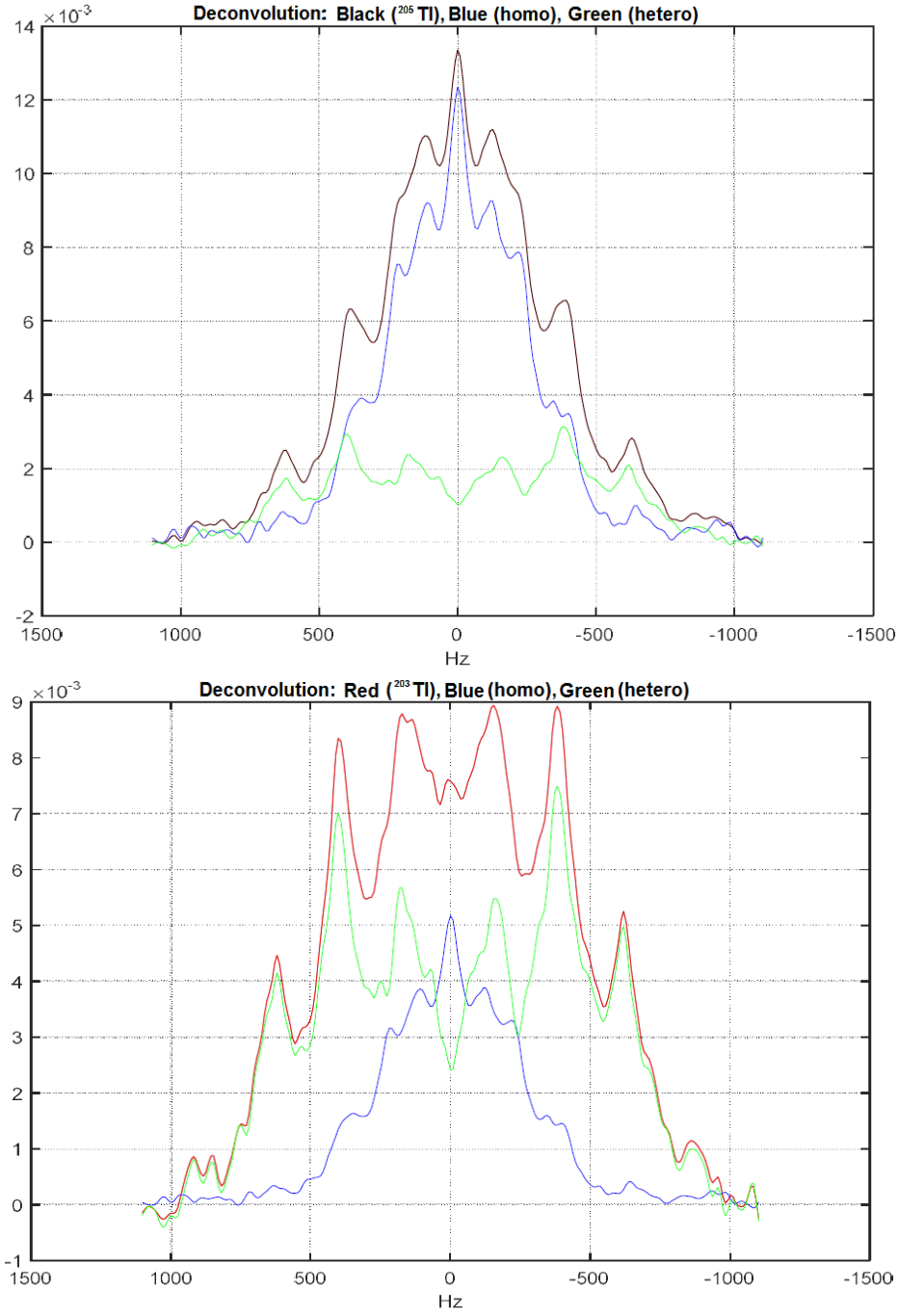

Figure 4.5.4 Deconvolution of the $[Tl_2\{P_2W_{15}O_{57}\}_2]^{22-}$ Tl NMR spectra: ^{205}Tl (above, black) and ^{203}Tl (red, below). Constituent spectrum

intensities are also shown in each (homonuclear: blue and heteronuclear: green)

5. Summary

This thesis deals with Tl(III)-complexes of two, fundamentally different multidentate ligand types,: organic polyaminopolycarboxylates and inorganic heteropolytungstates, which even so share some similarities. We have studied solution equilibrium and kinetic properties, as well as structural traits both in solid and solution phase, of various Tl(III)-complexes.

Structural properties of $[Tl(dota)]^-$ have been explored both in solid phase and solution. In solid state, the Tl^{3+} ion is directly coordinated to the eight donor atoms of the ligand, with the metal coordination environment being best described as twisted square antiprismatic (TSAP); the coordination of the ligand to the metal ion introduces two sources of stereoisomerism, one associated to the conformation of the cyclen moiety [(δδδδ) or (λλλλ)], and another related to the layout of the four acetate pendant arms [represented as Δ or Λ]. Inspection of the structure shows that crystals contain the Λ(λλλλ)/Δ(δδδδ) enantiomeric pair, the two enantiomers being centro-symmetrically related in accordance with the centro-symmetric character of the space group P-1. The "soft" nature of Tl^{3+} (and Bi^{3+}) according to the Pearson classification provokes a strengthening of the coordination bonds with the softer N donor atoms, which results in a deeper penetration of the metal ion into the macrocyclic cavity and the preclusion coordination of further water molecules or small ions to the metal center.

The acid–base properties and affinities towards mixed–complex formation were investigated for $[Tl(dota)]^-$ and $[Tl(cdo2a)]^+$. The coordinative saturation around the metal center and overall compactness in $[Tl(dota)]^-$ makes further coordination of small anions –even those with high affinity towards Tl(III)– unfavourable. $[Tl(cdo2a)]^+$ was found to form a relatively stable mixed–complex with iodide ions. The complexes are highly resistant towards dissociation via proton– or OH^-–assisted pathways. $[Tl(dota)]^-$ does not deprotonate in the pH–range 4–11, as there is no room for a Tl–coordinated water molecule in the complex, however a protonation constant of $pK^H_{[Tl(dota)]} = 1.4\pm0.1$ was be obtained from ^{205}Tl-NMR. This process most likely involves the protonation of one of the carboxylate arms. It is likely that $[Tl(dota)]^-$ may be stored on any measurable pH indefinitely. Conversely, $[Tl(cdo2a)]^+$ does have coordinated water and can be deprotonated twice ($lgK^{OH}_{Tl(cdo2a)} = -7.37\pm0.01$, $lgK^{OH}_{Tl(cdo2aOH)} = -11.10\pm0.01$). Protonation at low pH has not been measured, although the complex stays intact in the pH–range 0–12 for months.

$[Tl(dota)]^-$ does not form mixed–complexes generally, due to the metal being virtually completely wrapped by the ligand donor groups. Only the formation of a faint mixed $[Tl(dota)(CN)]^{2-}$ complex could be detected using ^{205}Tl-NMR, with $K_{mix} = 6.0 \pm 0.8$. This is several orders of magnitude lower than other cyanido–mixed Tl(III)–complexes (in case of $[Tl(edta)]^-$ **lg**Kmix = 8.7) and even the protonation of cyanide is enough for it to instantly dissociate. $[Tl(cdo2a)]^+$ readily forms halido–mixed ligand complexes, such as [Tl(*c*do2a)I] as evidenced by potentiometric titrations and Tl NMR. A formation constant of $lgK^I_{[Tl(cdo2a)]} = 4.1\pm0.1$ is obtained from both potentiometry with an iodide-selective electrode and

^{205}Tl NMR titrations in the pH–range 3–4 (avoiding the interference of OH^-).

Dissociation kinetics of $[Tl(cdo2a)]^+$ and $[Tl(dota)]^-$ were investigated with UV-spectrophotometry. Both complexes were found to be highly stable and inert against dissociation, requiring large excesses of competing agents –both for the metal and the ligand– for the dislocation of Tl(III) to occur in reasonable time spans. Several attempts were made to determine the stability of both $[Tl(cdo2a)]^+$ and $[Tl(dota)]^-$ using the double competition method previously described for $[Tl(edta)]^-$, using large (in some cases, several thousand–fold) excesses of both Br^- and H^+ in batch samples, followed via UV–spectrophotometry. True equilibriation could not however be reached in case of either complex, as some unknown side–reaction takes place which interferes with the evaluation of UV–spectra from then on.

Insight into the dissociation of $[Tl(dota)]^-$ was however obtained, showing quadratic dependence of k_{obs} on acidity, with no detectable spontaneous dissociation. This kind of rate law is in accordance with the related literature of dota-complexes, i.e. the dissociation is a dominantly proton-assisted process. Using the $k_{obs} = k_1[H^+] + k_2[H^+]^2$ rate law, the half–life of the complex at different pH values can be calculated. Half-life of $[Tl(dota)]^-$ is 32 h in 1 M $HClO_4$ and approximated to $5 \cdot 10^9$ h (more than half millon years) at pH = 7.4. The latter value indicates that the dissociation of $[Tl(dota)]^-$ at the physiological pH of blood is negligible. $[Tl(cdo2a)]^+$ behaves similarly, with faster dissociation and lower acid concentrations needed to initiate the process.

Solution dynamics of the isomer–interconversion observed in $[Tl(dota)]^-$ were elucidated. The complex is present in solution as an equilibrium mixture of two exchanging TSAP enantiomers $\Lambda(\lambda\lambda\lambda\lambda)$ and $\Delta(\delta\delta\delta\delta)$. Line shape changes in varied-temperature ^{13}C-NMR spectra have been attributed to the simple two–site exchange between the equally populated two isomers. This process involves both the inversion of the macrocyclic unit [$(\lambda\lambda\lambda\lambda) \leftrightarrow (\delta\delta\delta\delta)$] and the rotation of the four acetate pendant arms [$\Lambda \leftrightarrow \Delta$]. Fortunately, the complete transition from slow– to fast exchange can be observed at conventional temperatures and quantitative band-shape analysis of the two–step exchange process provides the exchange rates k_{exch} at every temperature, which were subsequently used to obtain activation parameters for the exchange process. The obtained values are in good agreement with those found by DFT.

Several attempts were made to prepare ternary $[Al(nota)F]^-$ from the parent complex [Al(nota)], to no avail. Contrary to literature, the formation of the ternary $[Al(nota)(F)]^-$ via direct reaction of [Al(nota)] and F^- cannot be detected either via potentiometry or ^{19}F NMR spectroscopy. The desired product can only be found in detectable amounts in solutions containing equimolar amounts of nota, Al(III) and F^- after heating, although no equilibrium data could be compiled. Yield of the ternary complex can be raised to almost 100% using 50% ethanol as solvent. What occurs is likely a multi-step competition reaction between the various Al(III)–fluorido species and nota through the intermediate $[Al(nota)F]^-$, as increased reaction times decrease yield and provide the parent complex [Al(nota)].

Solution structure of two thallium–containing POMs were investigated. In solid $(NH_4)_5K_7[Tl_2\{B\text{-}\beta\text{-}SiW_8O_{30}(OH)\}_2]\cdot 19H_2O$ the $[Tl_2\{B\text{-}\beta\text{-}SiW_8O_{30}(OH)\}_2]^{12-}$ architecture presents a polyanion with idealized C_{2h} symmetry, which consists of two thallium(III) centers and two $\{B\text{-}\beta\text{-}SiW_8O_{31}\}$ POM units. The two thallium(III) centers are both six-coordinated, and each thallium ion is coordinated to two $\{B\text{-}\beta\text{-}SiW_8O_{31}\}$ lacunary POM fragments via four terminal O atoms of the two complete tungsten-oxo triads and two terminal O atoms of two $\{SiO_4\}$ hetero groups. This structure is fully retained in solution and contains two thallium centers within scalar coupling distance, as evidenced by ^{205} and ^{203} Tl NMR spectra. Both spectra appear as pseudo-triplets attributed to the spin-spin coupling between two sterically identical Tl-atoms. Further fine structure can be observed due to spin-spin coupling with ^{183}W atoms (14.3%). The two different values for $^2J(^{203}Tl\text{-}^{183}W)$ are ca. 470 and 350 Hz, respectively, and the corresponding values for $^2J(^{205}Tl\text{-}^{183}W)$ are ca 1% larger. These values can be rationalized by coupling to two structurally inequivalent types of tungsten being two bonds away from the thallium centers. These couplings may actually be averaged effects of two types of ^{183}W centers (W_A, W_B) with similar chemical environments.

We have also simulated the Tl NMR spectra considering the symmetry of $[Tl_2\{B\text{-}\beta\text{-}SiW_8O_{30}(OH)\}_2]^{12-}$, the relative positions of the Tl and W atoms, the natural abundance of the NMR-active nuclei and the spin-spin coupling constants measured experimentally. Experimentally obtained NMR spectra are a superposition of several constituent spectra with different combinations of NMR-active nuclei. In our simulated model only the Tl-O-Tl and Tl-O-^{183}W couplings were considered,

leading to 54 different possible spin systems. The easily detectable shape difference between the central and the satellite peaks can be attributed to the fact that the ^{183}W atoms are coupled to homonuclearly-coupled Tl atoms (A_2 spin system), resulting in magnetic nonequivalence of the chemically equivalent two ^{205}Tl or ^{203}Tl atoms, creating an AA'X spin system. In such a spin system the Tl-W splitting is just half of that observed for the satellite signals.

The same is visible in $[Tl_2\{P_2W_{15}O_{57}\}_2]^{22-}$, although there is less distance between the central and satellite peaks and the two coupled ^{31}P nuclei (100% natural abundance) also provide added multiplicity to all thallium signals. The compound clearly retains its structure in solution and the obtained peak groups in ^{203} and ^{205}Tl NMR can both be nicely reconstructed as the sum of an adequate "amount" of pure central and satellite intensities. The spectra also contain a minor signal group which also seems to contain two Tl(III) nuclei, but is somewhat different in both chemical shift and peak structure.

NMR–titration of $[Tl_2\{B\text{-}\beta\text{-}SiW_8O_{30}(OH)\}_2]^{12-}$ with acetate ions as a competing agent for thallium has also yielded some insight into its stability. No visible reaction took place with large acetate–excess, even after several days. Considering the substance as an M_2L_2 complex comprised of 2 thallium ions and 2 $\{B\text{-}\beta\text{-}SiW_8O_{31}\}$ units an estimated minimum stability of lgK > 40 was calculated, although polytungstates are known to often possess extremely slow kinetics. From this it can be extrapolated that –barring any additional effect– the compound will only undergo dissociation due to dilution in the sub–nanomolar range. It is worth noting that $[Tl_2\{B\text{-}\beta\text{-}SiW_8O_{30}(OH)\}_2]^{12-}$ is shown to decay into a mixture of polytungstates, each containing only one Tl(III) by Tl NMR,

however this only occurs after several months and dissociated thallium – either as oxide or acetate-complex– remains absent.

6. Összefoglaló

Ezen doktori értekezés kétféle, egymástól alapjaiban különböző többfogú ligandum-csoport, egyrészt szerves poliamino-polikarboxilátok másrészt szervetlen heteropoliwolframátok, Tl(III)-komplexeivel foglalkozik. A választott ligandumok komplexei azonban mutatnak hasonlóságokat, ez tette lehetővé számunkra a cím adott megfogalmazását, utalva a komplexek robosztusságára, jelentős stabilitására és inertségére. Részletesen vizsgáltuk több Tl(III)-komplex szerkezeti tulajdonságait szilárd és oldatfázisban, valamint oldategyensúlyi és kinetikai jellemzőit.

Felderítettük a $[Tl(dota)]^-$ szerkezeti tulajdonságait szilárd– és oldatfázisban. Szilárd fázisban a Tl^{3+} ion közvetlenül koordinálódik a ligandum 8 donoratomjához, a fémion koordinációs környezete csavart négyzetes antiprizmás (twisted square antiprismatic, TSAP); a komplexképződés két sztereoizoméria-forrást hoz létre, az egyik a ciklénygyűrű konformációjához [(δδδδ) vagy (λλλλ)] kapcsolódik, a másik az acetát karok elhelyezkedéséhez [Δ vagy Λ]. Kristályos formában a Λ(λλλλ)/Δ(δδδδ) enantiomerpár található melyek centro-szimmetrikus kapcsolatban vannak, ahogy az a P-1 tércsoportra jellemző. A Tl^{3+} Pearson-besorolás szerinti "lágy" természete a N-donorokkal létrehozott koordinációs kötések erősségét megnöveli, melynek hatására a fémion mélyen, további koordinálható víz–, vagy egyéb kismolekuláktól elszigetelten ül a makrociklus üregében.

Megvizsgáltuk a $[Tl(dota)]^-$ és $[Tl(cdo2a)]^+$ sav-bázis tulajdonságait, inetségüket és a vegyeskomplex képzésére való hajlamát.

A törzskomplexek rendkívül ellenállóak proton– vagy OH^-–asszisztált disszociációval szemben. A $[Tl(dota)]^-$ nem veszít protont pH 4 és 11 közt, mivel a komplexben nincsen hely Tl–koordinált vízmolekula számára, viszont ^{205}Tl-NMR segítségével megállapítottunk egy $pK^{H}_{Tl(dota)}$ = 1,4±0,1 protonálódási állandót. Ez a folyamat legnagyobb valószínűség szerint egy karboxilát csoporton megy végbe. Könnyen meglehet, hogy a $[Tl(dota)]^-$ bármilyen mérhető pH–n hosszan eltartható. Ezzel ellentétben, a $[Tl(cdo2a)]^+$ tartalmaz koordinált vízmolekulát és így kétszer is deprotonálható ($lgK^{OH}_{[Tl(cdo2a)]}$ = –7,37±0,008, $lgK^{OH}_{[Tl(cdo2aOH)]}$ = –11,10±0,009). Kis pH–n való protonálódást nem mértünk, viszont ez a komplex is hónapokon át változatlan marad pH 0 és 12 közt.

A $[Tl(dota)]^-$ általánosságában nem képez vegyeskomplexeket, mivel a fémiont teljesen körbeveszik a ligandum donoratomjai. Mindössze egy igen gyenge $[Tl(dota)(CN)]^{2-}$ komplexet sikerült kimutatni ^{205}Tl NMR–el δ = 2463 ppm-nél, K_{mix} = 6,0 ± 0,8 állandóval. Ez nagyságrendekkel kisebb más Tl(III)–cianido vegyeskomplexekéhez képest ($[Tl(edta)]^-$ esetében a $\mathbf{lg}K_{mix}$ = 8,7) Potenciometriás titrálásokkal és ^{205}Tl NMR–el kimutattuk, hogy a $[Tl(cdo2a)]^+$ készségesen képez vegyeskomplexeket halogenid ionokkal. Jodid-szelektív elektróddal végzett potenciometriás– és ^{205}Tl NMR titrálásokkal pH 3 és 4 közt (az OH^- zavaró hatásait elkerülendő) megállapítottuk a terner [Tl(*c*do2a)I] komplex stabilitási állandóját: $lgK^{I}_{[Tl(cdo2a)]}$ = 4,13±0,08.

Megvizsgáltuk a $[Tl(cdo2a)]^+$ és $[Tl(dota)]^-$ disszociáció-kinetikáját. Mindkét komplex igen stabilnak és inertnek bizonyult disszociációval szemben, a Tl(III) kiszorítása csak nagy feleslegben alkalmazott kompetíciós ionok –mind a fémre, mind a ligandumra–

hatására játszódott le, akkor is igen lassan. Nagyszámú kísérletet végeztünk a $[Tl(cdo2a)]^+$ és $[Tl(dota)]^-$ stabilitási állandóinak meghatározására, a $[Tl(edta)]^-$–hoz korábban sikeresen használt kettős kompetíciós módszerrel, nagy (esetenként többezerszeres) feleslegben használt Br^- és H^+ ionokkal. Különmintás módszert használva, a változásokat UV–spektrofotometriával követtük. Valódi egyensúlyt nem értünk el, mivel hosszabb idő elteltével valamilyen ismeretlen mellékreakció is elindul és kiértékelhetetlenné teszi a további adatokat.

Sikerült azonban belátást nyerni a $[Tl(dota)]^-$ disszociációs folyamatába, a kezdeti sebességek módszerével. Az illesztett görbe azt mutatja, hogy k_{obs} négyzetesen függ a savkoncentrációtól, spontán disszociáció pedig nem észlelhető. Ez a fajta sebességi egyenlet egyezik a dota-komplexek ide vonatkozó irodalmában leírtakkal, a bomlás főként proton-asszisztált folyamat, A $k_{obs} = k_1[H^+] + k_2[H^+]^2$ egyenletet felhasználva kiszámítható a komplex felezési ideje különböző pH-kon. A $[Tl(dota)]^-$ esetében ez 32 óra 1 M $HClO_4$–ban és megközelítőleg $5 \cdot 10^9$ óra (több mint félmillió év) pH = 7.4–en. Ez utóbbi érték azt mutatja, hogy a vér fiziológiás pH-ján a komplex disszociációja elhangyagolható. A $[Tl(cdo2a)]^+$ hasonlóan viselkedik, de gyorsabban disszociál (4 óra 1 M $HClO_4$–ban és 786 óra pH = 7.4–en) és a folyamat alacsonyabb savkoncentrációknál is megkezdődik.

A $[Tl(dota)]^-$ oldatbeli izomer-interkonverziójának dinamikáját is vizsgáltuk. A komplex oldatban két TSAP enantiomer ($\Lambda(\lambda\lambda\lambda\lambda)$ és $\Delta(\delta\delta\delta\delta)$) egyensúlyi keverékeként van jelen. A különböző hőmérsékleteken felvett ^{13}C-NMR spektrumokban megfigyelt jelalak-változást az oldatban jelenlevő, egyenlő populációjú két izomer közti

egyszerű cserefolyamathoz rendeltük. A folyamat magában foglalja a makrociklus inverzióját [(λλλλ) ↔ (δδδδ)] és a négy acetát kar rotációját [Λ ↔ Δ]. Szerencsénkre, a teljes lassú–gyors csere átmenet végigkövethető volt szokványos hőmérsékleteken és kvantitatív jelalak-analízissel minden hőmérsékletre kiszámolható a kétlépéses folyamat cseresebessége k_{exch}, majd ezekből a folyamat aktiválási paraméterei. Az így kapott értékek jó egyezést mutatnak a DFT számolásokból származóakkal.

A $[Tl(dota)]^-$–hoz szerkezetében és robusztusságában némileg hasonló [Al(nota)] komplex részletes vizsgálatát elvégeztük. (Ilyen Al-komplexeket használnak anionhordozóként ^{18}F PET vizsgálatokhoz, amelyekben a „kemény" Al(III) köti meg a „kemény" fluoridot. Ez szolgált számunkra alapul „lágy-lágy" kölcsönhatáson alapuló Tl(III)-jodid vegyeskomplexek tervezésére.) Az irodalomban leírtakkal ellentétben, vegyesligandumú $[Al(nota)(F)]^-$ képződése nem figyelhető meg sem potenciometriával, sem ^{19}F NMR–el [Al(nota)] és F^- közvetlen reakciójában. A terner komplex Al(III)-t, F^--t és nota-t egyenlő koncentrációban tartalmazó oldatokból, melegítés hatására képződik észlelhető mennyiségben, de egyensúlyi adatok nem születtek. Ugyanakkor a vegyeskomplex szinte kvantitatíve képződik 15 perc melegítés után, ha oldószerként 50% etanolt választunk. Ez valószínűleg egy többlépéses kompetíciós reakció a különböző Al(III)-fluorido komplexek és a nota közt, melyben a $[Al(nota)(F)]^-$ egy intermedier, mivel hosszabb melegítés minden esetben csökkenti a vegyeskomplex arányát és [Al(nota)] képződik.

Megvizsgáltuk két tallium-tartalmú POM oldatbeli szerkezetét, a szilárd $(NH_4)_5K_7[Tl_2\{B\text{-}\beta\text{-}SiW_8O_{30}(OH)\}_2]\cdot 19H_2O$–ban a $[Tl_2\{B\text{-}\beta\text{-}SiW_8O_{30}(OH)\}_2]^{12-}$ szerkezet idealizált C_{2h} szimmetriájú polianion, mely két tallium(III) magból és két $\{B\text{-}\beta\text{-}SiW_8O_{31}\}$ POM egységből építhető fel. A $\{B\text{-}\beta\text{-}SiW_8O_{31}\}$ egységek a $[\gamma\text{-}SiW_{10}O_{36}]^{8-}$ prekurzorból képződnek rotációs izomerizáció és wolfram vesztés során. A két tallium(III) hatszorosan koordinált és mindkét tallium ion két $\{B\text{-}\beta\text{-}SiW_8O_{31}\}$ hiányos POM fragmenst köt össze, a két egész wolfram-oxo triád 4 terminális oxigénjével és két $\{SiO_4\}$ heterocsoport két terminális oxigénjével kapcsolódik. Ez a szerkezet változatlanul megmarad oldatfázisban is és két skalárisan csatoló tallium magot tartalmaz, amit ^{205}Tl és ^{203}Tl NMR spektrumok egyértelműen bizonyítanak. Első ránézésre mindkét spektrum pszeudo–tripletnek tűnik, amit a két sztérikusan azonos, spin-spin csatolásban lévő Tl-atomhoz rendelhetünk. A jelek további finom szerkezete is megfigyelhető a ^{183}W atomokkal (14.3%) történő csatolások miatt. A $^2J(^{203}Tl\text{-}^{183}W)$ két különböző értéke kb. 470 és 350 Hz és az ide tartozó $^2J(^{205}Tl\text{-}^{183}W)$ értékek ~1%–kal nagyobbak. Ezeket az értékeket kétféle, nem-ekvivalens wolfram atomokkal való csatolással lehet magyarázni.

A $[Tl_2\{B\text{-}\beta\text{-}SiW_8O_{30}(OH)\}_2]^{12-}$ szimmetriáját, a Tl és W magok relatív pozícióit, az NMR-aktív magok természetes előfordulásait és a mért csatolási állandókat figyelembe véve szimulált spektrumokat is készítettünk. Valójában a kísérletileg kapott spektrumok nagy számú rész-spektrum szuperpozíciói, melyekben különböző számban és helyen szerepelnek NMR-aktív magok. A szimulált modellünkben csak a Tl-O-Tl és Tl-O-^{183}W csatolásokat vettük figyelembe, így 54 különböző

lehetséges spinrendszert kaptunk. A középponti és szatelit csúcsok közti jól látható alakkülönbség annak tudható be, hogy a ^{183}W magok homonukleárisan csatolt (A_2 spinrendszer) Tl-atomokkal csatolnak, megzavarva a két sztérikusan azonos ^{205}Tl vagy ^{203}Tl mag mágneses ekvivalenciáját, ezzel AA'X spinrendszert eredményezve. Ilyen esetben a Tl-W felhasadás pontosan feleakkora, mint a szatelit jelekben.

Ez a jelenség megfigyelhető a $[Tl_2\{P_2W_{15}O_{57}\}_2]^{22-}$–ban is, viszont ebben az esetben kisebb a távolság a középponti és szatelit jelek közt és a két, csatolási távolságban levő ^{31}P mag (100% természetes előfordulással) további felhasadást eredményez minden tallium jelben. Ez a vegyület is jól láthatóan megőrzi szerkezetét oldatfázisban is, és a kísérletileg kapott ^{203}Tl és ^{205}Tl NMR jelek jól felépíthetőek megfelelő arányú tisztán centrális és szatellit jelek intenzitásainak öszegeként. A Tl-NMR spektrumokban található egy további, kisebb jelcsoport, ami szintén láthatóan két Tl(III) magot tartalmaz, de a jelalakja és a kémiai eltolódása is más.

A $[Tl_2\{B\text{-}\beta\text{-}SiW_8O_{30}(OH)\}_2]^{12-}$ NMR–titrálása, melyben kompetíciós ionként acetátot használtunk, a vegyület stabilitására enged következtetni. Nagy acetát felesleg mellett, több nap alatt sem történt kimutatható reakció. A vegyületet két tallium és két $\{B\text{-}\beta\text{-}SiW_8O_{31}\}$ egység M_2L_2 komplexeként kezelve, ismerve a $Tl(Ac)_4^-$ komplex stabilitását, becsülhető egy $lgK > 40$–es minimum stabilitási állandó. (Érdemes azonban megjegyezni, hogy a poliwolframátok reakciói gyakran extrém lassúak, tehat nem zárható ki „metastabilis", nem egyensúlyi viszonyok kialakulása sem). A látszólagos stabilitási állandó alapján extrapolálható, hogy hígulás miatti disszociáció a vegyületben

csak szub-nanomoláris koncentrációknál válik jelentőssé. Ezek mellett megemlítendő, hogy a $[Tl_2\{B\text{-}\beta\text{-}SiW_8O_{30}(OH)\}_2]^{12-}$ erősen savas közegben állás közben poliwolframátok keverékévé bomlik, melyek ^{205}Tl NMR vizsgálataink szerint már csak egy-egy Tl(III)-t tartalmaznak. Ehhez hónapokat kell várni és a mintákban disszociált talliumot – akár Tl(III) akva ionként, akár Tl_2O_3 oxidként, vagy acetáto-komplexként– továbbra sem lehet kimutatni.

7. References

[1] A. G. Lee, '*The Chemistry of Tha*llium', Elsevier, Amsterdam, NY, **1971**.

[2] A. J. Downs ed., '*Chemistry of Aluminium, Gallium, Indium and Thallium'*, Chapman & Hall, London, **1993**.

[3] J. Glaser 'Advances Thallium Aqueous Solution Chemistry' *Advances in Inorganic Chemistry*, **1995**, Vol. 43, pp. 1–78.

[4] K. Wade and A. J. Banister, *'Comprehensive Inorganic Chemistry'*, ed. J. C. Bailar, Pergamon, Oxford, **1973**, Vol. 1, p. 1119.

[5] J. G. Bednorz and K. A. Müller, '*Earlier and Recent Aspects of Superconductivity'*, Springer-Verlag, Berlin, **1991**.

[6] Glaser, J. 'On the Structure of Thallium(III) Halide Complexes and the Hydration of Thallium(III) in Solution and in Crystals' *Ph.D. Thesis*: KTH, Stockholm, **1981**.

[7] J. Blixt, J. Glaser, J. Mink, I. Persson, P. Persson and M. Sandström 'Structure of Thallium(III) Chloride, Bromide and Cyanide Complexes in Aqueous Solution' *J. Am. Chem. Soc.* **1995**, 117. 5089–5104

[8] R. Jószai 'Multinuclear NMR studies of the structure and fluxionality for the Al(III)– and Tl(III)–aminopolycarboxylate complexes and some metal-metal compounds formed by Tl(III) and transition metal cyanides' *PhD Thesis*, University of Debrecen, **2006.**

[9] P. Nagy 'Kinetics and Mechanisms of Platinum–Thallium Bonded Complexes and Structural Characterization of Some Thallium Cyanides in the Solid State' *PhD Thesis*, University of Debrecen, **2004.**

[10] F. H. Kemper and H. P. Bertram '*Metals and Their Compounds in the Environment'* ed. E. Merian, VCH, Weinheim, **1991**, Chap. II.29.

[11] A. McKillop and E.C. Taylor 'Thallium in Organic Synthesis' *Chem. In Britain*, **1973**, 9, 4.

[12] J. Emsley, '*The Elements'*, 2nd edn., Clarendon Press, Oxford, **1991**.

[13] George J. Taylor *'Primary Care Cardiology'* **2004**, Wiley-Blackwell. p. 100.

[14] Cannon, R. D. *'Electron Transfer Reactions'*; Butterworth-Heinemann, London, **1980**; p 87.

[15] J. Glaser and U. Henrikson 'Thallium-205 nuclear magnetic resonance study of thallium(III) halide complexes in aqueous solutions' *J. Am. Chem. Soc.*, **1981**, 103, 6642.

[16] J. Blixt 'Some aspects of thallium(III) halide and pseudohalide coordination in solution' *PhD Thesis*, KTH, **1993**.

[17] J. Glaser, H. Fjellvåg, A. Kjekshus, T.G. Strand 'Crystal and Molecular Structure of Thallium(III) Bromide Tetrahydrate and Thallium(III) Chloride Tetrahydrate, a Redetermination' *Acta Chem. Scand.*, **1979**, A33, 789-794.

[18] *a)* J. Glaser, B. Aurivillius, E. Wahlström, V.F. Sukhoverkhov 'Crystal and Molecular Structure of Potassium Tetrachlorothallate(III)' *Acta Chem. Scand.,* **1980**, A34, 75; *b)* J. Glaser, G. Johansson 'On the Structures of the Hydrated Thallium(III) Ion and its Bromide Complexes in Aqueous Solution' *Acta Chem. Scand.*, **1982**, A36, 125-135 *c)* J. Glaser, J. Koskikallio 'On the Structures of the Thallium(III) Chloride Complexes in Solution. I. Evidence for Tetrahedral $TlCl_4$(-) and Octahedral $TlCl_6$(3-) Species in Aqueous Solution' *Acta Chem. Scand.,* **1982**, A36, 451-458.

[19] J. Glaser, P. L. Goggin, M. Sandström 'The Structure of the Tetraiodothallate(III) Ion in its Tetrabutylammonium Salt and in a Dichloromethane Solution' *Acta Chem. Scand*., **1982**, A36, 55-62.

[20] J. Blixt, B. Győri, and J. Glaser, 'Determination of stability constants for thallium(III) cyanide complexes in aqueous solution by means of 13C and 205T1 NMR' *J. Am. Chem. Soc.,* **1989**, 111, 7784.

[21] D. G. Tuck, in '*Comprehensive Coordination Chemistry'*, ed. G. Wilkinson, Pergamon, Oxford, **1987**, Vol. 3, Chap. 25.2.

[22] M.A. Maliarik, A.B. Ilyukhin, 'Bis(nitrilotriacetato) Thallium(III) Complexes' *Russian Journal of Inorganic Chemistry* 43(6): 865-874, **1998**

[23] Anderegg, G. 'Critical Survey of Stability Constants of EDTA Complexes' *IUPAC Chemical Data Series 14,* Pergamon Press: Oxford, England, **1977**.

[24] Toth, I.; Brucher, E.; Zekany, L.; Veksin V. 'Equilibrium studies on the Al^{III}-, Ga^{III}-, In^{III}- and Tl^{III}-ethylenediaminetetraacetate-halide and -sulphide systems' *Polyhedron* **1989**, 8, 2057−2064.

[25] Bottari, E.; Anderegg 'Komplexone XLI. Die Komplexe des einwertigen und des dreiwertigen Thalliums mit einigen Polyaminocarboxylaten' *G. Helv. Chim. Acta* **1967**, 50, 2341−2349.

[26] J. Blixt, J. Glaser, P. Solymosi, and I. Tóth 'Equilibria and dynamics of thallium-EDTA ($Tl(edta)X^{2-}$) complexes (X = halide, pseudohalide) studied by multinuclear NMR' *Inorg. Chem.,* **1992**, 31, 5288

[27] P. Pyykkö 'Strong Closed-Shell Interactions in Inorganic Chemistry' *Chem. Rev.,* **1997**, 97, 5976.

[28] J. K. Nagle, A. L. Balch, and M. M. Olmstead '$Tl_2Pt(CN)_4$: A Noncolumnar, Luminescent Form of $Pt(CN)_4^{2-}$ Containing Pt-Tl Bonds' *J. Am. Chem. Soc*., **1988**, 110, 319.

[29] T. Ziegler, J. K. Nagle, J. G. Snijders, and E. J. Baerends 'A Theoretical Study on the Electronic Structures and Absorption Spectra of $Pt(CN)_4^{2-}$ and $Tl_2Pt(CN)_4$ Based on Density Functional Theory Including Relativistic Effects' *J. Am. Chem. Soc*., **1989**, 111, 5631.

[30] A. L. Balch and S. P. Rowley 'Solubilizing the thallium-platinum unit of Tl2Pt(CN)4. Preparation and use of a new crown ether/phosphine hybrid ligand for linking main-group and transition-metal ions' *J. Am. Chem. Soc.*, **1990**, 112, 6139.

[31] M. Maliarik, K. Berg, J. Glaser, M. Sandström, and I. Tóth 'New Class of Oligonuclear Platinum−Thallium Compounds with a Direct Metal−Metal Bond. 2. Structural Characterization of the Complexes' *Inorg. Chem*., **1998**, 37, 2910.

[32] F. Jalilehvand, L. Erikson, J. Glaser, M. Maliarik, J. Mink, M. Sandström, I. Tóth, and J. Tóth 'Tl−Pt(CN)5 in the Solid State—A Multimethod Study of an Unusual Compound Containing Inorganic Wires' *Chem. Eur. J.,* **2001**, 2167.

[33] M. Maliarik, J. Glaser, I. Tóth, M. W. da Silva, and L. Zékány 'New class of oligonuclear platinum-thallium compounds with a direct metal-metal bond. 3. Unusual equilibria in aqueous solution.' *Eur. J, Inorg. Chem*., **1998**, 565.

[34] P. Nagy, I. Tóth, I. Fábián, M. Maliarik, and J. Glaser 'Kinetics and mechanism of formation of the platinum-thallium bond: The $[(CN)_5Pt\text{-}Tl(CN)_3]^{3-}$ complex.' *Inorg. Chem.,* **2003**, 42, 6907.

[35] M. Maliarik 'Compounds with Non-Buttressed Metal-metal bond between Platinum and Thallium. Model Systems for Photoinduced Two-Electron-Transfer' *PhD Thesis*, KTH, **2001**.

[36] J. Autschbach and T. Ziegler 'A theoretical investigation of the remarkable spin-spin coupling pattern in $[(NC)_5Pt\text{-}Tl(CN)]^{-}$' *J. Am. Chem. Soc.,* **2001**, 123, 5320.

[37] M. T. Pope, '*Heteropoly and Isopoly Oxometalates'*, Springer-Verlag, Berlin, **1983**.

[38] M. T. Pope, in '*Comprehensive Coordination Chemistry'*, eds. J. McCleverty and T. J. Meyer, 2nd edition, John Wiley & Sons, Chichester, **2003**, Vol. 4, pp. 635–678.

[39] D. Fenske, M. Gnida, K. Schneider, W. Meyer-Klaucke, J. Schemberg, V. Henschel, A. K. Meyer, A. Knochel, and A. Müller 'A new type of metalloprotein: The Mo storage protein from Azotobacter vinelandii contains a polynuclear molybdenum-oxide cluster' *Chembiochem*, **2005**, 6, 405

[40] J. Schemberg, K. Schneider, U. Demmer, E. Warkentin, A. Müller, and U. Ermler ' Towards Biological Supramolecular Chemistry: A Variety of Pocket-Templated, Individual Metal Oxide Cluster Nucleations in the Cavity of a Mo/W-Storage Protein' *Angew. Chem. Int. Ed*., **2007**, 46, 2408.

[41] H. T. Evans Jr. 'Heteropoly and isopoly complexes of the transition elements of groups 5 and 6.' *Perspect. Struct. Chem*., **1971**, 4, 1.

[42] L. C. W. Baker, J. S. Figgis 'New fundamental type of inorganic complex: hybrid between heteropoly and conventional coordination complexes. Possibilities for geometrical isomerisms in 11-, 12-, 17-, and 18-heteropoly derivatives' *J. Am. Chem. Soc.* **1970**, 92, 3794.

[43] Pope, M. T.; Kortz, U. 'Polyoxometalates', *Encyclopedia of Inorganic and Bioinorganic Chemistry*, John Wiley, **2012**

[44] M. T. Pope, A. Müller '*Polyoxometalates: From Platonic Solids to Antiretroviral Activity'* Kluwer, Dordrecht, **1994**

[45] M. T. Pope, A. Müller *'Polyoxometalate Chemistry: From Topology via Self-Assembly to Applications'* Kluwer, Dordrecht, **2001**

[46] T. Yamase, M. T. Pope *'Polyoxometalate Chemistry for Nano-Composite Design'* Kluwer, Dordrecht, **2002**

[47] J. J. Borras-Almenar, E. Coronado, A. Müller, M. T. Pope '*Polyoxometalate Molecular Science'* Kluwer, Dordrecht, **2004**

[48] S. Mann, R. J. P. Williams, P. R. Sethuraman, and M. T. Pope 'New organo-metallic reagents for electron microscopy' *J. Chem. Soc., Chem. Commun.,* **1981**, 1083.

[49] R. Neumann 'Polyoxometalate Complexes in Organic Oxidation Chemistry' *Prog. Inorg. Chem.,* John Wiley & Sons, **1998**, 47, 317.

[50] D. E. Katsoulis 'A Survey of Applications of Polyoxometalates' *Chem. Rev*., **1998**, 98, 359.

[51] I. V. Kozhevnikov 'Catalysis by Heteropoly Acids and Multicomponent Polyoxometalates in Liquid-Phase Reactions' *Chem. Rev.*, **1998**, 98, 171.

[52] J. B. Moffat, '*Metal-Oxygen Clusters: The Surface and Catalytic Properties of Heteropoly Oxometalates*', Springer, New York, **2001**.

[53] N. Mizuno and K. Kamata 'Catalytic oxidation of hydrocarbons with hydrogen peroxide by vanadium-based polyoxometalates', *Coord. Chem. Rev*., **2011**, 255, 2358.

[54] M. Raynaud, J. C. Cherman, F. Plata, C. Jasmin, and G. Mathé 'Inhibitors of the murine leukemia sarcoma group viruses. Silicotungstates.' *C. R. Acad. Sci., Ser. D*, **1971**, 272, 347.

[55] R. H. Glew, M. A. Czuczman, W. F. Diven, R. L. Berens, M. T. Pope, and D. E. Katsoulis 'Metabolism of lysosomal enzymes in the protein-deficient weanling rat' *Comp. Biochem. Physiol*. **1982**, 72B, 581.

[56] G. Geisberger, S. Paulus, M. Carraro, M. Bonchio, and G. R. Patzke 'Synthesis, Characterisation and Cytotoxicity of Polyoxometalate/Carboxymethyl Chitosan Nanocomposites' *Chem. – Eur. J.,* **2011**, 17, 4619.

[57] J. T. Rhule, C. L. Hill, D. A. Judd, and R. F. Schinazi 'Polyoxometalates in Medicine.' *Chem. Rev.*, **1998**, 98, 327.

[58] A. Flütsch, T. Schröder, M. G. Grüter, and G. R. Patzke ' HIV-1 protease inhibition potential of functionalized polyoxometalates' *Bioorg. Med. Chem. Lett.,* **2011**, 21, 1162.

[59] Merbach A.E., Helm L., Tóth É. *'The chemistry of contrast agents in medical magnetic resonance imaging*' 2nd edn. Wiley, New York, **2013**

[60] (a) Stasiuk, G. J.; Long N. J. 'The ubiquitous DOTA and its derivatives: the impact of 1,4,7,10-tetraazacyclododecane-1,4,7,10-tetraacetic acid on biomedical imaging' *Chem. Commun.* **2013**, 49, 2732−2746. (b) Liu, S. 'Bifunctional coupling agents for radiolabeling of biomolecules and target-specific delivery of metallic radionuclides' *Adv. Drug Delivery Rev*. **2008**, 60, 1347−1370. (c) Lattuada, L.; Barge, A.; Cravotto, G.; Giovenzana, G. B.; Tei, L. 'The synthesis and application of polyamino polycarboxylic

bifunctional chelating agents' *Chem. Soc. Rev.* **2011**, 40, 3019−3049. (d) Viswanathan, S.; Kovacs, Z.; Green, K. N.; Ratnakar, S. J.; Sherry, A. D. 'Alternatives to Gadolinium-based MRI Metal Chelates for Magnetic Resonance Imaging' *Chem. Rev.* **2010**, 110, 2960−3018. (e) Tanaka, K.; Fukase, K. 'PET (positron emission tomography) imaging of biomolecules using metal–DOTA complexes: a new collaborative challenge by chemists, biologists, and physicians for future diagnostics and exploration of in vivo dynamics' *Org. Biomol. Chem*. **2008**, 6, 815−828.

[61] (a) Benetollo, F.; Bombieri, G.; Calabi, L.; Aime, S.; Botta, M. ' Structural Variations Across the Lanthanide Series of Macrocyclic DOTA Complexes: Insights into the Design of Contrast Agents for Magnetic Resonance Imaging' *Inorg. Chem.* **2003**, 42, 148−157. (b) Aime, S.; Barge, A.; Botta, M.; Fasano, M.; Ayala, J. D.; Bombieri, G. 'Crystal structure and solution dynamics of the lutetium(III) chelate of DOTA' *Inorg. Chim. Acta* **1996**, 246, 423−429.

[62] Parker, D.; Pulukkody, K.; Smith, F. C.; Batsanov, A.; Howard, J. A. K. 'Structures of the yttrium complexes of 1,4,7,10-tetraazacyclododecane-*N*,*N*′,*N*″,*N*‴-tetraacetic acid (H_4dota) and *N*,*N*″-bis(benzylcarbamoylmethyl)diethylenetriamine-*N*,*N*′,*N*″-triacetic acid and the solution structure of a zirconium complex of H_4dota' *J. Chem. Soc., Dalton Trans*. **1994**, 689−693.

[63] Heppeler, A.; André, J. P.; Buschmann, I.; Wang, X.; Reubi, J.-C.; Henning, M.; Kaden, T. A.; Maecke, H. R. 'Metal-ion-dependent biological properties of a chelator-derived somatostatin analogue for tumour targeting' *Chem.–Eur. J.* **2008**, 14, 3026−3034.

[64] Csajbok, E.; Baranyai, Z.; Banyai, I.; E. Brücher, E.; Kiraly, R.; Müller-Fahrnow, A.; Platzek, J.; Radüchel, B.; Schäfer M. 'Equilibrium, ^{1}H and ^{13}C NMR Spectroscopy, and X-ray Diffraction Studies on the Complexes Bi(DOTA)$^-$ and Bi(DO3A-Bu)' *Inorg. Chem.* **2003**, 42, 2342−2349.

[65] Anderson, O. P.; Reibenspies, J. H. '$\{Ca(OH_2)_3[Ca(DOTA)].7.7H_2O\}_n$' *Acta Crystallogr*. **1996**, C52, 792−795.

[66] Burai, L.; Tóth, E.; Moreau, G.; Sour, A.; Scopelliti, R.; Merbach, A. E. 'Novel macrocyclic EuII complexes: fast water exchange related to an extreme metal-coordinated water oxygen distance' *Chem.–Eur. J.* **2003**, 9, 1394−1404.

[67] Riesen, A.; Zehnder, M.; Kaden, T. A. 'Structures of two Zn^{2+} complexes with two tetraaza macrocyclic tetraacetates' *Acta Crystallogr.* **1991**, C47, 531−533.

[68] Chang, C. A.; Francesconi, L. C.; Malley, M. F.; Kumar, K.; Gougoutas, J. Z.; Tweedle, M. F. 'Synthesis, Characterization, and Crystal Structures of M(DO3A) (M = Fe, Gd) and Na[M(DOTA)] (M = Fe, Y, Gd)' *Inorg. Chem.* **1993**, 32, 3501−3508.

[69] Riesen, A.; Zehnder, M.; Kaden, T. A. 'Metal complexes of macrocyclic ligands. Part XXIII[†]. Synthesis, properties, and structures of mononuclear complexes with 12- and 14-membered tetraazamacrocycle-*N*,*N*′,*N*″,*N*‴-tetraacetic Acids' *Helv. Chim. Acta* **1986**, 69, 2067−2073.

[70] Viola-Villegas, N.; Doyle, R. P. 'The coordination chemistry of 1,4,7,10-tetraazacyclododecane-N,N′,N″,N‴-tetraacetic acid (H_4DOTA): Structural overview and analyses on structure–stability relationships' *Coord. Chem. Rev*. **2009**, 253, 1906−1925.

[71] (a) Kubicek, V.; Havlickova, J.; Kotek, J.; Tircso, G.; Hermann, P.; Toth, E.; Lukes, I. 'Gallium(III) Complexes of DOTA and DOTA−Monoamide: Kinetic and Thermodynamic Studies' *Inorg. Chem*. **2010**, 49, 10960−10969. (b) Drahos, B.; Kubicek, V.; Bonnet, C. S.; Hermann, P.; Lukes, I.; Toth, E. ' Dissociation kinetics of Mn2+ complexes of NOTA and DOTA' *Dalton Trans*. **2011**, 40, 1945−1951. (c) Toth, E.; Brucher, E.; Lazar, I.; Toth, I. 'Kinetics of Formation and Dissociation of Lanthanide(III)-DOTA Complexes' *Inorg. Chem*. **1994**, 33, 4070−4076. (d) Brucher, E.; Laurenczy, G.; Makra, Z. 'Studies on the kinetics of formation and dissociation of the cerium(III)-DOTA complex' *Inorg. Chim. Acta* **1987**, 139, 141−142.

[72] (a) Voracova, I.; Vanek, J.; Pasulka, J.; Strelcova, Z.; Lubal, P.; Hermann, P. 'Dissociation kinetics study of copper(II) complexes of DO3A, DOTA and its monosubstituted derivatives' *Polyhedron* **2013**, 61, 99−104. (b) Pniok, M.; Kubicek, V.; Havlickova, J.; Kotek, J.; Sabatie-Gogova, A.; Plutnar, J.; Huclier-Markai, S.; Hermann, P. 'Thermodynamic and Kinetic Study of Scandium(III) Complexes of DTPA and DOTA: A Step Toward Scandium Radiopharmaceuticals' *Chem.–Eur. J.* **2014**, 20, 7944−7955.

[73] (a) Wang, X.; Jin, T.; Comblin, V.; Lopez-Mut, A.; Merciny, E.; Desreux, J. F. 'A Kinetic Investigation of the Lanthanide DOTA Chelates. Stability and Rates of Formation and of Dissociation of a Macrocyclic Gadolinium(III) Polyaza Polycarboxylic MRI Contrast Agent' *Inorg. Chem*. **1992**, 31, 1095−1099. (b) Wu, S. L.; Horrocks, W., Jr. 'Kinetics of Complex Formation by Macrocyclic Polyaza Polycarboxylate Ligands: Detection and Characterization of an Intermediate in the Eu3+-dota System by Laser-Excited Luminescence' *Inorg. Chem.* **1995**, 34, 3724−3732. (c) Moreau, J.; Guillon, E.; Pierrard, J.-C.; Rimbault, J.; Port, M.; Aplincourt, 'Complexing Mechanism of the Lanthanide Cations Eu^{3+}, Gd^{3+}, and Tb^{3+} with 1,4,7,10-Tetrakis(carboxymethyl)-1,4,7,10-tetraazacyclododecane (dota)—Characterization of Three Successive Complexing Phases: Study of the Thermodynamic and Structural Properties of the Complexes by Potentiometry, Luminescence Spectroscopy, and EXAFS' *M. Chem.–Eur. J*. **2004**, 10, 5218−5232.

[74] Martins, A. F.; Prata, M. I. M.; Rodrigues, S. P. J.; Geraldes, C.; Riss, P. J.; Amor-Coarasa, A.; Burchardt, C.; Kroll, C.; Rösch, F. 'Spectroscopic, radiochemical, and theoretical studies of the Ga^{3+}-*N*-2-hydroxyethyl piperazine-*N*′-2-ethanesulfonic acid (HEPES buffer) system: evidence for the formation of Ga^{3+}- HEPES complexes in ^{68}Ga labeling reactions' *Contrast Media Mol. Imaging* **2013**, 8, 265−273.

[75] (a) Benazeth, S.; Purans, J.; Chalbot, M.-C.; Nguyen-van-Duong, M. K.; Nicolas, L.; Keller, F.; Gaudemer, A. 'Temperature and pH Dependence XAFS Study of Gd(DOTA)(-) and Gd(DTPA)(2)(-) Complexes: Solid State and Solution Structures' *Inorg. Chem*. **1998**, 37, 3667−3674. (b) Aime, S.; Botta, M.; Ermondi, G. 'NMR Study of Solution Structures and Dynamics of Lantbanide(II1) Complexes of DOTA ' *Inorg. Chem.* **1992**, 31, 4291−4299. (c) Hoeft, S.; Roth, K. 'Struktur und Dynamik von Lanthanoid-Tetraazacyclododecantetraacetat-(DOTA-)Komplexen in Lösung' *Chem.*

Ber. **1993**, 126, 869−873. (d) Fusaro, L.; Luhmer, M. '^{17}O NMR Study of Diamagnetic and Paramagnetic Lanthanide(III)–DOTA Complexes in Aqueous Solution' *Inorg. Chem*. **2014**, 53, 8717− 8722. (e) Aime, S.; Botta, M.; Fasano, M.; Marques, M. P. M.; Geraldes, C. F. G. C.; Purbanz, D.; Merbach, A. E. 'Conformational and Coordination Equilibria on DOTA Complexes of Lanthanide Metal Ions in Aqueous Solution Studied by (1)H-NMR Spectroscopy**.**' *Inorg. Chem.* **1997**, 36, 2059−2068. (f) Mayer, F.; Platas-Iglesias, C.; Helm, L.; Peters, J. A.; Djanashvili, K. '^{17}O NMR and Density Functional Theory Study of the Dynamics of the Carboxylate Groups in DOTA Complexes of Lanthanides in Aqueous Solution' *Inorg. Chem*. **2012**, 51, 170−178. (g) Esteban-Gomez, D.; de Blas, A.; Rodriguez-Blas, T.; Helm, L.; Platas-Iglesias, C. 'Hyperfine Coupling Constants on Inner-Sphere Water Molecules of Gd^{III}-Based MRI Contrast Agents' *ChemPhysChem* **2012**, 13, 3640−3650. (h) Powell, D. H.; Ni Dhubhghaill, O. M.; Pubanz, D.; Helm, L.; Lebedev, Y. S.; Schlaepfer, W.; Merbach, A. E. 'Structural and Dynamic Parameters Obtained from ^{17}O NMR, EPR, and NMRD Studies of Monomeric and Dimeric Gd^{3+} Complexes of Interest in Magnetic Resonance Imaging: An Integrated and Theoretically Self-Consistent Approach' *J. Am. Chem. Soc.* **1996**, 118, 9333−9346.

[76] Breeman, W. A. P.; De Blois, E.; Sze Chan, H.; Konijnenberg, M.; Kwekkeboom, D. J.; Krenning, E. P. '68Ga-labeled DOTA-Peptides and 68Ga-labeled Radiopharmaceuticals for Positron Emission Tomography: Current Status of Research, Clinical Applications, and Future Perspectives'. *Seminars in Nuclear Medicine.* **2011**, 41 (4): 314–321.

[77] Bodei, L.; Cremonesi, M.; Grana, C. M.; Fazio, N.; Iodice, S.; Baio, S. M.; Bartolomei, M.; Lombardo, D.; Ferrari, M. E.; Sansovini, M.; Chinol, M.; Paganelli, G. 'Peptide receptor radionuclide therapy with ^{177}Lu-DOTATATE: The IEO phase I-II study'. *European Journal of Nuclear Medicine and Molecular Imaging*. **2011**, 38 (12): 2125–2135.

[78] D'Souza C.A., McBride W.J., Sharkey R.M., Todaro L.J., Goldenberg D.M. 'High-Yielding Aqueous ^{18}F-Labeling of Peptides via Al^{18}F Chelation' *Bioconjugate Chem* **2011** 22:1793–1803

[79] Dijkgraaf I., Terry S.Y.A., McBride W.J., Goldenberg D.M., Laverman P., Franssen G.M., Oyen W.J.G.,Boerman O.C. 'Imaging integrin alpha-v-beta-3 expression in tumors with an ^{18}F-labeled dimeric RGD peptide' *Contrast Media Mol Imaging* **2013**, 8:238–245

[80] Glaser, J. 'On the structures of thallium(III) halide complexes and the hydration of thallium(III) in solution and in crystals' *PhD Thesis*, The Royal Institute of Technology (KTH), Stockholm, **1981**, p. 15

[81] Horvat, H. *Diploma work*: Investigation of the decomposition of the $[NaTl(edta)]^-$ complex, University of Debrecen, Debrecen, Hungary, **2010**.; https://dea.lib.unideb.hu/dea/handle/2437/101064

[82] Irving, H.M.; Miles, M.G.; Pettit, L.D. 'A study of some problems in determining the stoicheiometric proton dissociation constants of complexes by potentiometric titrations using a glass electrode' *Anal. Chim. Acta* **1967**, 38, 475−488.

[83] Reeves L. W.; Shaw K. N. 'Nuclear magnetic resonance studies of multisite chemical exchange. I. Matrix formulation of the Bloch equations' *Can. J. Chem*. **1970.** 48, 3641-3643.

[84] Kathó, Á.; Bényei, A. C.; Joó, F.; Sági, M. 'Formation and Solid State Structures of Highly Crystalline Guanidinium Salts of Sulfonated Tertiary Phosphanes' *Adv. Synth. Catal.* **2002**, *344*, 278-282.

[85] Altomare, A.; Cascarano, G.; Giacovazzo, C.; Guagliardi, A. 'Completion and refinement of crystal structures with SIR92' *J. Appl. Cryst.* **1993**, *26*, 343-350.

[86] Sheldrick, G.M. 'A short history of SHELX' *Acta Cryst.* **2008**, *A64*, 112-122.

[87] Tao, J.M.; Perdew, J.P.; Staroverov, V.N.; Scuseria, G.E. 'Climbing the Density Functional Ladder: Nonempirical Meta–Generalized Gradient Approximation Designed for Molecules and Solids' *Phys. Rev. Lett.* **2003**, *91*, 146401.

[88] Gaussian 09, Revision A.01, Frisch, M.J.; Trucks, G.W.; Schlegel, H.B.; Scuseria, G.E.; Robb, M.A.; Cheeseman, J.R.; Scalmani, G.; Barone, V.; Mennucci, B.; Petersson, G. A.; Nakatsuji, H.; Caricato, M.; Li, X.; Hratchian, H.P.; Izmaylov, A.F.; Bloino, J.; Zheng, G.; Sonnenberg, J.L.; Hada, M.; Ehara, M.; Toyota, K.; Fukuda, R.; Hasegawa, J.; Ishida, M.; Nakajima, T.; Honda, Y.; Kitao, O.; Nakai, H.; Vreven, T.; Montgomery, Jr., J.A.; Peralta, J.E.; Ogliaro, F.; Bearpark, M.; Heyd, J.J.; Brothers, E.; Kudin, K.N.; Staroverov, V.N.; Kobayashi, R.; Normand, J.; Raghavachari, K.; Rendell, A.; Burant, J.C.; Iyengar, S.S.; Tomasi, J.; Cossi, M.; Rega, N.; Millam, N.J.; Klene, M.; Knox, J.E.; Cross, J.B.; Bakken, V.; Adamo, C.; Jaramillo, J.; Gomperts, R.; Stratmann, R.E.; Yazyev, O.; Austin, A.J.; Cammi, R.; Pomelli, C.; Ochterski, J.W.; Martin, R.L.; Morokuma, K.; Zakrzewski, V.G.; Voth, G.A.; Salvador, P.; Dannenberg, J.J.; Dapprich, S.; Daniels, A.D.; Farkas, Ö.; Foresman, J.B.; Ortiz, J.V.; Cioslowski, J.; Fox, D.J. Gaussian, Inc., Wallingford CT, **2009**.

[89] Ross, R.B.; Powers, J.M.; Atashroo, T.; Ermler, W.C.; LaJohn, L.A.; Christiansen, P.A. 'Ab initio relativistic effective potentials with spin-orbit operators' *J.Chem. Phys.* **1990**, *93*, 6654-6670.

[90] (a) Peng, C.; Ayala, P.Y.; Schlegel, H.B.; Frisch, M.J. ' Using redundant internal coordinates to optimize equilibrium geometries and transition states' *J. Comput. Chem*. **1996**, *17*, 49-56; (b) Peng, C.; Schlegel, H. B. ' Combining synchronous transit and quasi-newton methods for finding transition states' *Isr. J. Chem*. **1994**, *33*, 449-454.

[91] Wolinski, K.; Hilton, J.F.; Pulay, P. 'Efficient implementation of the gauge-independent atomic orbital method for NMR chemical shift calculations' *J. Am. Chem. Soc.* **1990**, *112*, 8251-8260.

[92] Tomasi, J.; Mennucci, B.; Cammi, R. 'Quantum mechanical continuum solvation models' *Chem. Rev.* **2005**, *105*, 2999-3093.

[93] Parker, D.; Dickins, R.S.; Puschmann, H.; Crossland, C.; Howard, J.A.K. 'Being Excited by Lanthanide Coordination Complexes: Aqua Species, Chirality, Excited-State Chemistry, and Exchange Dynamics' *Chem Rev.* **2002**, *102*, 1977-2010.

[94] Shannon, R. D. 'Revised effective ionic radii and systematic studies of interatomic distances in halides and chalcogenides' *Acta Cryst.* **1976**, *A32*, 751-767.

[95] Aime, S.; Barge, A.; Benetollo, F.; Bombieri, G.; Botta, M.; Uggeri, F. 'A Novel Compound in the Lanthanide(III) DOTA Series. X-ray Crystal and Molecular Structure of the Complex Na[La(DOTA)La(HDOTA)]·10H_2O' *Inorg. Chem.* **1997**, *36*, 4287-4289.

[96] a) Vojtisek, P.; Cigler, P.; Kotek, J.; Rudovsky, J.; Hermann, P.; Lukes, I. 'Crystal Structures of Lanthanide(III) Complexes with Cyclen Derivative Bearing Three Acetate and One Methylphosphonate Pendants' *Inorg. Chem.* **2005**, *44*, 5591-5599; b) Kotek, J.; Rudovsky, J.; Hermann, P.; Lukes, I. 'Three in One: TSA, TSA', and SA Units in One Crystal Structure of a Yttrium(III) Complex with a Monophosphinated H4dota Analogue' *Inorg. Chem.* **2006**, *45*, 3097-3102.

[97] Parr, R.G.; Pearson, R.G. 'Absolute hardness: companion parameter to absolute electronegativity' *J. Am. Chem. Soc.* **1983**, *105*, 7512-7516.

[98] Glaser, J. '*Advances in Inorganic Chemistry'*, Sykes, G. Ed., Academic Press: San Diego, CA, **1995**, Vol. 43, pp. 1–78

[99] Jalilehvand, F.; Maliarik, M.; Sandström, M.; Mink, J.; Persson, I.; Persson, P.; Tóth, I.; Glaser, J. 'New Class of Oligonuclear Platinum-Thallium Compounds with a Direct Metal-Metal Bond. Structure of Heterodimetallic Cyano Complexes in Aqueous Solution by EXAFS and Vibrational Spectroscopy' *Inorg. Chem.* **2001**, *40*, 3889-3899.

[100] Blixt, J.; Dubey, R.K.; Glaser, J. 'Oxidation of Thiocyanate by Thallium(III) in Aqueous Solution Studied by Multinuclear NMR Spectroscopy. Evidence for a $Tl(SCN)^{2+}$ Intermediate' *Inorg. Chem.* **1991**, *30*, 2824-2826.

[101] Nagy, P.; Joszai, R.; Fabian, I.; Toth, I.; Glaser, J. 'The decomposition and formation of the platinum–thallium bond in the $[(CN)_5Pt–Tl(edta)]^{4–}$ complex: kinetics and mechanism' *J. Mol. Liq.* **2005**, *118*, 195-207.

[102] Hijnen, N.M.; de Vries, A.; Blange, R.; Burdinski, D.; Grüll, H. 'Synthesis and in vivo evaluation of ^{201}Tl(III)–DOTA complexes for applications in SPECT imaging' *Nucl. Med. Biol.* **2011**, *38*, 585-592.

[103] Banyai, I.; Glaser, J. 'Equilibrium dynamics in the thallium(III)-bromide system in acidic aqueous solution. A thallium-205 NMR study' *J. Am. Chem. Soc.* **1990**, *112*, 4703-4710.

[104] Banyai, I.; Blixt, J.; Glaser, J.; Toth, I. 'On the Dissociation of Hydrogen Cyanide in Aqueous Solutions Containing Different Ionic Media. A Combined Potentiometric and Carbon-13 NMR Study' *Acta Chem Scand.* **1992**, *46*, 138-141.

[105] Toth, I.; Brucher, E.; Zekany, L.; Veksin, V. 'Equilibrium studies on the Al^{III}-, Ga^{III}-, In^{III}- and Tl^{III}-ethylenediaminetetraacetate-halide and -sulphide systems' P*olyhedron* **1989**, *8*, 2057-2064.

[106] (a) Karplus, M. 'Vicinal Proton Coupling in Nuclear Magnetic Resonance' *J. Am. Chem. Soc.* **1963**, *85*, 2870−2871; (b) Geraldes, C.F.G.C.; Sherry, A.D.; Kiefer, G.E.

'The solution structure of Ln (DOTP)$^{5-}$ complexxes. A comparison of lanthanide-induced paramagnetic shifts with the MMX energy-minimized structure' *J. Magn. Reson.* **1992**, *97*, 290−304.

[107] Rodríguez-Rodríguez, A.; Esteban-Gomez, D.; de Blas, A.; Rodriguez-Blas, T.; Fekete, M.; Botta, M.; Tripier, R.; Platas-Iglesias, C. *Inorg. Chem.* **2012**, *51*, 2509-2521.

[108] Rodríguez-Rodríguez, A.; Esteban-Gomez, D.; de Blas, A.; Rodriguez-Blas, T.; Botta, M.; Tripier, R.; Platas-Iglesias, C. 'Solution Structure of Ln(III) Complexes with Macrocyclic Ligands Through Theoretical Evaluation of ^{1}H NMR Contact Shifts' *Inorg. Chem.* **2012**, *51*, 13419-13429.

[109] van Wüllen, C. 'On the use of effective core potentials in the calculation of magnetic properties, such as magnetizabilites and magnetic shieldings' *J. Chem. Phys.* **2012**, *136*, 114110.

[110] Purgel, M.; Baranyai, Z.; de Blas, A.; Rodriguez-Blas, T.; Banyai, I.; Platas-Iglesias, C.; Toth, I. 'An NMR and DFT Investigation on the Conformational Properties of Lanthanide(III) 1,4,7,10-Tetraazacyclododecane-1,4,7,10-tetraacetate Analogues Containing Methylenephosphonate Pendant Arms' *Inorg. Chem.* **2010**, *49*, 4370-4382.

[111] Platas-Iglesias, C. 'The Solution Structure and Dynamics of MRI Probes Based on Lanthanide(III) DOTA as Investigated by DFT and NMR Spectroscopy' *Eur. J. Inorg. Chem.* **2012**, 2023-2033.

[112] a) Regueiro-Figueroa, M.; Esteban-Gómez, D.; de Blas, A.; Rodríguez-Blas, T.; Platas-Iglesias, C. 'Structure and Dynamics of Lanthanide(III) Complexes with an *N*-Alkylated do3a Ligand (H_3do3a = 1,4,7,10-Tetraazacyclododecane-1,4,7-triacetic Acid): A Combined Experimental and DFT Study' *Eur. J. Inorg. Chem.* **2010**, 3586-3595; b) Regueiro-Figueroa, M.; Bensenane, B.; Ruscsák, E.; Esteban-Gómez, D.; Charbonnière, L. J.; Tircsó, G.; Tóth, I.; de Blas, A.; Rodríguez-Blas, T.; Platas-Iglesias, C. 'Lanthanide dota-like Complexes Containing a Picolinate Pendant: Structural Entry for the Design of Ln^{III}-Based Luminescent Probes' *Inorg. Chem.* **2011**, *50*, 4125-4141; c) Lima, L.M.P.; Lecointre, A.; Morfin, J.-F.; de Blas, A.; Visvikis, D.; Charbonnière, L.J.; Platas-Iglesias, C.; Tripier, R. 'Positively Charged Lanthanide Complexes with Cyclen-Based Ligands: Synthesis, Solid-State and Solution Structure, and Fluoride Interaction' *Inorg. Chem.* **2011**, *50*, 12508-12521; d) Cosentino, U.; Villa, A.; Pitea, D.; Moro, G.; Barone, V.; Maiocchi, A. *J. Am. Chem. Soc*. **2002**, *124*, 4901-4909; e) Natrajan, L.S.; Khoabane, N.M.; Dadds, B.L.; Muryn, C.A.; Pritchard, R.G.; Heath, S.L.; Kenwright, A.M.; Kuprov, I.; Faulkner, S. 'Probing the Structure, Conformation, and Stereochemical Exchange in a Family of Lanthanide Complexes Derived from Tetrapyridyl-Appended Cyclen' *Inorg. Chem.* **2010**, *49*, 7700-7709; f) Di Vaira, M.; Stoppioni, P. 'Theoretical investigation on the geometries of DOTA and DOTA-like complexes and on the transition states of their conformational equilibria' *New J. Chem.* **2002**, *26*, 136-144.

[113] A. Rodríguez-Rodríguez, D. Esteban-Gómez, R. Tripier, G. Tircsó, Z. Garda, I. Tóth, A. de Blas, T. Rodríguez-Blas, and C. Platas-Iglesias 'Lanthanide(III) Complexes with a Reinforced Cyclam Ligand Show Unprecedented Kinetic Inertness' *J. Am. Chem. Soc.*, **2014**, 136 (52), pp 17954–17957.

[114] Laverman P., McBride W.J., Sharkey R.M., Eek A., Joosten L., Oyen W.J.G., Goldenberg D.M., Boerman O.C. 'A Novel Facile Method of Labeling Octreotide with ^{18}F-Fluorine' *J. Nucl. Med.* **2010**, 51:454–461

[115] Nemes J., Tóth I., Zékány L. 'Formation kinetics of an aluminium(III)-ethylenedinitrilotetraacetatefluoride mixed ligand complex' *J. Chem. Soc. Dalton Trans.* **1998,** 2707-2713

[116] Bodor A., Tóth I., Bányai I., Szabó Z., Hefter G.T. '^{19}F NMR Study of the Equilibria and Dynamics of the Al^{3+}/F^- System' *Inorg. Chem.* **2000**, 39:530–2537

[117] Rorabacher D.B., MacKellar W.J., Shu F.R., Bonavita S.M. 'Solvent effects on protonation constants. Ammonia, acetate, polyamine, and polyaminocarboxylate ligands in methanol-water mixtures' *Anal. Chem*. **1971**, 43:561–573

[118] Shivahare, G. C. 'Electrometric studies on tungstates of thallium (I) and the effect of ageing' *Naturwissenschaften*, **1964**, 51, 406

[119] Bierstedt, P.E.; Bither, T.A.; Darnell, F.J. 'Superconductivity of some new hexagonal tungsten bronzes' *Solid State Comm.* **1966**, *4*, 25-26

[120] Bassil, B.S.; Nellutla, S.; Kortz, U.; Stowe, A. C.; van Tol, J.; Dalal, N. S.; Keita, B.; Nadjo, L. 'The Satellite-Shaped Co-15 Polyoxotungstate, $[Co_6(H_2O)_{30}\{Co_9Cl_2(OH)_3(H_2O)_9(\beta\text{-}SiW_8O_{31})_3\}]^{5-}$' *Inorg. Chem.* **2005**, *44*, 2659-2665.

[121] Winter, R.S. Long, D.L. Cronin, L. 'Synthesis and Characterization of a Series of $[M_2(\beta\text{-}SiW_8O_{31})_2]^{n-}$ Clusters and Mechanistic Insight into the Reorganization of $\{\beta\text{-}SiW_8O_{31}\}$ into $\{\alpha\text{-}SiW_9O_{34}\}$' *Inorg. Chem.* **2015**, *54*, 4151-4155.

[122] Brown, I.D.; Altermatt, D. 'Bond-valence parameters obtained from a systematic analysis of the Inorganic Crystal Structure Database' *Acta Crystallogr.* **1985**, *B41*, 244-247.

[123] Fox, A.R.; Wright, R.J.; Rivard, E.; Power, P.P. '$Tl_2[Aryl_2P_4]$: A Thallium Complexed Diaryltetraphosphabutadienediide and its Two-Electron Oxidation to a Diaryltetraphosphabicyclobutane, $Aryl_2P_4$' *Angew. Chem. Int. Ed.* **2005**, *44*, 7729-7733.

[124] Hinton, J. F. 'Thallium NMR Spectroscopy' *Bulletin of Magnetic Resonance*, **1992**, *13*, 90-108.

[125] Schneider, W. G.; Buckingham, A.D. 'Mercury, thallium and lead resonances' *Discuss. Faraday Soc.* **1962**, *34*, 147-155.

[126] van Hal, J.W.; Alemany, L.B.; Whitmire, K.H. 'Solution Dynamics of Thallium-Metal Carbonyl Compounds Using (205)Tl NMR Spectroscopy' *Inorg. Chem.* **1997**, *36*, 3152-3159.

[127]) (a) Ito, T.; Yamase, T. 'Investigation of Intermediates Involved in the Photochemical Formation of Mo-Blue Nanoring by Capillary Electrophoresis–Mass Spectrometry' *Eur. J. Inorg. Chem.* **2009**, 5205–5210; (b) Yan, J.; Gao, J.; Long, D.L.; Miras H.N.; Cronin, L. 'Self-Assembly of a Nanosized, Saddle-Shaped, Solution-Stable Polyoxometalate Anion Built from Pentagonal Building Blocks: $[H_{34}W_{119}Se_8Fe_2O_{420}]^{54-}$' *J. Am. Chem. Soc.* **2010**, *132*, 11410–11411; (c) Cao, J.; Li, C.; Zhang, Z.; Xu, C.; Yan,

J.; Cui, F.; Hu, C. 'Intriguing role of a quaternary ammonium cation in the dissociation chemistry of keggin polyoxometalate anions.' *J. Am. Soc. Mass Spectrom.* **2012**, *23*, 366–374. (d) Lin, Z.; Wang, B.; Cao, J.; Chen, B.; Xu, C.; Huang, X.; Fan, Y.; Hu, C. 'Controlled Synthesis of Polyoxopalladates, and Their Gas-Phase Fragmentation Study by Electrospray Ionization Tandem Mass Spectrometry' *Eur. J. Inorg. Chem.* **2013**, 3458–3463; (e) Cao, J.; Xu, C.; Fan, Y.; Fan, L.; Zhang, X.; Hu, C. 'Selective Production of Electrostatically-Bound Adducts of Alkyl Cations/Polyoxoanions by the Collision-Induced Fragmentations of Their Quaternary Ammonium Counterparts' *J. Am. Soc. Mass Spectrom.* **2013**, *24*, 884–894.

[128] Kohguchi, K.; Ede, K.I.; Sagara, Y.; Nakamura, M. 'EFFECT OF THALLIUM ACETATE ON THE GROWTH OF BACTERIA' *Kurume Med. J.* **1969**, *16*, 163-168.

[129] Al-Karablieh, N.; Weingart, H, Ullrich, M.S. ' The outer membrane protein TolC is required for phytoalexin resistance and virulence of the fire blight pathogen Erwinia amylovora' *Microb. Biotechnol.* **2009**, *2*, 465-475.

8. Scientific publications of Tamás Fodor

(in reverse chronological order)

8.1. Papers related to the dissertation

3. Wassim W. Ayass**,** Tamás **Fodor**, Zhengguo Lin, Rachelle M. Smith, Linyuan Fan, Jie Cao, Imre Tóth, László Zékány, Magda Pascual-Borràs, Antonio Rodríguez-Fortea, Josep M. Poblet, and Ulrich Kortz:
Introducing Thallium in Discrete Metal-Oxide Chemistry: The Tl^{3+}-Containing $[Tl_2\{B\text{-}\beta\text{-}SiW_8O_{30}(OH)\}_2]^{12-}$,
Inorganic Chemistry (beküldve/submitted) IF: 4.820 (2015)

2. Tamás **Fodor**, István Bányai, Attila Bényei, Carlos Platas-Iglesias, Mihály Purgel, Gábor Horváth, László Zékány, Gyula Tircsó and Imre Tóth:
$[Tl^{III}(dota)]^-$: An extraordinary robust macrocyclic complex
Inorg. Chem., **2015,** *54 (11),* pp 5426–5437. IF: 4.762 (2014)

1. Edit Farkas, Tamás **Fodor**, Ferenc K. Kálmán*, Gyula Tircsó and Imre Tóth:
Equilibrium and Dissociation Kinetics of [Al(1,4,7-triazacyclononane-1,4,7-triacetate)] ([Al(nota)]) Complex,
Reaction Kinetics, Mechanisms and Catalysis, **2015,** *116(1),* 19-33. IF: 0.983 (2013)

8.2. Presentations related to the dissertation

5. **Fodor** Tamás, Ayass W. W., Zékány László, Bodor Andrea, Kortz U., Tóth Imre:
Dimer vagy monomer? $^{203/205}$Tl NMR homo- és heteronukleáris spin-spin csatolások heteropolimetallátok oldataiban
50. Komplexkémiai Kollokvium, Balatonvilágos, 2016. május 30-június 1,

4. T. **Fodor**, W. W. Ayass, L. Zékány, A. Bodor, U. Kortz and I. Tóth: **Homonuclear and heteronuclear Tl-Tl NMR spin-spin coupling as structural tool in solution**

Magyar NMR Munkabizottság 2016. évi ülése, MTA DAB Székház, Debrecen, 2016. május 20-21.

3. **Fodor** Tamás, Rozinka Felícia, Carlos Platas-Iglesias, Zékány László, Bényei Attila, Purgel Mihály, Kálmán Ferenc Krisztián, Tircsó Gyula, Tóth Imre: **Vegyesligandumú Tl(III)-komplexek egyensúlyi és kinetikai vizsgálata,** *20. Nemzetközi Vegyészkonferencia*, **2014,** November 6-9, Kolozsvár, Románia.

2. **Fodor** Tamás, Garda Zoltán, Rozinka Felícia, Kálmán Ferenc Krisztián, Kovács Zoltán, Tircsó Gyula és Tóth Imre: **Vegyesligandumú tallium(III)-komplexek egyensúlyi és kinetikai vizsgálata,** *XLVIII Komplexkémiai Kollokvium*, **2014,** Május 28-30, Siófok, Magyarország.

1. Tamás **Fodor**, Carlos Platas-Iglesias, Mihály Purgel, László Zékány, Attila Bényei, Imre Tóth:
TlDOTA: an extraordinarily stable complex
XLVI. Komplexkémiai Kollokvium, **2012,** Május 21-23, Mátrafüred, Magyarország

8.3. Posters related to the dissertation

5. Tamás **Fodor**, Zoltán Garda, Felícia Rozinka, Gyula Tircsó, Imre Tóth
Ternary complexes as anion binders: a new approach to radiolabeling
Medicinal flavor of metal complexes: diagnostic and therapeutic applications, **2015**. december 7-9., Orleans; Franciaország

4. Edit Farkas, Tamás **Fodor**, Ferenc K. Kálmán, Gyula Tircsó, Imre Tóth
Equilibrium and Dissociation Kinetics of [Al(nota)] Complex
Medicinal flavor of metal complexes: diagnostic and therapeutic applications, **2015**. december 7-9., Orleans; Franciaország

3. Edit Farkas, Tamás **Fodor**, Ferenc K. Kálmán, Gyula Tircsó and Imre Tóth
Equilibrium and Dissociation Kinetics of [Al(nota)] Complex
COST Action TD1004, **2015**. szeptember 10-11., Belgrád, Szerbia

2. **Fodor** Tamás, Farkas Edit Carlos Platas Iglesias, Zékány László, Purgel Mihály, Bényei Attila, Kálmán Ferenc Krisztián, Tircsó Gyula**,** Tóth Imre: **Vegyesligandumú fémkomplexek, mint lehetséges izotóphordozók,** *19. Nemzetközi Vegyészkonferencia*, **2013,** November 21-24, Nagybánya, Románia.

1. Tamás **Fodor**, Edit Farkas, Gyula Tircsó**,** Carlos Platas Iglesias, Mihály Purgel, László Zékány, Attila Bényei, Imre Tóth:
Mixed ligand metal-complexes modeling anion binding: the hard aluminum(III) and the soft thallium(III)
11th International Symposium on the Synthesis and Applications of Isotopes and Isotopically Labelled Compounds, September 9-13, **2012,** Heidelberg/Freiburg, Germany

8.4. Paper not involved in the dissertation

1. Enikő Molnár, Nathalie Camus, Véronique Patinec, Gabriele A. Rolla, Mauro Botta, Gyula Tircsó***,** Ferenc K. Kálmán, Tamás **Fodor**, Raphaël Tripier***** and Carlos Platas-Iglesias*****:
Picolinate-Containing Macrocyclic Mn2+ Complexes as Potential MRI Contrast Agents
Inorg. Chem. **2014,** *53,* 5136−5149 IF: 4.762 (2013)

8.5. Presentations not related to the dissertation

3. Molnár Enikő, Nathalie Camus, Véronique Patinec, Gabriele A. Rolla, Mauro Botta, Kálmán Ferenc Krisztián, **Fodor** Tamás, Raphaël Tripier, Carlos Platas-Iglesias, és **Tircsó Gyula: Pikolinátcsoportot tartalmazó makrociklusos ligandumok Mn(II)-komplexei: egyensúly és kinetika,** *XXXXVIII Komplexkémiai Kollokvium*, **2014,** Május 28-30, Siófok, Magyarország.

2. Tircsó Gyula**,** Garda Zoltán, Molnár Enikő, **Fodor** Tamás, Kálmán Ferenc, Tei Lorenzo, Kovács Zoltán, Tóth Imre: **Mn^{2+}-komplexek: az MRI kontrasztanyag kutatás jövője vagy zsákutcája?** *19. Nemzetközi Vegyészkonferencia*, **2013,** November 21-24, Nagybánya, Románia.

1. Garda Zoltán, Kálmán Ferenc Krisztián, Botár Richárd, Molnár Enikő, **Fodor** Tamás, Kovács Zoltán, Tóth Imre, Tircsó Gyula:
7-, 8-, 10-, és 12-tagú (makro) ciklusos ligandumok Mn^{2+}-komplexeinek egyensúlyi és bomláskinetikai jellemzése
XLVII. Komplexkémiai Kollokvium, **2013,** Május 29-31, Mátraháza, Magyarország

8.6. Posters not related to the dissertation

2. Zoltán Garda, Enikő Molnár, Richárd Botár, Tamás **Fodor**, Ferenc K. Kálmán, Zoltán Kovács, Imre Tóth, Gyula Tircsó:
Tuning of the thermodynamic and kinetic properties of Mn^{2+} complexes formed with cyclododecane derivatives: the effect of the nature of donor atoms
16. International Conference on BioInorganic Chemistry (ICBIC-16), 22-26 July, **2013**, Grenoble, France.

1. Zoltán Garda, Enikő Molnár, Richárd Botár, Tamás **Fodor**, Ferenc K. Kálmán, Zoltán Kovács, Imre Tóth, Gyula Tircsó**:**
Tuning of the thermodynamic and kinetic properties of Mn^{2+} complexes formed with cyclododecane derivatives: the effect of the nature of donor atoms
Debrecen Colloquium on Inorganic Reaction Mechanisms, 11-15 June **2013**, Debrecen, Hungary.

8.7. Patent claims not directly related to the dissertation

4. Botár R., Garda Z., **Fodor** T., Kálmán F., K., Nagy V., Tircsó Gy., Tóth I., **Új ciklononán alapú vegyületek és alkalmazásuk Mn(II)-alapú MRI kontrasztanyagok ligandumaiként** Magyar szabadalom, P1500563, Benyújtva: **2015. november 30.**

3. Botár R., Garda Z., **Fodor** T., Kálmán F., K., Nagy V., Tircsó Gy., Tóth I., **Új 3,6,9,15-t tetraaza-bicklo[9.3.1]pentadeka-1(14),11(15),12-trién alapú vegyületek és alkalmazásuk Mn(II)-alapú MRI kontrasztanyagok ligandumaiként,** Magyar szabadalom, P1500564, Benyújtva: **2015. november 30.**

2. Botár R., Garda Z., **Fodor** T., Kálmán F., K., Nagy V., Tircsó Gy., Tóth I., **Új 2,11-diaza[3.3](2,6)-piridinofán alapú vegyületek és alkalmazásuk Mn(II)-alapú MRI kontrasztanyagok ligandumaiként,** Magyar szabadalom, P1500565, Benyújtva: **2015. november 30.**

1. Botár R., Garda Z., **Fodor** T., Kálmán F., K., Nagy V., Tircsó Gy., Tóth I., **Új 6-oxa-3,9,15-triaza-biciklo[9.3.1]pentadeka-1(14),11(15),12-trién alapú vegyületek és alkalmazásuk Mn(II)-alapú MRI kontrasztanyagok ligandumaiként,** Magyar szabadalom, P1500566, Benyújtva: **2015. november 30.**

9. Acknowledgement

I would like to express my gratitude to Prof. Imre Tóth for supervising me all these years, always showing me new ways to tackle obstacles and for all the help he has given me.

I am grateful to Dr. Gyula Tircsó for deepening my understanding of practical synthetic chemistry and insight into finer aspects of potentiometry and relaxometry.

Köszönöm Zékány Lászlónak a bonyolultabb számításokban, szimulációkban nyújtott elengedhetetlen segítségét, valamint történelmi és világpolitikai ismereteim kiterjesztését.

I would like to thank Dr. István Bányai for getting me acquainted with some lesser-known inner workings of NMR and for his help with measurements.

I would like to thank Dr. Mihály Purgel for his help with in silico calculations and interpretation thereof.

I am grateful to Dr. Attila Bényei for his help in solving crystal structures and his patience when waiting for said crystals.

Köszönöm Rózsa Bélának a munkában, különösképp a tallium-elektrolízisben nyújtott segítségét.

I thank Prof. Ernő Brücher for constantly providing new wisdom and knowledge.

I thank my current and previous colleagues and students at the Dept. of Inorganic and Analytical Chemistry, University of Debrecen for their help and for providing a friendly, fun atmosphere.

Végül szeretném megköszönni családomnak, hogy mindvégig támogattak és megteremtették a munkához szükséges atomszférát.

I am grateful to the hungarian Science Research Fund (OTKA, projects K-84291 & K-109029) and COST action TD1004 for financial support.